



Republic of Iraq
Ministry of Higher Education
and Scientific Research
University of Diyala
College of Science



Effect of SWCNTs-Polymers Nanocomposites on Cancer Cell Line Applications

A Thesis

Submitted to the Council of College of Science
University of Diyala in Partial Fulfillment of Requirements for the
Degree of Doctor of Philosophy (Ph.D.) in Physics

By

Marwa Rashed Jwameer

(B.Sc. in Physics 2010)

(M.Sc. in Physics 2016)

Supervised by

Prof. Dr.

Sabah A. Salman

1444 A. H.

Prof. Dr.

Farah T. M. Noori

2022 A. D.

بِسْمِ اللَّهِ الرَّحْمَنِ الرَّحِيمِ

(مَنْ يَتَّقِ اللَّهَ يَجْعَلْ لَهُ مَخْرَجًا وَيَرْزُقْهُ مِنْ حَيْثُ لَا يَحْتَسِبُ وَمَنْ يَتَوَكَّلْ عَلَى اللَّهِ فَهُوَ حَسْبُهُ إِنَّ اللَّهَ بَلِّغُ أَمْرِهِ قَدْ جَعَلَ اللَّهُ لِكُلِّ شَيْءٍ قَدْرًا)

بِسْمِ اللَّهِ الرَّحْمَنِ الرَّحِيمِ

[الزُّمَرُ: ٢-٣]

Dedication

To my Country AL-Iraq...

To my Family....

To my Teacher and my Father Prof.

Dr. Tahseen H. Mubarak

To my Friends.....

To all who have given me a hand

throughout this work.....

Marwa Al-Soabei

Acknowledgments

First and foremost, I thank Allah (SWT) for letting me live to see this thesis through and gave me chance and courage to complete this work, and our prophet Muhammad (peace and blessings of Allah be upon him) who invites us to science and knowledge.

I would like to express my sincere gratitude to my supervisors **Prof. Dr. Sabah A. Salman** and **Prof. Dr. Farah T. M. Noori** who granted me the opportunity to do this research. I am indebted to them for their suggestions and valuable remarks.

Special thank are extended to the Dean of the College of Science University of Diyala **Prof. Dr. Tahseen H. Mubarak** and to head of Physics Department **Assist. Prof. Dr. Ammar A. Habeeb** and all the Staff of the Department of Physics for their assistance and especially for **Prof. Dr. Nabeel Ali Bakr**.

Special thank are extended to head of **Biological Department Prof. Dr. Ibrahim hadi Mohamed and Iraqi Center for Cancer /Al-Mustansiriyah University**.

My greatest indebtedness goes to **my Parents** for their valuable advice, my Brothers (**Ali and Hasan**), my Sisters (**Hajer and Rooa**) and my uncle (**Esraa**) for their endless support.

Finally, my deepest gratitude is dedicated to my Studying Partners: Shahlaa, Laith and Omer, and Special thanks to my close friend **Dr. Olfat Ahmed, Dr. Nada Suheel, Asst. Prof. Hind Walled, Dr. AWS, Dr. Muhammed Hameed, Ali A. Salal, Hayder, Noor Sabah, Rana Talib, Iraq Ali** and **Marwa Adib** who shares every happy and sad moments with me...

Marwa 2022

Published and Accepted Research Articles

List of Publications

- 1- Marwa R.Jwameer, Farah T. M. Noori, Sabah A. Salman, **Carbon Nanotube Conjugate with PEG as a Drug Delivery in to AMJ13 and HepG2 Cell**, Journal of Mechanical Engineering Research and Developments, ISSN: 1024-1752, Volume 44, No.8, PP. 44-56, 2021.
- 2- Marwa R.Jwameer, Sabah A. Salman, Farah T. M. Noori, **Smart Drug Delivery Systems Based on Single-Wall Carbon Nanotubes Loaded with Nanocurcumin Extract for Cancer therapy and Toxicity**, Diyala Journal for Pure Science, No. 96, Date of acceptance 10-8-2022.

Abstract

This study included three parts; the first part included functionalization of single wall carbon Nanotubes (SWCNTs) using (HCl) and mixture of acids (H_2SO_4 , HNO_3) to convert them to (SWCNTs-COOH), and then followed by an esterification process of (SWCNTs-COOH) with (PEG, PEG-PEI), an ester reaction was performed between the group of carboxylic acids PEG and PEG-PEI which contains amino groups. Then the physical properties were studied using XRD, FTIR, UV-Vis, RS, TEM and AFM the techniques to characterize the composite (PEG – SWCNTs). SWCNTs had a sharp peak at (291 nm) in UV-vis, whereas (PEG – SWCNTs) and (PEG-PEI-SWCNTs) had a peak at 289 nm and 300.98 nm. In Fourier transforms infrared spectroscopy (FTIR) spectra, a strong OH bond can be seen for both materials, as well as the C–H bond of (PEG-SWCNTs) and C –H, N-H, C-N bond of (PEG- PEI-CNTs) also showed. In XRD pattern SWCNTs have a sharp peak at $2\theta = 25.6299^\circ$, which is related to 002 with d – spacing (3.4729 Å) while functionalization of PEG-SWCNTs is conformed to a broad peak at $2\theta = 23.4473^\circ$ with d – spacing (3.8447Å) and functionalization of PEG-PEI-SWCNTs conform by broad peak at ($2\theta = 23.51^\circ$) with d – spacing (3.7816Å). The values of crystallite size for SWCNTs, PEG-SWCNTs and PEG-PEI-SWCNTs equals ((3nm), (7.7nm) and (8.48nm)), respectively. Atomic force microscopy (AFM) and SWCNTs images show a single wall carbon nanotube with a grain size of (60 nm). In PEG-SWCNTs and PEG-PEI-SWCNTs, the grain size increases with functionalization to (83.60 nm, 80.68 nm), respectively. In Raman Spectroscopy, we notice a shift in the D and G bands in PEG-SWCNTs and PEG-PEI-SWCNTs. In TEM the raw

SWCNTs are long curved aggregates, which appear to be a bundle of inhomogeneous aggregates consisting of many tubes, The tubular structure of CNTs-PEG-PEI is rough, and some particles appear to be attached and distributed along the SWCNTs sidewalls, maybe indicating that PEG and PEI groups are conjugated onto nanotubes.

The second part included loading nanocurcumin (N.Cur) on to SWCNTs containing polyethylene glycol (PEG) and polyethyleneimine (PEI), which contains amino groups, were synthesized (PEG-PEI-SWCNTs). The spectral and structural characteristics of (PEG-PEI-SWCNTs-N.Cur) were comprehensively analyzed by XRD, FTIR, UV- Vis, RS, TEM and AFM. XRD patterns revealed that PEG-PEI-SWCNTs had different crystalline structures and defects, as well as a higher interlayer spacing. AFM results showed SWCNTs with the grain size of (60 nm), while PEG-PEI-SWCNTs revealed SWCNTs aggregation with the grain size of (79.6 nm) after loading N. Curcumin extract, which was verified by TEM examination. A strong OH bond appeared in FTIR spectra. Furthermore, UV- Vis absorbance peaks at (289, 300.98, (282,425) and (273,431)) nm seemed to be correlated with SWCNTs, PEG-PEI-SWCNTs, N. Curcumin extract, and PEG- PEI-SWCNTs- N. Curcumin extract. The Raman spectra for PEG-PEI-SWCNTs-N. Cur, the radial breathing mode (RBM) band, the disorder band (D band), the tangential mode (G band) and the overtone of the D band (2D band) shifting to ((171,264),1283, 1593 and 2131 cm^{-1}) respectively. The peaks for the nanocurcumin around (958, 1183 and 1428) cm^{-1} experienced shift to (939, 1168 and 1470) cm^{-1} in the drug loaded sample due to nano-encapsulation and indicates successful drug loading. The lines at (716 and 853) cm^{-1} can be assigned to the C-N stretching vibrations.

Part third included the samples in the all parts of this study using in three type of bio application, first type of bio application include effect SWCNTs and PEG-SWCNTs on two type of anti-bacterial Gram-negative bacterial strain *Pseudomonas aeruginosa* and Gram-positive bacterial strain *bacillus spp.* were exposed to a series of concentrations from prepared (PEG-SWCNTs) ((25-100) $\mu\text{g/ml}$). The results exhibited significant inhibitory activity and that the rate of bacterial growth inhibition increased with increasing concentration. Second type of bio application include effect SWCNTs, PEG-SWCNTs, PEG-PEI-SWCNTs and PEG-PEI-SWCNTs-N.Cur on two type of anticancer the breast cancer AMJ13 cell line and liver cancer HepG2 cell line were exposed to a series of prepared (SWCNTs, PEG-SWCNTs, PEG-PEI-SWCNTs, PEG-PEI-SWCNTs-N.Cur) concentrations ((6.25- 100) $\mu\text{g/ml}$), and the inhibition rate of growth in cells was measured for 72 h. The cytotoxicity screening showed that there was a highly toxic effect on the cancer cells. Third type of bio application include effect (SWCNTs, PEG-PEI-SWCNTs and PEG-PEI-SWCNTs-N.Cur) on the normal cell line (RD). Inhibition rates in the normal cell line RD by the effect of different concentrations ((6.25- 100) $\mu\text{g/ml}$) of (SWCNTs, PEG-PEI-SWCNTs and PEG-PEI-SWCNTs-N.Cur) for an exposure period of (72 hours) and a temperature of (37 ° C).

List of Contents

Chapter One		
<i>Introduction and Previous Studies</i>		
1-1	Introduction	1
1-2	Composites Material	3
1-3	The Materials Used in This Study	5
1-3-1	Polyethylene Glycol (PEG)	5
1-3-2	Polyethyleneimine (PEI)	6
1-3-3	Carbon Nanotube	7
1-3-4	Nanocurcumin	9
1-4	Literature Survey	12
1-5	Aims of the Study	31
Chapter Two		
<i>Theoretical Part</i>		
2-1	Introduction	32
2-2	Optical Properties	32
2-2-1	UV-VIS	32
2-2-2	Electronic Transitions	32
2-2-3	Absorbing Species Containing π , σ , and n Electrons	33
2-3	Raman Spectroscopy	36
2-3-A	Basic Principles and Instrumentation	37
2-3-B	Radial Breathing Mode (RBM)	39
2-3-C	The G-band	40

2-3-D	The D-band	40
2-4	X-Ray Diffraction	41
2-5	Bacterial Strains	43
2-6	Antibacterial Activity of Nanoparticles	43
2-7	Structure of the Bacterial Cell Walls	44
2-8	Bacterial Types	46
2-8-1	Pseudomonas Aeruginosa (P. aeruginosa)	46
2-8-2	Bacillus SPP	46
2-9	Interactions between Bacteria and Nanoparticles	47
2-10	Mechanism of Antimicrobial Activity of Carbon Nanotubes	49
2-11	Core -Shell Particles	52
2-12	Cancer	54
2-13	Mechanism of NPs action against tumor	57
2-14	Cell Lines	59
2-14-1	AMJ13 Cell Line	60
2-14-2	Hep-G2 Cell Line	60
2-14-3	R.D Cell Line	61
2-15	Nanoparticles for Drug Delivery	61
2-16	CNTs in Drug Delivery	63
2-17	CNT Functionalization Techniques	63
2-17-1	Noncovalent Functionalization	64
2-17-2	Covalent Functionalization	64
Experimental Work		
Chapter Three		

3-1	Introduction	67
3-2	Chemical and Biomedical Material Reagents	67
3-3	Preparation of Material	69
3-3-1	Functionalization of SWCNTs by PEG	69
3-3-2	Functionalization of SWCNTs with PEG and PEI mixture	69
3-3-3	Loading Nanocurcumin on PEG-PEI-SWCNTs	70
3-4	Measurement of Optical Properties	70
3-5	Structural Properties and Surface Morphology Measurements	71
3-5-1	X-Ray Diffraction	71
3-5-2	Atomic Force Microscopy (AFM) Measurements	71
3-5-3	Transmission Electron Microscopy (TEM)	71
3-6	Chemical Properties	72
3-6-1	Fourier Transform Infrared (FTIR) Spectroscopy	72
3-6-2	Raman Measurement	72
3-7	Bioactivity	73
<i>Chapter Four</i>		
<i>Results and Discussion</i>		
4-1	Introduction	76
4-2	Optical Properties	76
4-3	Chemical Properties	78
4-3-A	Fourier Transform Infrared (FTIR)	78
4-3-B	Raman Spectroscopy (RS)	81
4-4	Morphological Properties	87
4-4-1	Atomic Force Microscopy (AFM) Analysis	87

4-4-2	Transmission Electron Microscopy (TEM) Analysis	90
4-5	Structural Properties	92
4-5-1	X-Ray Diffraction Analysis	92
4-6	Biomedical Application Results	94
4-6-1	Antibacterial Activity	94
4-6-2	Anti-Proliferative Activity of Against Cancer Cell Line	98
4-6-2-A	Anti-Proliferative Activity Of (SWCNTs) Against Cancer Cell Line	98
4-6-2-B	Anti-Proliferative Activity Of (PEG-SWCNTs) Against Cancer Cell Line	100
4-6-2-C	Anti-Proliferative Activity Of (PEG-PEI-SWCNTs) Against Cancer Cell Line	102
4-6-2-D	Anti-Proliferative Activity Of (PEG-PEI-SWCNTs-N. Cur) Against Cancer Cell Line	104
4-6-3	Anti-Proliferative Activity of Normal Cancer Cell Line	107
4-6-3-A	Effect of SWCNTs on Normal Cell Line	107
4-6-3-B	Effect of PEG-PEI-SWCNTs on Normal Cell Line	109
4-6-3-C	Effect of PEG-PEI-SWCNTs-N.Cur on Normal Cell Line	111
4-7	Conclusions	113
4-8	Future Recommendations	114

List of Figures

No.	Title	Page No.
(1-1)	Illustrative image of polyethylene glycol material	6
(1-2)	Chemical structure of polyethylenimine	7
(1-3)	Difference type of CNTs	9
(1-4)	Different functional and biological features of curcumin or nanocurcumin.	11
(1-5)	Chemical structure of nano curcumin.	12
(2-1)	Rotational and vibrational electronic levels	33
(2-2)	Electronic transition	34
(2-3)	The photograph of Raman spectroscopy	36
(2-4)	The diagram showing the type of transition of the electrons and the Rayleigh and Raman scattering	38
(2-5)	Raman Spectrum of SWCNT, DWCNT and MWCNT samples	39
(2-6)	Bragg's diffraction. Two beams with identical wavelength and phase approach a crystalline solid and are scattered of two different atoms within it	42
(2-7)	Structural distinguishes between Gram's positive and the Gram's negative bacterial cell wall	45
(2-8)	The Image for P.aeruginosa bacteria	46
(2-9)	The image for bacillus Spp bacteria	47
(2-10)	Mechanism of antibacterial activity of nanoparticles	49
(2-11)	Mechanism of antimicrobial activity of carbon nanotubes	51
(2-12)	Variety of core-shell particles: (a) Surface modified core particles anchored with shell particles. (b) Smooth	53

	coating of dielectric core with shell. (c) Encapsulation of very small particles with dielectric material and (d) Quantum bubble deposited on inexpensive core	
(2-13)	Schematic representation of the nanocarriers used in smart drug delivery systems	56
(2-14)	The Mechanism of action of nanoparticles against Tumor-cells	58
(2-15)	The active and passive targets of nanoparticles	59
(2-16)	Carbon nanotubes (CNT) before and after oxidization using a combination of nitric and sulfuric acid. This method resulted in chemical nanotubes and formation of carboxylate groups on the surface modifications carbon.	66
(3-1)	Schematic diagram laboratory experiments carried out to achieve the aim of the present study	68
(4-1)	The absorbance of SWCNTs and PEG-SWCNTs as a function of wavelength	76
(4-1)	The absorbance of (a) SWCNTs and PEG-PEI-SWCNTs, (b) Nano Cur and PEG-PEI-SWCNTs-N. Cur as a function of wavelength.	77
(4-2)	FTIR spectrum of (a) SWCNTs, (b) PEG-SWCNTs, (c) PEG-PEI-SWCNTs (d) Nano Curcumin and (e) PEG-PEI-SWCNTs-N. Cur	80
(4-3)	Raman Spectroscopy (a)SWCNTs, (b)PEG- SWCNTs and (c) SWCNTs, PEG-SWCNTs	82
(4-4)	Raman Spectroscopy (a)SWCNTs, (b) PEG-PEI-SWCNTs and (c) SWCNTs, PEG-PEI-SWCNTs	84
(4-5)	Raman Spectroscopy (a) N. Cur, (b) PEG-PEI-SWCNTs-N. Cur and (c) N. Cur, PEG-PEI- SWCNTs-N. Cur.	86
(4-6)	Surface images by AFM for (a) SWCNTs and (b) SWCNTs – PEG4000.	89
(4-7)	Surface images by AFM for (a) PEG-PEI-SWCNTs (b) Nanocurcumin (N. Cur) and (c) PEG-PEI-SWCNTs-N. Cur.	89

(4-8)	TEM images of (a)SWCNTs, (b) PEG-PEI-SWCNTs, (c)N. Cur and (d) PEG-PEI-SWCNTs-N. Cur	91
(4-9)	The XRD pattern for (a) SWCNTs, (b) PEG-SWCNTs, (c) PEG-PEI-SWCNTs, (d) N. Cur and (e) PEG-PEI-SWCNTs- N. Cur.	93
(4-10)	Anti-bacterial activity of (a) SWCNTs (b) PEG-SWCNTs Bacillus SPP, the inhibited zones of bacterial growth for both strains are illustrated when exposed to variety concentrations as follows; (1) 25 mL, (2): 50 mL, (3): 75 mL, (4): 100 mL.	96
(4-11)	Anti-bacterial activity of (a)SWCNTs (b) PEG-SWCNTs Pseudomonas aeruginosa, the inhibited zones of bacterial growth for both strains are illustrated when exposed to variety concentrations as follows; (1) 25 mL, (2): 50 mL, (3): 75 mL, (4): 100 mL.	97
(4-12)	Cytotoxic effect of (a) SWCNTs in AMJ13 cell, (b) SWCNTs in HepG2 cells.	99
(4-13)	Morphological changes in (AMJ13, HepG2) Cells after treated with SWCNTs.	99
(4-14)	Cytotoxic effect of (a)PEG-SWCNTs in AMJ13 cell, (b) PEG- SWCNTs in HepG2 cells.	101
(4-15)	Morphological changes in (AMJ13, HepG2) Cells after treated with PEG- SWCNTs.	101
(4-16)	Cytotoxic effect of (a) PEG-PEI-SWCNTs in AMJ13 cell, (b) PEG-PEI- SWCNTs in HepG2 cells.	103
(4-17)	Morphological changes in (AMJ13, HepG2) Cells after treated with PEG-PEI- SWCNTs.	104
(4-18)	Cytotoxic effect of (a)-PEG-PEI-SWCNTs-N. Cur in AMJ13 cell, (b)- PEG-PEI- SWCNTs-N. Cur in HepG2 cells.	106
(4-19)	Morphological changes in (AMJ13, HepG2) Cells after treated with PEG-PEI- SWCNTs-N.Cur.	106
(4--20)	Cytotoxic effect of of SWCNTs on normal cell line (RD).	107
(4-21)	Inverted microscope image showing effect of different concentrations of SWCNTs.	108
(4-22)	Cytotoxic effect of of PEG-PEI- SWCNTs on normal cell line (RD).	109

(4-23)	Inverted microscope image showing effect of different concentrations of PEG-PEI- SWCNTs.	110
(4-24)	Cytotoxic effect of of PEG-PEI- SWCNTs-N. Cur on normal cell line (RD).	111
(4-25)	Inverted microscope image showing effect of different concentrations of PEG-PEI- SWCNTs -N.Cur.	112

List of Tables

No.	Title	Page No.
(2-1)	The different types of nanoparticle-based system for drug delivery	62
(3-1)	The Chemical and Biomedical Material Reagents	67
(4-1)	The FTIR Peaks Assignments of SWCNTs, PEG-SWCNTs, PEG-PEI-SWCNTs, N. Cur and PEG-PEI-SWCNTs-N.Cur.	79
(4-2)	Surface roughness, root mean square (RMS) and grain size of (SWCNTs, PEG-SWCNTs, PEG-PEI-SWCNTs, N. Cur and PEG-PEI-SWCNTs-N. Cur)	88
(4-3)	Inhibition rates in the normal cell line RD by the effect of different concentrations of SWCNTs for an exposure period of 72 hours and a temperature of 37 ° C.	108
(4-4)	Inhibition rates in the normal cell line RD by the effect of different concentrations of PEG-PEI-SWCNTs for an exposure period of 72 hours and a temperature of 37 ° C.	110
(4-5)	Inhibition rates in the normal cell line RD by the effect of different concentrations of PEG-PEI-SWCNTs-N.Cur for an exposure period of 72 hours and a temperature of 37 ° C	112

List of Abbreviations

Symbol	Definition
DNA	Deoxyribonucleic Acid
CNTs	Carbon nanotubes
MMCs	Metal-Matrix Composite
CMCs	Ceramic -Matrix Composite
OMCs	Organic-Matrix Composite
PMCs	Polymer- Matrix Composite
CMCs	Carbon-Matrix Composite
PEG	Polyethylene Glycol
PEI	Polyethyleneimine
DB	Degree of Branch
NH ₂	Primary Amine end Groups
NH	Secondary Amine Linear Unite
PDT	Photo Dynamic Therapy
SWCNTs	Single-Walled Carbon Nanotubes
MWCNTs	Multi-Walled Carbon Nanotubes
GCNTs	Graphene-Nanotubes
MSN	Mesoporous Silica Nanoparticles
CNS	Central Nervous System
BBB	Blood Brain Barrier
PI-PEGs	Phospholipid-Polyethylene glycols
MCF7	Human Breast Cancer Cell Lines
FITC	Fluorophore Fluorescein Isothiocyanate
SEM	Scanning Electron Microscopy
TEM	Transmission Electron Microscope
DLS	Dynamic Laser Light Scattering
XRD	X-ray Diffraction
ALT	Alanine Aminotransferase
AST	Aspartate Aminotransferase
PVA	Poly Vinyl Alcohol
AGS	Gastric Cancer Cell Lines

UV-VIS	Ultra violet-Visible
GO	Graphene Oxide
SAED	Selected Area Electron Diffraction
FE-TEM	Field Emission Transmission Electron Microscopy
FTIR	Fourier Transform Infrared Spectroscopy
VSM	Vibrating Sample Magnetometer
PEG-diPBI	Polyethylene Glycol Modified diperylene bisimide
CVD	Chemical Vapor Deposition
TGA	Thermogravimetric Analysis
E2	β - estradiol
HBCCs	Human Breast Cancer Cells
LBP	Lobaplatin
RS	Raman Spectroscopy
Cur	Curcumin
<i>EDC</i>	Hydrochloride C ₆ H ₁₇ N ₃ -HCL
NHS	N-Hydroxy succinimide
TENG	Triboelectric Nano generator
FA	Folic Acid
AFM	Atomic Force Microscopy
FCM	Flow Cytometry
NPs	Nanoparticles
N. sativa	Ba _{0.7} Sr _{0.3} TiO ₃
UCNPs	Up Conversion Nanoparticles
PLGA	Poly (lactic-co-glycolic Acid)
HEM	High Energy Mode
RBM	Radial Breathing Mode
SERS	Surface Enhanced Raman Scattering
G-Band	Verified the Tangential Modes
LPS	Lipopolysaccharides
P. aeruginosa	Pseudomonas Aeruginosa

ROS	Reactive Oxygen Species
E. coli	Escherichia Coli
S. enteric	Salmonella Enteric
PG	Pentaglycines
MDR	Multi Drug Resistance
SDDSs	Smart Drug Delivery System
MSNs	Meso-Porous Silica Nanoparticle
GNPs	Gold Nanoparticles
SPIONs	Super Paramagnetic Iron Oxide Nanoparticles
QDs	Quantum Dots
EPR	Enhanced Permeability
AFP	α -fetoprotein
CEA	Carcinoembryonic Antigen
EPR	Enhanced Permeation and Retention
AMJ13	Ahmed Murtatha Jabria 13
Hep-G2	Hepatocellular Carcinoma2
PLA	Polylactic Acid
PCL	Polycaprolactone
PACA	Polyacrylate
rpm	Revolution Per Minute
IMVC	Indole Methyl Red Vokes Proskauer
MTT	Methyl Thiazolyl Tetrazolium
DMSO	Dimethyl Sulfoxide
RMS	Root Mean Square
RNA	Ribonucleic Acid

Chapter One
Introduction and Previous Studies

1-1 Introduction

The word “biomaterial” is generally used to categorize materials used for biomedical applications and is different from a biological material such as bone which is produced by a biological system [1]. A biomaterial may be defined as a natural or synthetic substance that can be used for any period of time to treat, strengthen or substitute any tissue, organ or function of the body [2]. Another definition of biomaterial is “a synthetic material used to replace part of a living system or to function in intimate contact with living tissue” [3]. From material’s standpoint, biological tissue can be considered as a composite consisting of nano-biomaterials, for example, nano-muscle fibers, nano-apatite grains, nano-membrane, etc. [2]. Nano-biomaterials have long been a focus of active research owing to their unique properties that can be utilized for biomedical applications such as tissue engineering, biosensing, bioimaging, drug and gene delivery, wound healing, medical implant and diagnostic systems like protein and DNA microarrays. The rapid growth of nanotechnology has enabled the researchers to produce nanoparticles, nanofibers, nanocoating and nanocomposites for biomedical applications [4,5]. Have suggested that a nano-functionalized surface has promising biological properties. Hence, clinical applications of biomaterials can be improved by producing a nanostructured surface. In general, the biomaterials with medical applications can be divided into four groups: polymers, metals, ceramics and composites [4].

Biopolymers can be described as naturally occurring macromolecules which are usually produced by living systems including plants, animals, and microorganisms [6]. In recent years, there is a growing tendency to use more of natural polymers for developing various food and biomedical products [7,8]. It is noteworthy to mention over here that the mankind has

been using biopolymers not only for food and biomedical applications, where it has found numerous applications, but also in textile, cosmetics, pharmaceuticals, and paper industries [9]. Biopolymers contain repeating units of monomers and are usually derived from plants, animals, and microorganisms. In general, the repeating units of a biopolymer may either be sugars, amino acids, or fermentative products like aliphatic polyesters [10]. These biopolymers may have different functional groups like hydroxyl, amino, amide, carboxyl, phosphate, phenolic, etc. [11], which impart to their different biological activities [12]. The biopolymers are usually broadly classified into three groups, namely, polysaccharides, proteins, and polynucleotides. Recently, there has been a great thrust on the usage of biopolymers for a number of applications, especially in the biomedical and pharmaceutical [13]. The functional efficiency of the biopolymer molecules depends on the composition, physicochemical properties and structural features [14]. It is possible to rationally design the composition and structure of the biopolymer to obtain the appropriate functional attributes [15]. The internal structure of the polymer molecule determines many functional characteristics such as permeability, chargeability and integrity [16]. The stability of the biopolymer particles and their ability to aggregate is influenced by the electrical characteristics. Biopolymer particles with a high electric charge will repel and prevent aggregation. Molecules of biopolymers and their electrical properties influence the interaction with other molecules present in the surrounding environment [16]. Among natural biopolymers, alginate is one of the most popular and intensely studied [17].

Current cancer treatments mostly involve surgery, chemotherapy and/or radiotherapy. The purpose of chemotherapy and of radiation is to kill the tumor cells, as they are more susceptible to the actions of these

methods. However, the well-known side effects strongly minimize their actual benefits, and they reduce the potential candidates. Nanotechnology provides innovative and promising alternatives to conventional strategies to defeat tumors [18]. Among nanotechnology, carbon nanotubes (CNTs) have gained intensive attention and interest during the past 20 years because of their unique mechanical properties, in addition to very interesting values in electrical and thermal conductivity. Moreover, the possibility of functionalizing their surface with a wide group of bio/chemical species paves the way for numerous therapeutic and drug delivery applications. For these reasons, they stand out within the newest approaches for cancer “theragnostic” treatment, i.e. treatments that combine both the diagnosis and therapy in the same nanostructure [19].

1-2 Composite Materials

A composite material is a materials system composed of two or more physically distinct phases whose combination produces aggregate properties that are different from those of its constituents [20]. The composite biomaterials have been used successfully in the field of dentistry as restorative materials or dental cements for decades. The combination of low density/weight and high strength properties in composite materials make them ideal for prosthetic limbs. The carbon-carbon and carbon-reinforced polymer composites have attracted attention of researchers, particularly for bone repair and joint replacement applications, because of their low elastic modulus levels, but these materials have not displayed the mechanical and biological properties required for these applications [21]. Composites materials can be classified according to two aspects. Composites are firstly classified based on the matrix constituent. They are called by the part which is mostly present in the composites. The composites classes depending on matrix component are listed below [22]:

1. Metal- Matrix Composites (MMCs).
2. Ceramic- Matrix Composites (CMCs).
3. Organic- Matrix Composites (OMCs).

The organic matrix composites are divided in to two types: carbon-matrix composites (CMCs) and polymer matrix composites (PMCs) [23]:

(A) Carbon – Matrix Composites (CMCs)

Carbon matrix composites are usually produced from PMCs by including the extra types of carbonizing and the original polymer matrix. Hence, C/C composites are used in high temperature applications. Mechanical properties of carbon matrix composites do not degrade until (2200C°). Conversely; the main drawback is the high cost of material and fabrication. The (CMCs) find wide application areas in aerospace and military system [23].

(B) Polymer –Matrix Composites (PMCs)

PMCs are widely used composites materials in the world. In this type of composites, polymer base resin is used as a matrix material in mixture with reinforcing agents. They are widely used in industrial, military, aerospace and automobile applications. The main advantage of these composites is the easy fabrication of large complex shapes [24]. In PMCs applications, both thermoplastic and thermoset polymers can be used as a matrix constituent. PMCs with thermoplastic polymers soften up on heating, therefore, service temperature for the thermoplastic PMCs is limited, i.e., usually they are not suitable for high temperature applications. Conversely, thermoset PMCs cannot be reshaped after curing process.

Because, thermoset PMCs have crosslinked molecular structure which is an insoluble and infeasible three-dimensional network [25].

1-3 The Materials Used in This Study

1-3-1 Polyethylene Glycol (PEG)

Polyethylene glycol (PEG) is one of the most widely used synthetic materials for biomedical applications. PEG is soluble in water, methanol, ethanol, acetonitrile, benzene, and dichloromethane, and is insoluble in diethyl ether and hexane. It is coupled to hydrophobic molecules to produce non-ionic surfactants. PEG is used as an excipient in many pharmaceutical products. Lower-molecular-weight variants are used as solvents in oral liquids and soft capsules, whereas solid variants are used as ointment bases, tablet binders, film coating, and lubricants. PEG is also used in lubricating eye drops [26]. Figure (1-1) shows an image of PEG material. PEG is a polyether compound with many applications from industrial manufacturing to medicine. The structure of PEG is $[\text{HO}-(\text{CH}_2\text{CH}_2\text{O})_n-\text{CH}_2\text{CH}_2-\text{OH}]$. PEG is also known as polyethylene oxide (PEO) or poly-ox ethylene (POE), depending on its molecular weight. PEG is produced by the interaction of ethylene oxide with water, ethylene glycol, or ethylene glycol oligomers. The reaction is catalyzed by acidic or basic catalysts. Ethylene glycol and its oligomers are preferable as a starting material instead of water, because they allow the creation of polymers with a low poly disparity (narrow molecular weight distribution). Polymer chain length depends on the ratio of reactants [27].

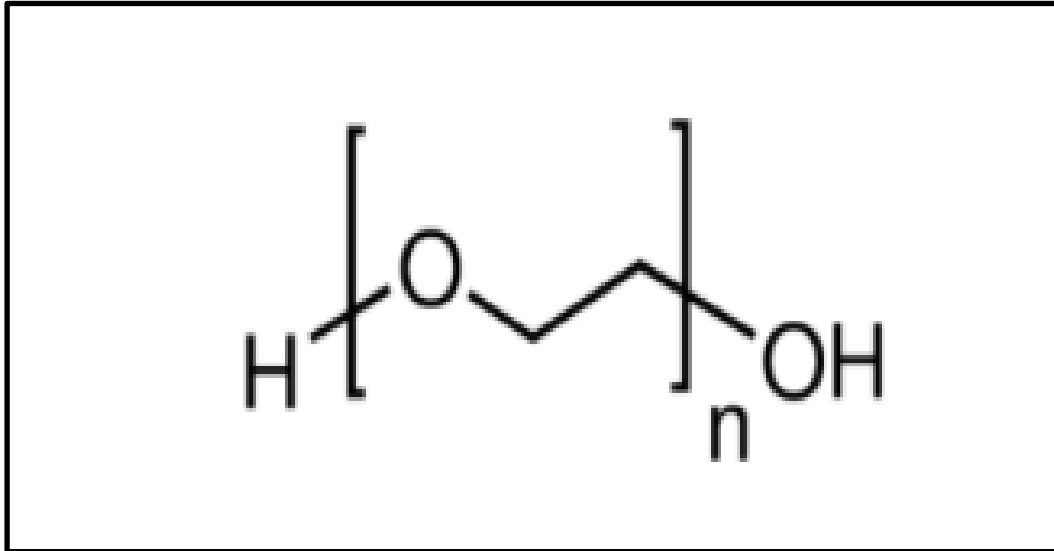


Figure (1-1): Illustrative image of polyethylene glycol material [27].

1-3-2 Polyethyleneimine (PEI)

PEI is a low molecular weight branched polymer with molecular weights varying between 0.8 and 750 kDa. PEI, as shown in figure (1-2), consists essentially of amino groups: (1) primary amine end groups (NH₂), (2) secondary amine linear units (NH), (3) tertiary amine branched (i.e., dendritic) units and is characterized by a degree of branching (DB) defined as: $DB = 2D / (2D + L)$, where D is the dendritic unit and L is the linear unit [28]. Some of the primary and secondary groups are protonated to ammonium ions, according to the pH of the solution [29], which give the PEI a cationic character. Most importantly, the PEI is considered as an eco-friendly material that was approved for food contact in the USA [30]. PEI was employed in a wide range of applications: mainly in medicinal chemistry as a DNA transfection agent and a drug delivery agent alongside with other uses [31] and in other applications such as water treatment, carbon dioxide capture and cosmetics [32] thanks to its structure, its high ionic charge and its high nucleophilicity. The latter was the main reason to

employ PEI in crosslinked polymer gels. In fact, and during the last 2 decades, PEI was shown to effectively crosslink with various acrylamide-based polymers through different mechanisms (nucleophilic attack, transamination reaction, acid–base interaction) [33]. PEI's application fields may be divided according to its use in:

- 1- Use of PEI as a drug.
- 2- Use of PEI for delivery of small drugs, and for the photo dynamic therapy (PDT).
- 3- Use of PEI for antimicrobial coating.
- 4- Use of PEI for the preparation of nanosized delivery vectors.
- 5- Use of PEI for non-invasive optical imaging devices.

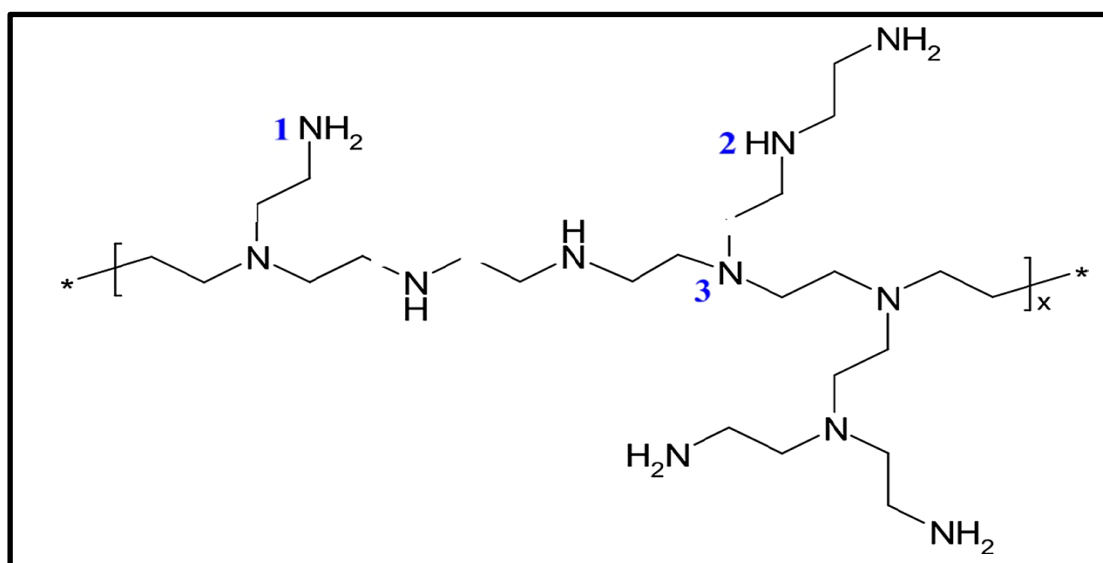


Figure (1-2): Chemical structure of polyethylenimine [33].

1-3-3 Carbon Nanotubes (CNTs)

Carbon nanotubes fundamentally fall into two classes: single-walled carbon nanotubes (SWCNTs) and multi-walled carbon nanotubes (MWCNTs). Despite the obvious commonality, SWCNTs and MWCNTs

have significantly different physical properties from each other because of their structural differences [34]. The most important feature that distinguishes SWCNTs is that the wall of the nanotube consists of the only one graphene layer. In other words, single-walled carbon nanotubes can be described as graphene sheets seamlessly rolled up to form hollow cylinders. That is why they often referred to as graphene nanotubes (GNTs). Unlike a single-walled nanotube, a multi-walled carbon nanotube can be viewed as a concentric arrangement of SWCNTs, i.e. consisting of multiple layers of graphene rolled up seamlessly into a tube shape. Figure (1-3) shows difference type of CNTs, these differences between single-walled and multi-walled carbon nanotubes result in substantially different properties and corresponding impacts on materials after their introduction [35]. SWCNTs are proving their great potential for utilization as a multifunctional additive and for creating new products with previously unattainable properties. They allow improvement of various features in practically all known materials: to impart conductive and anti-static properties, and to increase strength, crack resistance, flexibility and adhesion, and many other parameters depending on the required application. Moreover, this is often achieved at SWCNTs concentrations of tenths or hundredths of a percent, which generally makes it possible to retain the existing technologies for manufacturing the end products [36]. There are several approaches to classification of SWCNT applications. The most common are by the industry, material or type of industrial product. Classification by the type of industrial product can also be further classified depending on the potential volume of SWCNT consumption. Composite materials and reinforced plastics, industrial coatings, car tires and rubber technical goods, structural materials, and materials for electrochemical power sources account for the most significant volume of SWCNT consumption. The next group of applications in terms of the volume of

SWCNTs used includes adhesives and lubricants, anti-static plastics, transparent conductive films, and cables. Then there are a few niche applications that use limited quantities of single-walled carbon nanotubes [37]. Owing to their chemical compatibility with biomolecules (DNA and protein), single-walled carbon nanotubes can be used as components of biosensors and medical equipment. Tests of SWCNTs in implants show that they can be further used as coatings for catheters and neural implants. Solutions are also being developed for application in vivo, in particular for targeted delivery of substances encapsulated in SWCNTs-[38].

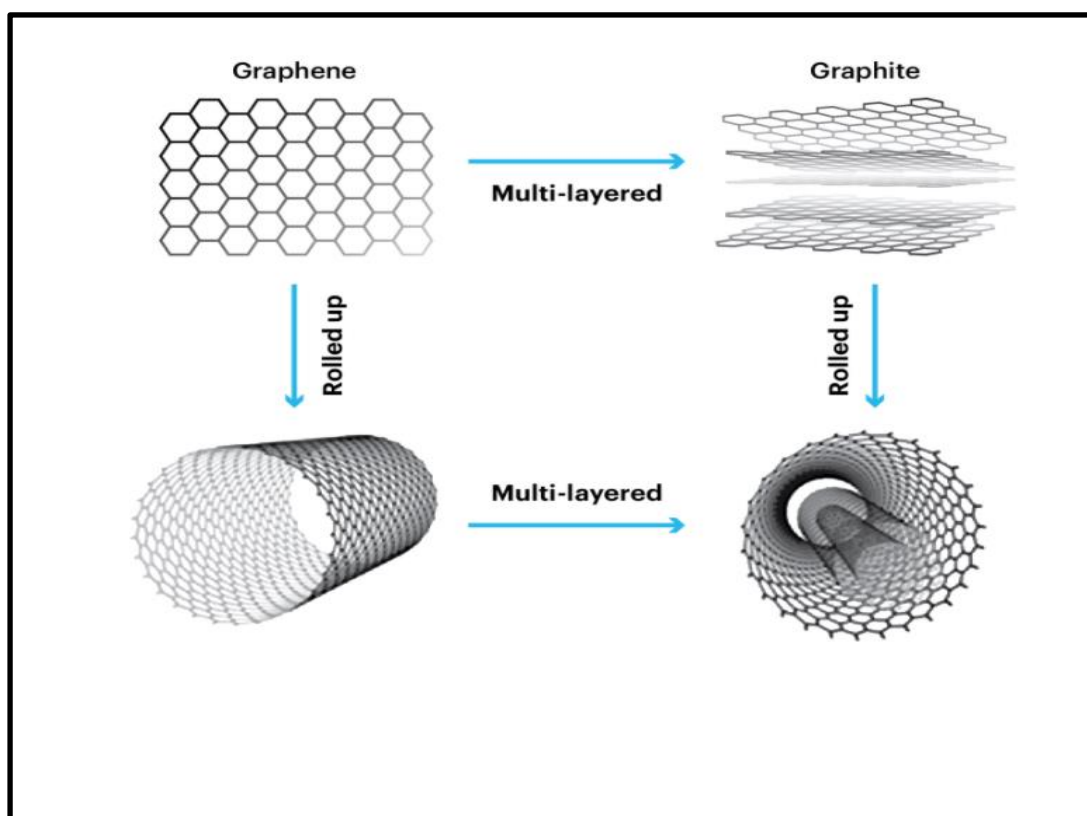


Figure (1-3): Different types of CNTs [38].

1-3-4 Nanocurcumin

Curcumin in the form of a nanoparticle (hereafter, curcumin nanoparticle) is a widely reported form for enhancing the bioavailability and solubility of lipophilic curcumin [39,40]. Kurita and Makino as well as

Hani and Shivakumar reported that the solubility and absorption rate of nanocurcumin is higher than the normal curcumin form, respectively [41,42]. Furthermore, curcumin nanoparticles can be more bioavailable and deposited more highly than the normal curcumin in comparison of the tissues of the Sprague-Dawley rat model [43,44]. However, no form of curcumin or its closely related analogues poses the properties required for a good drug or additive candidate in terms of chemical stability, high water solubility, potent and selective target activity, high bioavailability, broad tissue distribution, stable metabolism and low toxicity [45]. Due to the problems of water insolubility and low bioavailability of curcumin or curcumin nanoparticles, it has been reported that biodistribution and bioavailability of curcumin or curcumin nanoparticles would be increased by encapsulation processes such as nanoemulsions, liposomes, micelles, polymeric micro or nanoparticles, phospholipid complexes and hydrogels which showed the potential for efficient drug delivery systems that minimize the delay and reduce the vulnerability of diseases in organisms [46]. Prasad et al. postulated that an increased amount and length of curcumin in blood circulation could enhance the tissue deposition and biological activity in animals [47]. Furthermore, Mohamed et al. opined that hydrogen-bromide-treated curcumin can be exclusively used as a source of antioxidant in bioactive food materials [48]. As an organic curcumin nanocarrier, liposomal curcumin is considered as the best way of improving bioavailability of curcumin in cellular level and the commodities based on liposomal formulations are being marketed for different dietary applications of curcumin [49,50]. In addition, in case of inorganic nano formulations, mesoporous silica nanoparticles (MSN) are the most used nano systems for improving the bioavailability of poorly water-soluble drugs [51-53]. Among herbal and natural compounds, curcumin is a very attractive herbal supplement considering its

multipurpose properties. The potential effects of curcumin on glia cells and its therapeutic and protective properties in central nervous system (CNS)-related disorders is relevant. However, curcumin is unstable and easily degraded or metabolized into other forms posing limits to its clinical development. This is particularly important in brain pathologies determined blood brain barrier (BBB) obstacle. To enhance the stability and bioavailability of curcumin, many studies focused on the design and development of curcumin nano delivery systems (nanoparticles, micelles, dendrimers, and diverse nanocarriers). These nano constructs can increase curcumin stability, solubility, in vivo uptake, bioactivity and safety. Recently, several studies have reported on a curcumin exosome-based delivery system, showing great therapeutical potential. Figure (1-4) shows curcumin contains many valuable biological properties [54]. The chemical structure of nanocurcumin is shown in figure (1-5).

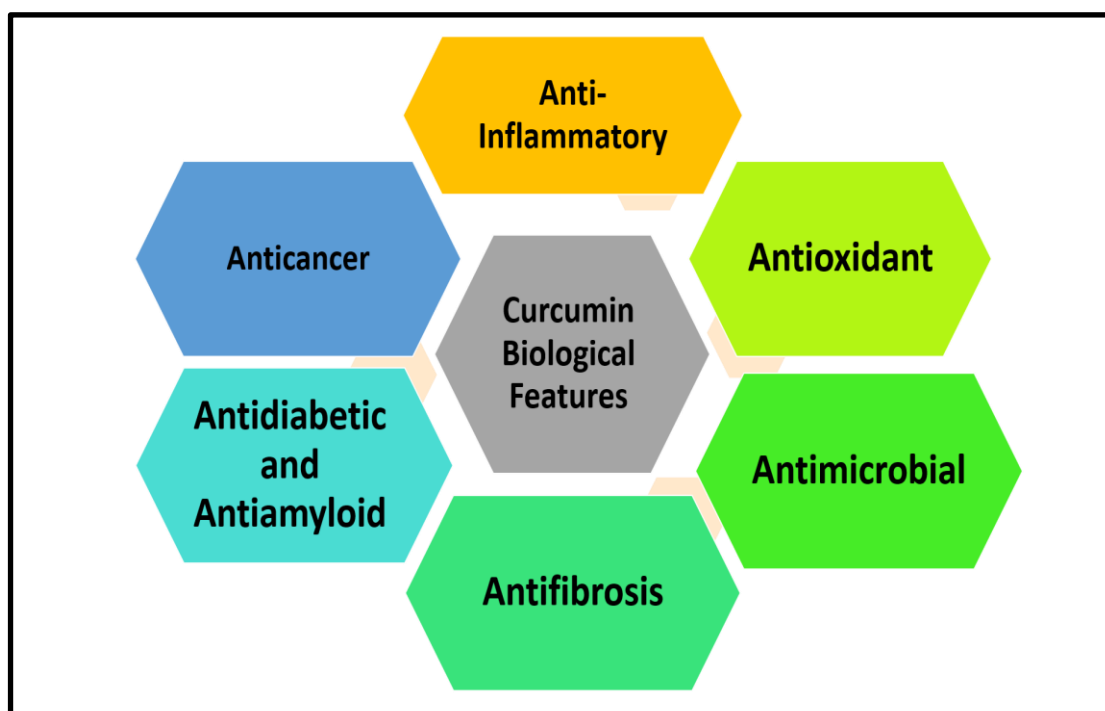


Figure (1-4): Different functional and biological features of curcumin or nanocurcumin [54].

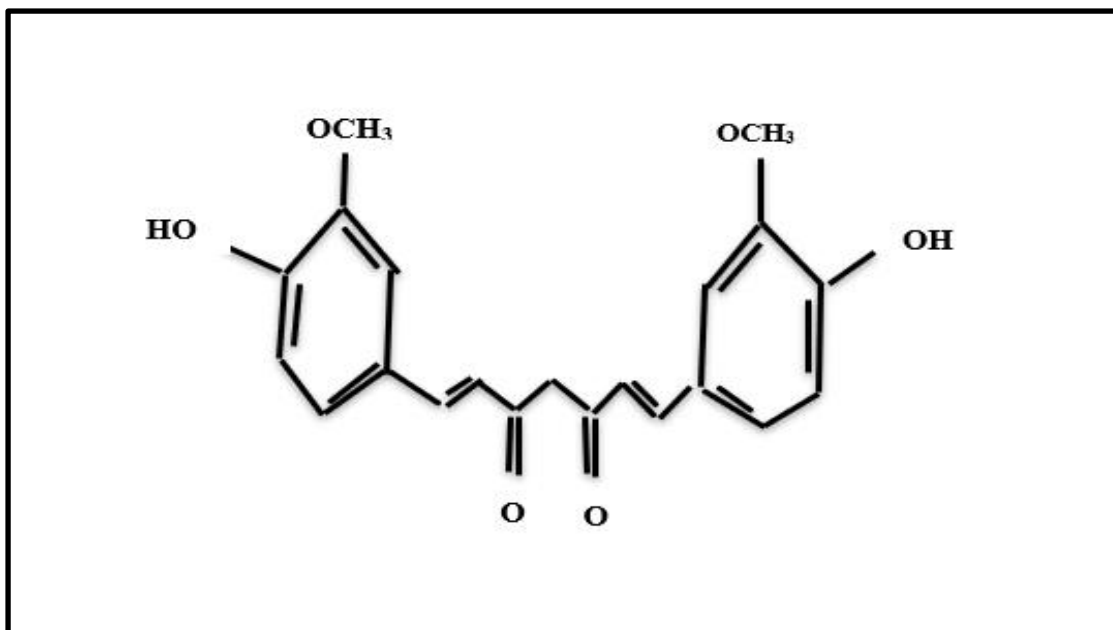


Figure (1-5): Chemical structure of nano curcumin [54].

1-4 Literature Survey

Bhirde et al. (2010) studied the distribution and clearance of polyethylene glycol (PEG)-ylated single-walled carbon nanotube (SWCNTs) as drug delivery vehicles for the anticancer drug cisplatin in mice. In this study PEG-SWCNTs were efficiently dispersed in aqueous media compared with controls, and did not induce apoptosis in vitro. Hematoxylin and eosin staining, and Raman bands for SWCNTs in tissues from several vital organs from mice injected intravenously with nanotube bioconjugates revealed that control SWCNTs were lodged in lung tissue as large aggregates compared with the PEG-SWCNTs, which showed little or no accumulation. Characteristic SWCNT Raman bands in feces revealed the presence of biliary or renal excretion routes. Attachment of cisplatin on bioconjugates was visualized with Z-contrast scanning transmission electron microscopy. PEG-SWCNT–cisplatin with the attached targeting ligand EGF successfully inhibited growth of head and neck tumor xenografts in mice [55].

Hadidi et al. (2011) studied optimization of single-walled carbon nanotube solubility by noncovalent PEGylation using experimental design methods. In this study, noncovalent functionalization of single walled carbon nanotubes (SWCNTs) with phospholipid-polyethylene glycols (PI-PEGs) was performed to improve the solubility of SWCNTs in aqueous solution. Two kinds of PEG derivatives, ie, PI-PEG 2000 and PI-PEG 5000, were used for the PEGylation process. An experimental design technique (D-optimal design and second-order polynomial equations) was applied to investigate the effect of variables on PEGylation and the solubility of SWCNTs. The type of PEG derivative was selected as a qualitative parameter, and the PEG/SWCNT weight ratio and sonication time were applied as quantitative variables for the experimental design. Optimization was performed for two responses, aqueous solubility and loading efficiency. The grafting of PEG to the carbon nanostructure was determined by thermogravimetric analysis, Raman spectroscopy, and scanning electron microscopy. Aqueous solubility and loading efficiency were determined by ultraviolet-visible spectrophotometry and measurement of free amine groups, respectively. Results showed that PI-PEGs were grafted onto SWCNTs. Aqueous solubility of (0.84 mg/mL) and loading efficiency of nearly (98%) were achieved for the prepared PI-PEG 5000-SWCNT conjugates. Evaluation of functionalized SWCNTs showed that our noncovalent functionalization protocol could considerably increase aqueous solubility, which is an essential criterion in the design of a carbon nanotube-based drug delivery system and its biodistribution [56].

Bhattacharya et al. (2012) studied antibacterial activities of polyethylene glycol, tween 80 and sodium sodecyl sulphate coated silver nanoparticles in normal and multi-drug resistant bacteria. In this study antibacterial activity of silver nanoparticles coated with different

functionalizing agents i.e., polyethylene glycol, tween 80 and sodium dodecyl sulphate were evaluated on both normal and multi-drug resistant strains of bacteria. Under the same reaction conditions, these functionalizing agents were added separately to coat silver nanoparticles. Among these, poly- ethylene glycol coated nanoparticles were most effective in killing all the bacterial strains which includes *Escherichia coli* DH5_, *Bacillus subtilis*, *Micrococcus luteus*, *Staphylococcus aureus* and multi-drug resistant clinical isolates of *Shigella* spp. (*flexneri*, *boydii*, *sohnea*) and *Vibrio cholerae*. The minimum inhibitory concentration of polyethylene glycol coated silver nanoparticles was also less compared to the other two sets of nanoparticles. Consistence with that polyethylene glycol coated nanoparticles produced more intracellular reactive oxygen species in bacteria. Moreover, when human cell lines MCF7 and chang liver were incubated in presence of these nanoparticles for (18 h) with same concentrations as used for bacteria, no toxicity was observed. But significant increase in cell killing was observed with longer incubation time. Thus, our present investigation implicates the potential therapeutic use of silver nanoparticles as antibacterial agent particularly the polyethylene glycol coated one [57].

Hadidi et al. (2012) studied evaluation of the effect of PEGylated single-walled carbon nanotubes on viability and proliferation of jurkat Cells. In this study, They were linked the PEGylation of single-walled CNTs (SWCNTs) with phospholipid-PEG (PI-PEG) conjugates to prepare water-dispersible nanostructures, the present study was designed to evaluate whether the functionalization with PI-PEG derivatives could alter the cytotoxic response of cells in culture, affect their viability and proliferation. In-vitro cytotoxicity screens were performed on cultured Jurkat cells. The SWCNTs samples used in this exposure were pristine

SWCNTs, PI-PEG 2000/5000-SWCNTs at various concentrations. Jurkat cells were first incubated for (3 h) at (37° C) with test materials and seeded in 6-well culture plates at a given concentration. The plates were then incubated for (24, 48 and 72 h) at (37° C) in a 5% CO₂ humidified incubator. Cell viability and proliferation assay were performed using trypan blue exclusion test and the cell cycle kinetic status of jurkat cells was analyzed by flow cytometry. Cell morphology was finally studied using double staining technique and a fluorescence microscope. There found that, regardless of the duration of exposure, functionalized SWCNTs were substantially less toxic, compared to pure SWCNTs and that the molecular weight of PI-PEGs played an important role at higher concentrations. In conclusion, our noncovalent protocol seemed to be effective for increasing SWCNTs biocompatibility [58].

Khandare et al. (2012) studied PEG-conjugated highly dispersive multifunctional magnetic multi-walled carbon nanotubes for cellular imaging. Theirs report synthesis of a highly versatile multicomponent nanosystem by covalently decorating the surface of multiwalled carbon nanotubes (CNTs) by magnetite nanoparticles (Fe₃O₄), poly (ethylene glycol) (PEG), and fluorophore fluorescein isothiocyanate (FITC). The resulting Fe₃O₄-PEG-FITC-CNT nanosystem demonstrates high dispersion ability in an aqueous medium, magnetic responsiveness, and fluorescent capacity. Transmission electron microscopy images revealed that Fe₃O₄ nanoparticles were well anchored onto the surfaces of the CNT. In vitro time kinetic experiments using confocal microscopy demonstrated a higher uptake of the Fe₃O₄-PEG-FITC-CNT nanosystem localized at the perinuclear region of MCF7 cells compared to the free FITC. In addition, the CNT nanosystem demonstrated no evidence of toxicity on cell growth. Surface conjugation of multicomponents, combined with in vitro non-

toxicity, enhanced cellular uptake for FITC and site-specific targeting ability makes this fluorescent Fe_3O_4 -PEG-FITC-CNT nanosystem an ideal candidate for bioimaging, both in vitro and in vivo [59].

Hadidi et al. (2013) studied PEGylated single-walled carbon nanotubes as nanocarriers for cyclosporin a delivery. In this study great attempts have been made in the development of SWCNTs as advanced nanomaterials for biomedical applications. Studies performed in our laboratories and other investigations have indicated that SWCNTs could be considered as promising nano vectors for the delivery of a variety of therapeutic agents, following their surface modification to increase their water dispersibility, render them biologically compatible, decrease their toxicity, and increase their ability to cross the cell membranes. First planned to PEGylate SWCNTs with PI-PEG5000 through hydrophobic interaction between CNT sidewalls and the hydrocarbon chain of the phospholipid component of a PI-PEG moiety in order to obtain non-covalent functionalized PI-PEG5000-SWCNTs. Then, following the cytotoxicity studies, our observations confirmed that the noncovalent PEGylation protocol proposed in this project could improve the SWCNTs' biocompatibility significantly. The present study was planned to use PEGylated SWCNTs for the delivery of CsA. Although lacking in certain aspects, the results obtained by our research until now clearly showed the potential of PEGylated SWCNT-based systems for drug delivery [60].

Son et al. (2013) studied effect of nanocurcumin particles prepared by top-down method on CCl_4 - induced hepatic fibrosis mice. In this study nanocurcumin particles were prepared by top-down method as it can improve hydrophilic and increase bioavailability. As a result, curcumin concentration was yielded up to (10%) (w/w), and the particle size was defined less than (1,000 nm) in diameter. The particles were characterized

by scanning electron microscope (SEM), transmission electron microscope (TEM), dynamic laser light scattering (DLS), and X-ray diffraction (XRD). The acute oral toxicity was done with a dose up to (500 mg) per kg of body weight and no dead mice were found indicating the nanocurcumin particles are safe for long-term use. The model of hepatic fibrosis mice was induced by intraperitoneal (i.p) injection of 0.8 mL of carbon tetrachloride (CCl₄) in olive oil (1:3 v/v) per kg of body weight. Nanocurcumin particles (15 mg/kg of body weight) were orally administered to hepatic fibrosis mouse model in 4 weeks to evaluate the therapeutic potential in comparison to other groups. The results indicate that nanocurcumin have significant effects on reducing levels of serum alanine aminotransferase (ALT) and aspartate aminotransferase (AST) in CCl₄-induced hepatic fibrosis mice. Histological examination shows that hepatic fibrotic livers of mice treated with nanocurcumin particles were recovered after 4 weeks [61].

Ravelli et al. (2013) studied PEGylated carbon nanotubes: preparation, properties and applications. This review focuses on the different approaches available to PEGylate CNTs, either covalently or non-covalently, as well as on the most common techniques adopted to characterize the resulting materials. Finally, the applications of PEGylated CNTs to different fields (mainly drug delivery) are briefly reported [62].

Tan et al. (2014) studied a review on characterizations and biocompatibility of functionalized carbon nanotubes in drug delivery design. This review focuses on recent advances in drug delivery design based on f-CNTs with an emphasis on the determination of various parameters involved and characterization methods used in order to achieve higher therapeutic efficacy of targeted drug delivery. In particular, theirs will highlight a variety of different analytical techniques which can be used

to characterize the elemental composition, chemical structure, and functional groups introduced onto the CNTs after surface modification. They also review the current progress of available *in vitro* biocompatibility assays based on f-CNTs and then discuss their toxicological profile and biodistribution for advanced drug delivery [63].

Annaraj et al. (2014) studies on the enhanced biological applications of PVA loaded nanocurcumin. Curcumin has been shown to be a powerful suppressor of chronic inflammation mediated disease processes. PVA loaded curcumin is highly potent, nontoxic. The antimicrobial properties as demonstrated in both Gram positive and Gram-negative bacteria and anti-cancer properties were studied on gastric cancer cell lines (AGS). Transmission electron microscopy confirms an even size distribution of PVA loaded curcumin nanoparticles in the range of 50 nm. PVA loaded curcumin freely soluble in water unlike bulk curcumin. Its activity against gastric cancer cells also has been investigated [64].

Markovic et al. (2015) studied facile synthesis of water-soluble curcumin nanocrystals. Solvent exchange method was applied to synthesize curcumin nanocrystals. Different techniques were used to characterize the structural and photophysical properties of the curcumin nanocrystals. It was found that the nanocurcumin prepared by this method had good chemical and physical stability, could be stored in the powder form at room temperature, and was freely dispersible in water. It was established that the size of curcumin nanocrystals varied in the range of (20–500 nm). Fourier transform infrared spectroscopy and UV–Vis analyses showed the presence of tetrahydrofuran inside the curcumin nanocrystals. Furthermore, it was found that the nanocurcumin emitted photoluminescence with a yellow–green color [65].

Dizaj et al. (2015) studied antimicrobial activity of carbon-based nanoparticles. In this study carbon-based nanomaterials such as fullerenes, carbon nanotubes (CNTs) (especially single-walled carbon nanotubes (SWCNTs)) and graphene oxide (GO) nanoparticles show potent antimicrobial properties. In present review, there have briefly summarized the antimicrobial activity of carbon-based nanoparticles together with their mechanism of action. Reviewed literature show that the size of carbon nanoparticles plays an important role in the inactivation of the microorganisms. As major mechanism, direct contact of microorganisms with carbon nanostructures seriously affects their cellular membrane integrity, metabolic processes and morphology. The antimicrobial activity of carbon-based nanostructures may interestingly be investigated in the near future owing to their high surface/volume ratio, large inner volume and other unique chemical and physical properties. In addition, application of functionalized carbon nanomaterials as carriers for the ordinary antibiotics possibly will decrease the associated resistance, enhance their bioavailability and provide their targeted delivery [66].

Anbarasu et al. (2015) studied synthesis and characterization of polyethylene glycol (PEG) coated Fe₃O₄ nanoparticles by chemical co-precipitation method for biomedical applications, with polyethylene glycol (PEG) as a stabilizer and dispersant. The X-ray diffraction and selected area electron diffraction (SAED) results show that the cubic inverse spinel structure of pure phase polycrystalline Fe₃O₄ was obtained. The scanning electron microscopy (SEM) and field emission transmission electron microscopy (FE-TEM) results exhibited that the resulted Fe₃O₄ nanoparticles were roughly spherical in shape with narrow size distribution and homogenous shape. Fourier transform infrared spectroscopy (FT-IR) results suggested that PEG indicated with Fe₃O₄ via its carbonyl groups.

Results of vibrating sample magnetometer (VSM) indicated that the prepared Fe₃O₄ nanoparticles exhibit superparamagnetic behavior and high saturation magnetization at room temperature. Such Fe₃O₄ nanoparticles with favorable size and tunable magnetic properties are promising biomedical applications [67].

Malhotra et al. (2016) studied nanomaterials-based biosensors for cancer biomarker detection. In this study discussed the prospects of CP based biosensors for cancer biomarker detection. Compared to the conventional electrode used for detection of CEA, CP based electrochemical biosensors are flexible, cost effective, light weight and can be easily disposed. The studies suggest doped with MWCNT and graphene results in enhanced sensitivity, lower detection limit and wider linear detection range and have a great potential for early cancer detection. This nanomaterial modified paper-based platform should be used in the development of medical diagnostics kits, flexible electronics and energy storages devices [68].

Farvadi et al. (2017) studied polyionic complex of single-walled carbon nanotubes and PEG-grafted-hyperbranched polyethyleneimine (PEG-PEI-SWNT) for an improved doxorubicin loading and delivery: development and in vitro characterization. In this study a new approach was developed to modify and stabilize SWNTs efficiently without necessity of any catalyst such as EDC, which results in SWNT aggregation or harsh conditions such as long-time exposure to high temperature or ultrasonication, which may destroy homing biomolecule ligands attached to nanotubes. Additionally, there obtained an ultra-high loading capacity (900%) significantly superior to other drug carriers, including dendrimers, liposomes, and micelles and even to those previously reported for SWNTs

(120% (Zhang et al. 2009) and (400%) (Ali-Boucetta et al. 2008, Liu et al 2010). Moreover, the release profile was improved and more sustained in comparison with PEG-modified SWNTs that showed more burst release. Taking into consideration, the above-mentioned properties of the modified SWNT, and the pH dependency of drug loading and release profile due to protonation and deprotonation of doxorubicin, suggest SWNTs as a successful delivery system that should be studied in vivo [69].

Sun and Li (2017) studied aqueous dispersion of single walled carbon nanotubes stabilized by PEG modified diperylene bisimide and their application as an antibacterial agent. In this study polyethylene glycol modified diperylene bisimide (PEG-diPBI) was synthesized and applied to disperse single-walled carbon nanotubes (SWCNTs) in water. The aqueous dispersion efficiency of PEG-diPBI on SWCNTs is investigated by UV-vis, Raman spectroscopy, and transmission electron microscopy. It is found that the enhanced dispersing capability of PEG-diPBI can be attributed to the diperylene aromatic core, which can strongly interact with SWCNT via synergistic p-p and hydrophobic interactions. The dispersing solution properties are closely related to the hydrophilic part of PEG-diPBI. Moreover, the well-dispersed SWCNTs show excellent antibacterial activities [70].

Assali et al. (2017) studied single-walled carbon nanotubes ciprofloxacin nanoantibiotic: strategy to improve ciprofloxacin antibacterial activity. This study describe the covalent functionalization of the single-walled carbon nanotubes (SWCNTs) with multiple molecules of ciprofloxacin. The prepared nano antibiotics were characterized using different techniques, including transmission electron microscopy, Raman spectroscopy, and thermogravimetric analysis. The characterization of the

nano antibiotics confirmed the successful covalent functionalization of the SWCNTs with (55%) of functionalization as has been observed by thermogravimetric analysis. The release profile revealed that (90%) of the loaded ciprofloxacin was released within (2.5 h) at pH 7.4 showing a first-order release profile with $R^2=0.99$. Interestingly, the results of the antibacterial activity indicated that the functionalized SWCNTs have significant increase in the antibacterial activity against the three strains of bacteria – by 16-fold for staphylococcus aureus and pseudomonas aeruginosa and by 8-fold for escherichia coli – in comparison to the ciprofloxacin free drug. Moreover, the synthesized nano antibiotic showed high hemocompatibility and cytocompatibility over a wide concentration range [71].

Oskoueian et al. (2018) studied fabrication, characterization, and functionalization of single-walled carbon nanotube conjugated with tamoxifen and its anticancer potential against human breast cancer cells, aimed to fabricate SWCNT conjugated with tamoxifen and evaluated its anticancer potential against human breast cancer cells (MCF-7). The results showed that SWCNT was synthesized successfully using chemical vapor deposition (CVD) method. The results of Raman spectroscopy, SEM, and TEM analyses confirmed the synthesis of highly pure SWCNT. The functionalization of SWCNT was performed by oxidizing of SWCNT, attachment of polyethylene glycol (PEG) to oxidized SWCNT, and attachment of azelaic acid to the polyethylene glycol group. As a result, the SWCNT with free functional carboxylic acid and hydroxyl groups (SWCNT-PEG) was developed. The SWCNT-PEG was then conjugated with tamoxifen (SWCNT-PEG-TAM). The FT-IR together with NMR results confirmed the conjugation of tamoxifen to functionalized SWCNT (SWCNT-PEG-TAM). The cytotoxic concentrations (CC50) of SWCNT-

PEG, tamoxifen, and SWCNT-PEG-TAM were >100 , 12.67 ± 2.69 , and 5.49 ± 1.34 mg/ml, respectively. Linking tamoxifen to functionalized SWCNT enhanced the cytotoxic action of tamoxifen against breast cancer cells up to 2.3 times. The results of the morphological examination and caspase-3 activity confirmed the higher cytotoxic action of SWCNT-PEG-TAM as compared to free tamoxifen. The results obtained in this study indicated that this delivery system enhanced the therapeutic effects and anticancer potential of tamoxifen against human breast cancer cells [72].

Siresha et al. (2018). A review on carbon nanotubes in biosensor devices and their applications in medicine, their found CNTs consist of versatile features that combine the potential to serve for diagnostic and therapeutic applications. While they may serve as biosensors of cancer biomarkers, they can be loaded with anticancer drugs and used as therapeutic platforms in oncology. Although, CNTs-based biosensors are promising it still has many practical concerns in applications. For example, for the fabrication of biosensors usually needs specific size and helicity, but it is very hard to control size of CNTs while manufacturing. It is also very difficult to make cost-effective and high purity in mass production of CNTs, that is the reason why the current market prices of CNTs is too high for any realistic commercial applications. In CNT-based biosensors, enzyme always needs to immobilize onto surface of CNTs. However, immobilization may damage their biological activity, biocompatibility and structure stability and need to perform their cytotoxicity. As it stated that, the structural stabilization and surface characteristics of CNTs are need to be standardized for the cytotoxicity determination. The continuous CNT fibers avoid the leaching of CNT, implantable electrodes for in vivo testing. All the above-mentioned issues must be evaluated by a scientific and systematic methods. It is clear that much further advancement needed to be

addressed before CNTs technology can be applied in carcinogenic treatments [73].

Sharmeen et al. (2018) studied polyethylene glycol functionalized carbon nanotubes/gelatin-chitosan nanocomposite: an approach for significant drug release. This research work blooms the new idea of developing a safe and controlled drug releasing matrix using multi-walled carbon nanotubes (MWCNTs). In aqueous solution, uniform and highly stable dispersion of MWCNTs was obtained after secondary functionalization with polyethylene glycol (PEG) which was studied by Fourier transmission infrared spectroscopy (FTIR) and thermogravimetric analysis (TGA). Solution casting method was used to prepare MWCNTs/gelatin chitosan nanocomposite films and the effect of MWCNTs on physico-mechanical, thermal and water uptake properties of the nanocomposites were evaluated. Incorporation of MWCNTs into the porous gelatin-chitosan matrix showed interesting stiffness and dampness along with developed microfibrillar structures within the pore walls intended at being used in tissue engineering of bone or cartilage. A common antibiotic drug, ciprofloxacin was incorporated into nanocomposite matrix. The evaluation of the effect of MWCNTs on drug release rate by dissolution test and antimicrobial susceptibility test was performed. Sharp release of the drug was found at early stages (~1 h), but the rate was reduced afterwards, showing a sustained release. It was observed that for all microorganisms, the antibacterial activities of drug loaded MWCNTs/gelatin-chitosan nanocomposites were higher than that of drug loaded gelatin-chitosan composite films containing no MWCNTs. Comparative statistical studies by ANOVA techniques also showed remarkable difference between the antibacterial activities, exhibited by MWCNTs-incorporated and non-incorporated composite films [74].

Shiping et al. (2018) studied antitumor effects of carbon nanotube-drug complex against human breast cancer cells. In this study has been improved the bio-solubility and sustained-release properties of a carbon nanotube (CNT)-drug complex, the present study used a hydrophilic polymer, polyethylene glycol (PEG), and β -estradiol (E2), which targets the estrogen receptor in human breast cancer cells (HBCCs), to modify CNTs carrying lobaplatin (LBP) to form E2-PEG-CNT-LBP. The in vitro inhibitory effects against HBCCs and the in vivo pharmacological effect of the complex on heart, liver and kidney tissues were also evaluated. The results indicated that the inhibitory effects of this complex against HBCCs reached (80.44%) within (72 h). A blood biochemical test of normal mice indicated that this complex reduced platelet counts, while aspartate aminotransferase levels were increased compared with those in the control group. Histopathological analysis revealed no obvious adverse effects on the heart, liver and kidneys. The in vivo results indicated that the novel E2-PEG-CNT-LBP complex had no obvious toxic effects while exhibiting sustained-release properties. The clearance of E2-PEG-CNT-LBP by non-specific uptake systems was delayed and its clearance was increased compared with LBP alone [75].

Joly and Latha (2019) studied synthesis of nanocurcumin alginate conjugate and Its characterization by XRD, IR, UV VIS and Raman spectroscopy. In this study the effect of stabilization of both free curcumin and nano curcumin–alginate conjugate in honey was studied by UV–Vis absorption, IR, vibrational spectroscopy (Raman) and XRD. Curcumin is degraded in acid and alkaline medium is highly stable with the nano formulation. From this work it was deduced that in presence of surfactant honey curcumin-alginate inhibits the formation of small sub-products. This work reveals the complexation of curcumin with alginate in presence of surfactant honey was demonstrated to protect this molecule from the

degradation. UV–Vis, FTIR, XRD and Raman spectroscopy were important to determine the nature of the structural modifications [76].

Charmi et al. (2019) studied Polyethylene glycol (PEG) decorated graphene oxide nanosheets for controlled release curcumin delivery. In this study, firstly GO synthesized by the improved Hummers chemical method and then polyethylene glycol polymer was conjugated to it by using EDC/NHS catalyst. Finally, curcumin (Cur) as anti-cancer drug has been loaded onto the PEGylated graphene oxide (GO-PEG). Next, curcumin loaded onto PEGylated graphene oxide (GO-PEG-Cur) were evaluated by using ultraviolet, Fourier transform infrared spectroscopy, differential scanning calorimeter, atomic microscopic force and dynamic light scattering. The amount of loaded drug was calculated about (4.5%) with the help of the standard curcumin curve and UV/Vis spectrometer [77].

Roy et al. (2019) studied synergistic effect of polydopamine polyethyleneimine copolymer coating on graphene oxide for EVA nanocomposites and high-performance triboelectric nanogenerators. This article reports a novel modification of graphene oxide (GO) encapsulated by the copolymer of polydopamine (PD) and polyethylenimine (PEI) *via* a michael addition reaction, aiming to create robust ethylene vinyl acetate copolymer (EVA) nanocomposites even at very low amounts of filler loading by overcoming the above hindrances. It has been found that the addition of only (1.2 wt%) modified GO (*i.e.*, PD–PEI–rGO) increased the tensile strength, Young's modulus and storage modulus of EVA composites by (80%), (50%) and (24%), respectively. These increments surpass many recent claims on relevant composites. Excellent molecular level dispersion was also observed from the fracture surface SEM images. Being amine-rich with high electron-donating capability and mechanically robust, the

nanocomposite served as an outstanding tribopositive material, thereby generating (7.49 V) and (4.06 μ A) output voltage and current, respectively, when employed in a triboelectric nanogenerator (TENG). The high electrical outputs led the device to light up 43 blue LEDs instantaneously upon hand pressing, demonstrating that the nanocomposite is indeed a promising candidate for harvesting green energy. Moreover, the nanogenerator displayed outstanding cyclic performance stability (even after 8000 cycles) and environmental durability [78].

Wang et al. (2020) studied functionalized folate-modified graphene Oxide/PEI siRNA nanocomplexes for targeted ovarian cancer gene therapy. In this study, we synthesized a novel gene vector PEG-GO-PEI-FA by functionalized graphene oxide (GO), in which folic acid (FA) can specifically bind to the folate receptor (FR), which is overexpressed in ovarian cancer. Characterizations of the nanocomplexes were evaluated by dynamic light scattering (DLS), atomic force microscopy (AFM), and fourier transform infrared spectroscopy (FTIR). The siRNA condensation ability and stability were assessed by agarose gel electrophoresis. Cellular uptake efficiency and lysosomal escape ability in ovarian cancer cells were investigated by confocal laser scanning microscopy. Furthermore, cellular biosafety of the system and inhibitory of the siRNA tolerability were evaluated by CCK-8 assay. The size of the PEG-GO-PEI-FA nanocomplexes was 216.1 ± 2.457 nm, exhibiting mild cytotoxicity in ovarian cancer cells. With high uptake efficiency, PEG-GO-PEI-FA can escape from the lysosome rapidly and release the gene. Moreover, PEG-GO-PEI-FA/siRNA can effectively inhibit the growth of ovarian cancer cells. By and large, the PEG-GO-PEI-FA/siRNA may offer a promising strategy for siRNA delivery in the treatment of FR-positive ovarian carcinoma or similar tumors [79].

Yang et al. (2020) studied PEG/PEI-functionalized single-walled carbon nanotubes as delivery carriers for doxorubicin: synthesis characterization, and in vitro evaluation. In this study, raw SWCNTs were purified with different oxidizing acids, and the resulting shortened CNTs were conjugated with poly (ethylene glycol) (PEG) and polyethylenimine (PEI). The different nanocarriers, that is, CNTs-COOH (CNTs), CNTs-PEG and CNTs-PEG PEI, were systematically characterized and evaluated in terms of drug loading, in vitro release, cytotoxicity towards MCF-7 cells and cellular uptake. The results showed that all CNT carriers had a high drug loading capacity. In comparison with CNTs-COOH and CNTs PEG, CNTs-PEG-PEI showed a more rapid drug release under acidic conditions and a higher antitumor activity. Furthermore, fluorescence detection and flow cytometry (FCM) analysis results indicated that the internalization into cells of CNTs-PEG-PEI was significantly enhanced, thus inducing tumor cell death through apoptosis more efficiently. The above series of benefits of CNTs PEG-PEI may be attributed to their good dispersibility and comparably higher affinity to tumor cells due to the difunctionalization. In summary, the PEG- and PEI-conjugated CNTs may be used as novel nanocarriers and the findings will contribute to the rational design of multifunctional delivery vehicles for anticancer drugs [80].

Hanna and Saad (2020) studied nanocurcumin: preparation, characterization and cytotoxic effects towards human laryngeal cancer cells. The aim of the present study was to prepare curcumin nanoparticles (nanocurcumin) by a sol-oil method to improve curcumin absorption and bioavailability, and to investigate the therapeutic effects of the prepared nanoparticles on the inhibition mechanisms towards human Hep-2 cancer cells. The nanoparticles were characterized by fourier transform infrared spectroscopy, transmission electron microscopy, X-ray diffraction, and

zeta potential analysis. The prepared curcumin nanoparticles possessed a narrow particle size distribution with an average diameter of (28 nm). The inhibition effects on the growth of human Hep-2 cells were investigated using neutral red uptake and lactate dehydrogenase assays. The results indicated that the nanocurcumin has a selective effect in inhibiting Hep-2 cell growth in a dose- and time-dependent mode with the most effective IC₅₀ value (17-^{+0.31} mg ml⁻¹) obtained after (48 h) of incubation without any cytotoxic effects on normal cells. This IC₅₀ value of nanocurcumin revealed a significant increase of early and late apoptotic cells with an intense comet nucleus of Hep-2 cells as a marker of DNA damage. Flow cytometry analysis of the progression of apoptosis in nanocurcumin Hep-2 treated cells showed that arresting in the cell cycle in the G₂/M phase with increasing apoptotic cells in the sub-G₁ phase. At the same time, real-time PCR analysis indicated that the treatment of Hep-2 cells with nanocurcumin resulted in upregulation of P53, Bax, and Caspase-3, whereas there was downregulation of Bcl-XL. These findings gave insights into understanding that the inhibition mechanisms of nanocurcumin on the proliferation of Hep-2 cancer cells was through the G₂/M cell cycle arrest and the induction of apoptosis was dependent on Caspase-3 and p53 activation. However, in vivo studies with an animal model are essential to validate these results [81].

Jihad et al. (2021) studied polyethylene glycol functionalized graphene oxide nanoparticles loaded with nigella sativa extract: a smart antibacterial therapeutic drug delivery system. In this study flaky graphene oxide (GO) nanoparticles (NPs) were synthesized using hummer's method and then capped with polyethylene glycol (PEG) by an esterification reaction, then loaded with nigella sativa (*N. sativa*) seed extract. Aiming to investigate their potential use as a smart drug delivery system against staphylococcus aureus and escherichia coli, the spectral and structural characteristics of

GO-PEG NPs were comprehensively analyzed by XRD, AFM, TEM, FTIR, and UV-Vis. XRD patterns revealed that GO-PEG had different crystalline structures and defects, as well as a higher interlayer spacing. AFM results showed GONPs with the main grain size of (24.41 nm), while GONPs-PEG revealed graphene oxide aggregation with the main grain size of (287.04 nm) after loading *N. sativa* seed extract, which was verified by TEM examination. A strong OH bond appeared in FTIR spectra. Furthermore, UV-Vis absorbance peaks at (275, 284, 324, and 327 nm) seemed to be correlated with GONPs, GO-PEG, *N. sativa* seed extract, and GO-PEG-*N. sativa* extract. The drug delivery system was observed to destroy the bacteria by permeating the bacterial nucleic acid and cytoplasmic membrane, resulting in the loss of cell wall integrity, nucleic acid damage, and increased cell-wall permeability [82].

Lakshmanan et al. (2021) studied nanocurcumin-loaded UCNPs for cancer theranostics: physicochemical properties, in vitro toxicity, and in vivo imaging studies. In this study Formulation of promising anticancer herbal drug curcumin as a nanoscale-sized curcumin (nanocurcumin) improved its delivery to cells and organisms both in vitro and in vivo. We report on coupling nanocurcumin with upconversion nanoparticles (UCNPs) using poly (lactic-co-glycolic Acid) (PLGA) to endow visualisation in the near-infrared transparency window. Nanocurcumin was prepared by solvent-antisolvent method. NaYF₄: Yb, Er (UCNP1) and NaYF₄: Yb, Tm (UCNP2) nanoparticles were synthesised by reverse microemulsion method and then functionalized it with PLGA to form UCNP-PLGA nanocarrier followed up by loading with the solvent-antisolvent process synthesized herbal nanocurcumin. The UCNP samples were extensively characterised with XRD, Raman, FTIR, DSC, TGA, UV-VIS-NIR spectrophotometer, upconversion spectrofluorometer, HRSEM,

EDAX and zeta potential analyses. UCNP1-PLGA-nanocurcumin exhibited emission at (520, 540, 660 nm) and UCNP2-PLGA-nanocurcumin showed emission at (480 and 800 nm) spectral bands. UCNP-PLGA-nanocurcumin incubated with rat glioblastoma cells demonstrated moderate cytotoxicity, (60–80%) cell viability at (0.12–0.02 mg/mL) marginally suitable for therapeutic applications. The cytotoxicity of UCNPs evaluated in tumour spheroids models confirmed UCNP-PLGA-nanocurcumin therapeutic potential. As-synthesised curcumin-loaded nanocomplexes were administered in tumour bearing laboratory animals (Lewis lung cancer model) and showed adequate contrast to enable in vivo and ex vivo study of UCNP-PLGA-nanocurcumin bio distribution in organs, with dominant distribution in the liver and lungs. Our studies demonstrate promise of nanocurcumin-loaded upconversion nanoparticles for theranostics applications [83].

1-5 Aims of the Study

The aim of the study included four parts as below:

Part 1: Functionalization of SWCNTs by PEG and study its bio applications on bacteria inhibition and anticancer activity.

Part 2: Functionalization of SWCNTs with PEG and PEI mixture and comparing its bio applications on anticancer activity with the results of part 1.

Part 3: Study of the effect of loading the nano curcumin on PEG-PEI-SWCNTs and study its anticancer activity compared with part1 and part 2.

Part 4: The samples in the all parts of this study were characterized by following analysis: UV-vis spectroscopy (UV-VIS), Fourier transform Infra-Red analysis (FTIR), Raman spectroscopy (RS), X-ray diffraction (XRD), Atomic force microscopy (AFM), and Transmission electron microscopy (TEM).

Chapter Two
Theoretical Part

2-1 Introduction

This chapter includes a general description of the theoretical part of this study, physical concepts, scientific clarifications, relationships, and laws used to interpret the study results.

2-2 Optical Properties

2-2-1 UV-VIS Spectroscopy

Many molecules absorb ultraviolet or visible light. The absorbance of a solution increases as attenuation of the beam increases. Absorbance is directly proportional to the path length (b), and the concentration (c) of the absorbing species. Beer's law states that [84]:

$$A = \epsilon bc \dots \dots \dots (2-1)$$

where ϵ is a constant of proportionality, called the absorptivity.

Different molecules absorb radiation of different wavelengths. An absorption spectrum will show a number of absorption bands corresponding to structural groups within the molecule. For example, the absorption that is observed in the UV region for the carbonyl group in acetone is of the same wavelength as the absorption from the carbonyl group in diethyl ketone [84].

2-2-2 Electronic Transitions

The absorption of UV or visible radiation corresponds to the excitation of outer electrons. There are three types of electronic transitions which can be considered:

1. Transitions involving π , σ and n electrons
2. Transitions involving charge-transfer electrons
3. Transitions involving d and f electrons (not covered in this Unit)

When an atom or molecule absorbs energy, electrons are promoted from their ground state to an excited state. In a molecule, the atoms can rotate and vibrate with respect to each other. These vibrations and rotations also have discrete energy levels, which can be considered as being packed on top of each electronic level, it shown in figure (2-1) [84].

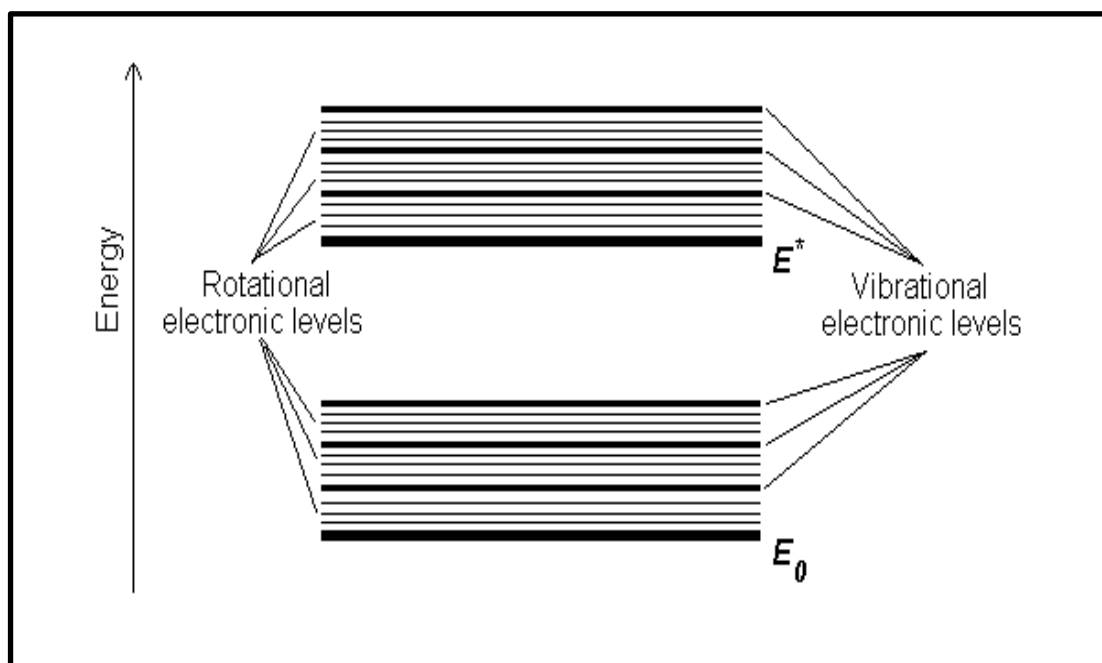


Figure (2-1): Rotational and vibrational electronic levels [84].

2-2-3 Absorbing Species Containing π , σ , and n Electrons

Absorption of ultraviolet and visible radiation in organic molecules is restricted to certain functional groups (chromophores) that contain valence electrons of low excitation energy. The spectrum of a molecule containing these chromophores is complex. This is because the superposition of rotational and vibrational transitions on the electronic transitions gives a

combination of overlapping lines. This appears as a continuous absorption band [84]. Possible electronic transitions of π , σ , and n electrons are shown in figure (2-2).

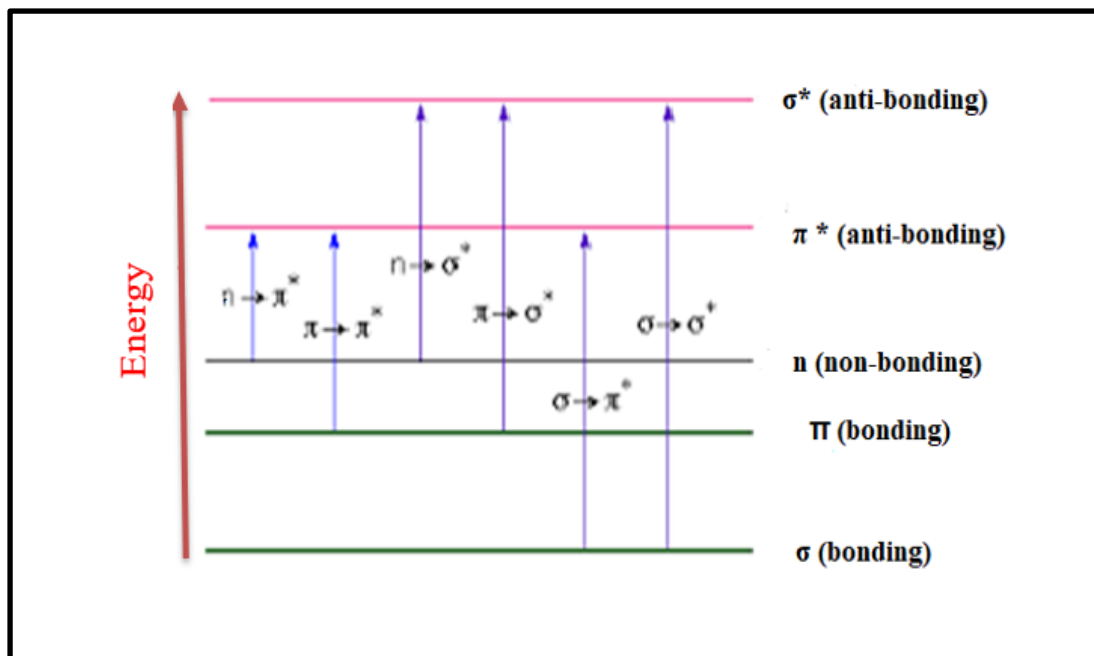


Figure (2-2): Electronic transitions [84].

A- $\sigma \rightarrow \sigma^*$ Transitions

An electron in a bonding s orbital is excited to the corresponding antibonding orbital. The energy required is large. For example, methane (which has only C-H bonds, and can only undergo ($\sigma \rightarrow \sigma^*$) transitions) shows an absorbance maximum at (125 nm). Absorption maxima due to ($\sigma \rightarrow \sigma^*$) transitions are not seen in typical UV-Vis. Spectra (200 - 700 nm) [84].

B- $n \rightarrow \sigma^*$ Transitions

Saturated compounds containing atoms with lone pairs (non-bonding electrons) are capable of ($n \rightarrow \sigma^*$) transitions. These transitions usually

need less energy than ($\sigma \rightarrow \sigma^*$) transitions. They can be initiated by light whose wavelength is in the range (150 - 250 nm). The number of organic functional groups with ($n \rightarrow \sigma^*$) peaks in the UV region is small [84].

C- $n \rightarrow \pi^*$ and $\pi \rightarrow \pi^*$ Transitions

Most absorption spectroscopy of organic compounds is based on transitions of n or π electrons to the π^* excited state. This is because the absorption peaks for these transitions fall in an experimentally convenient region of the spectrum (200 - 700 nm). These transitions need an unsaturated group in the molecule to provide the π electrons [84].

Molar absorptivities from ($n \rightarrow \pi^*$) transitions are relatively low, and range from 10 to 100 $\text{L mol}^{-1} \text{cm}^{-1}$. ($\pi \rightarrow \pi^*$) transitions normally give molar absorptivities between (1000 and 10,000 $\text{L mol}^{-1} \text{cm}^{-1}$) [84].

The solvent in which the absorbing species is dissolved also has an effect on the spectrum of the species. Peaks resulting from ($n \rightarrow \pi^*$) transitions are shifted to shorter wavelengths (blue shift) with increasing solvent polarity. This arises from increased solvation of the lone pair, which lowers the energy of the n orbital. Often (but not always), the reverse (i.e. red shift) is seen for ($\pi \rightarrow \pi^*$) transitions. This is caused by attractive polarisation forces between the solvent and the absorber, which lower the energy levels of both the excited and unexcited states. This effect is greater for the excited state, and so the energy difference between the excited and unexcited states is slightly reduced - resulting in a small red shift. This effect also influences ($n \rightarrow \pi^*$) transitions but is overshadowed by the blue shift resulting from solvation of lone pairs [84].

2-3 Raman Spectroscopy

Figure (2-3) shows the photograph of the instrument. The innovatory progress in instrumentation had led the Raman spectroscope to be more influential investigative tool used for the evaluation and characterization of great variety of materials for many applications. Mostly this technique can comprise of the structural component investigation, crystallographic orientation, electronic devices inorganic or organic thin film and mechanical stresses without any limitations [85].

In this procedure, the line of Raman spectral are attained through a sample illumination with a potent infrared laser source or a source of visible monochromatic light. Moreover, a hybrid technique amongst the microscopy and Raman spectroscopy is termed as a Raman microscopy. Hence, this technique is utilized to keep the Raman maps record while utilizing a process of point mapping just to signify the spatial dispersion of various chemical components [85].

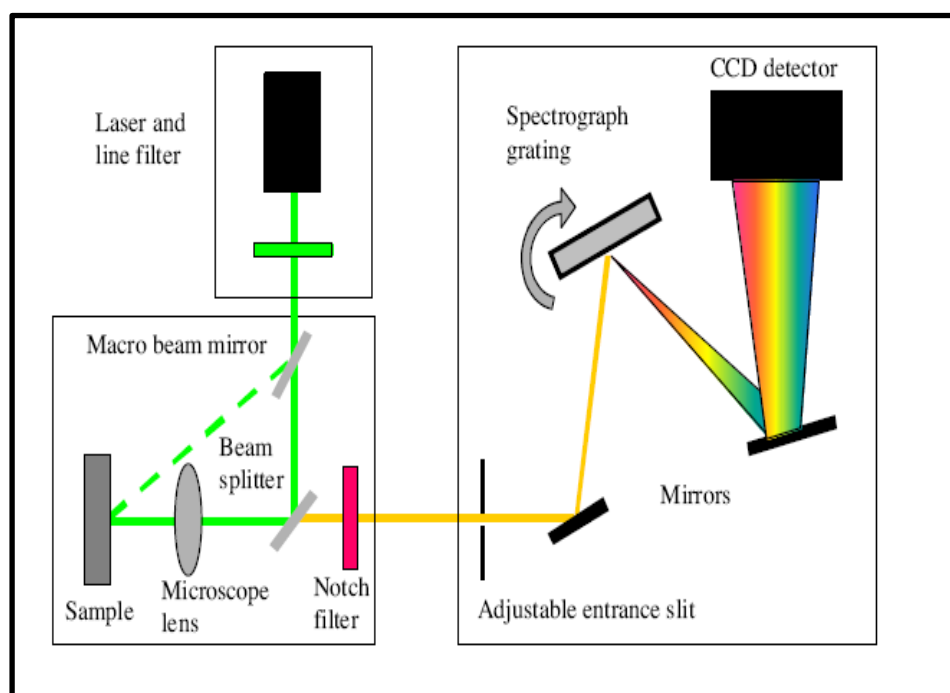


Figure (2-3): The Raman spectrophotometer [85].

2-3-A Basic Principles and Instrumentation

The encroachment of monochromatic light on a molecule occurs which lead to the inelastic and elastic scatterings that are being presented as significant scattering procedures. The occurrence of inelastic scattering is due to the alteration in photon energy while elastic scattering happens because no variation in photon energy. Therefore, three categories of the scattering phenomenon can be exhibited in figure (2-4).

First: having an identical frequency and wavelength of the scattered light as that of the incident photon turns the procedure to be elastic in nature as the loss of energy is insignificant termed this phenomenon as a Rayleigh scattering method. A minor section of the elastically scattered photons happens because shift the frequency. Therefore, the incident photon frequency through the quantity of vibrational energy gained or lost by a molecule is acknowledged as a Raman scattering.

Second: the attainment of the vibrational energy from incident photons for molecules terms the scattering as a Stokes Raman Scattering. This represents the scattered photon's energy would be less than the incident photons energy.

Third: losing a molecules' vibrational energy to the incident photon terms the scattering as anti-Stokes Raman scattering, in which the scattered photon's energy would be greater than that of the incident photons. The higher incidence probability, Stokes Raman Scattering is utmost frequently utilized in molecular vibrational studies than that of the anti-Stokes Raman scattering [86].

Raman spectroscopy produces the related to the defects, tube alignment and purity. This further contributes distinctive occurrence of MWCNTs

compared to the other allotropes of carbon. This procedure has been amazingly effective to describe the SWCNTs' structural properties [87].

The Raman spectrum of CNTs can be categorized into three distinguishable features: the high energy mode (HEM), D mode and radial breathing mode (RBM). Each of these features demonstrates different properties of SWCNTs, with two dominant features appear in every Raman spectra of CNT samples [88]. Presently, the indication in figures (2-4) and (2-5) assists in evaluating the approximate key annotations for each concerned region to the CNT Raman spectra.

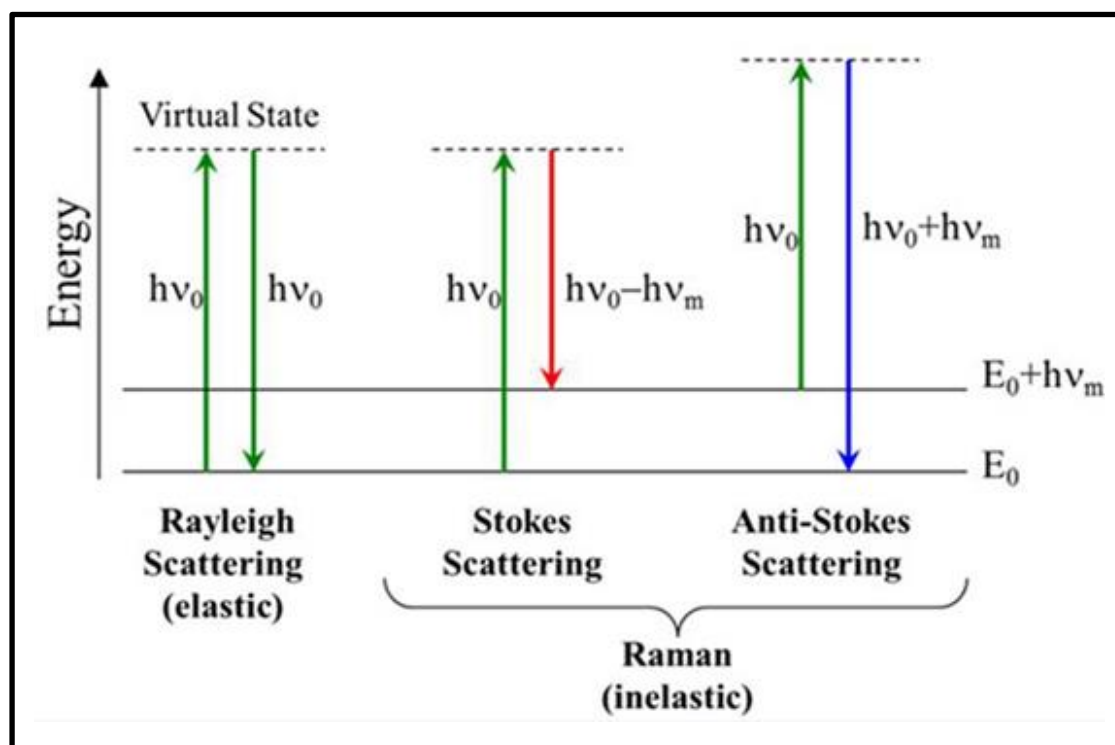


Figure (2-4): The diagram showing the type of transition of the electrons and the Rayleigh and Raman scattering [89].

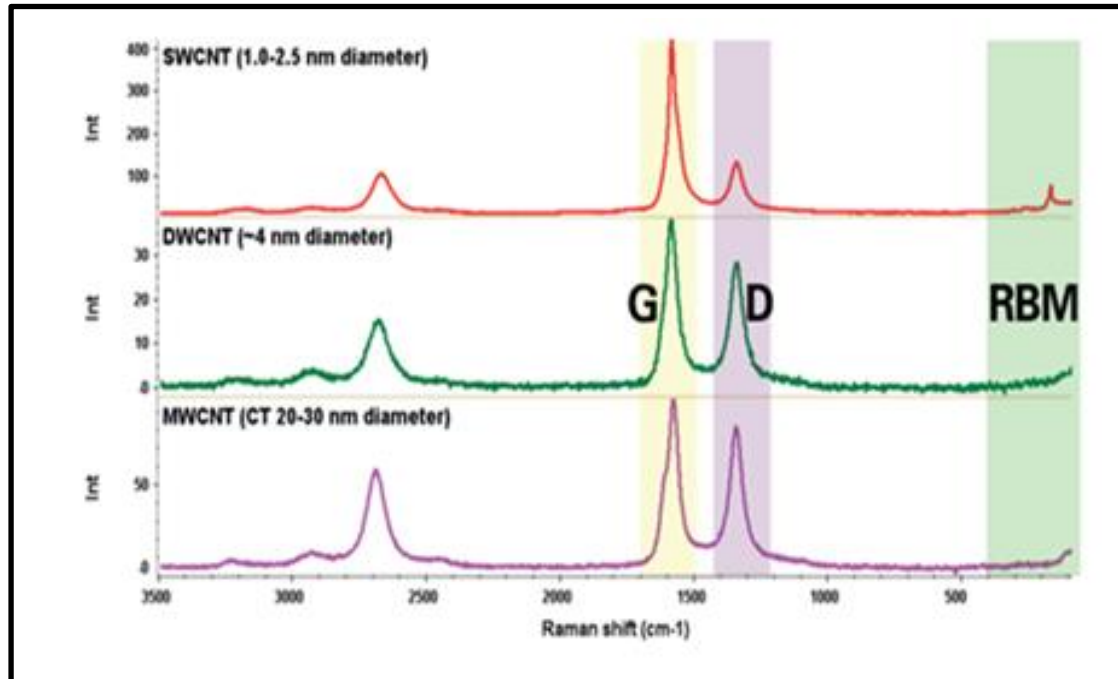


Figure (2-5): Raman Spectrum of SWCNT, DWCNT and MWCNT samples [90].

2-3-B Radial Breathing Mode (RBM)

The mode of radial breathing is normally observed in a range of (100-300 cm^{-1}), these bands signify shows difference between SWCNTs and other forms of carbon since these components are not observed in any other sp^2 bonded carbon material. The in-phase symmetric dispositions of entire carbon atoms nearby the tube, which provides some indication of the diameters in the sample, and also identifies whether the tubes are multi or single-walled. In MWNTs, the RBM band can be seen if the inner tube diameters are very small (less than 5nm usually). Moreover, the RBM band's frequency (ω_{RBM}) relies upon the tube's diameter which can be articulated by [91]:

$$\omega_{\text{RBM}} = \frac{A}{d} + B \dots \dots \dots (2 - 2)$$

where, d represents the tube's diameter, A is a proportionality constant, and B is a damping variable caused by the environment around the tube. Which mostly zero for tube, B is expected to be zero [92,93]. Whereas, the outer curvature sheet of MWCNT is adjacent to the graphene while, inner sheets being identical to SW-carbon Nanotubes. Conversely, the innermost shell's diameter considerably relies on the procedure's sensitivity which has been utilized for the development [94].

2-3-C The G-band

The double peak structure, referred to earlier, is associated with the G-band, tangential vibrational modes of the CNTs, which is associated with the Raman graphite spectra. The G band in CNT's is due to the curvature of the graphene sheet and is split into two peaks: G^- peak and G^+ peak. The G^- peak has a lower frequency which is more visible in semiconducting tubes, as in metallic tube samples it also has a lower intensity and is much broader, making it less visible. The G^+ peak is higher frequency and has no significant difference in frequency or width between metallic and semiconducting tubes [91-93]. In samples of MWNTs where a large portion are metallic, the G-band is visible as a single peak. The D-band is found at frequencies between (1250 and 1450 cm^{-1}), while its overtone appears at approximately double the frequency ranging between (2500 and 2900 cm^{-1}).

2-3-D The D-band

D-band is generally termed as defect band due to the D band's intensity which is relative to the tube's number of defects. The D bands' estimated intensity and width can be utilized for determining the graphitic material's fraction existing in the sample material [91-93]. A common quality idea

of grown nanotubes can be attained measuring the D & G bands' ratios. The D band's intensity can be used to oversee damage being inflicted on the sample from various processes used in its purification, such as tip sonication or centrifugation. Gohil and Ghosh observed the MWCNT Raman spectra placed over an active substrate of SERS (surface enhanced Raman scattering) and verified the tangential mode's (G-band) multiple splitting occurrence. Likewise, the splitting of D band induced by a disorder into distinctive features which are absent at room temperature otherwise [94]. Moreover, the D-band splitting ($\sim 1350 \text{ cm}^{-1}$) observations designated the double resonance conditions fulfilled for the MWCNTs which had been deposited on the active substrates of SERS at lower temperatures.

To utilize the Raman spectroscopy for purity assessment by distinctive methodologies depend on the G-band peak and D-band peak's intensity ratio. Moreover, the D band represents a double resonance peak induced by a defect happens because of the elastic scattering through defect and inelastic scattering via a phonon. Henceforth, the unorganized samples should demonstrate a higher intensity for D band integrated intensity ratio to the G band (I_D/I_G) which is an upright indicator for the quality of sample [95-99].

2-4 X-Ray Diffraction

XRD is an important experimental technique that has long been used to address all issues related to the crystal structure of solids, including lattice constants and geometry, identification of unknown materials, the orientation. In XRD, a collimated beam of X-rays with a wavelength typically ranging from 0.7 to 2 Å is incident on a specimen and diffracted by the crystalline phases in the specimen. According to Bragg's law:

$$n\lambda = 2d\sin\theta \dots \dots \dots (2 - 3)$$

where n is a positive integer (0, 1, 2, ...) called the order of reflection, d is the spacing between atomic planes in the crystalline phase and λ is the X-ray wavelength. The intensity of the diffracted X-rays is measured as a function of the diffraction angle 2θ and the specimen's orientation.

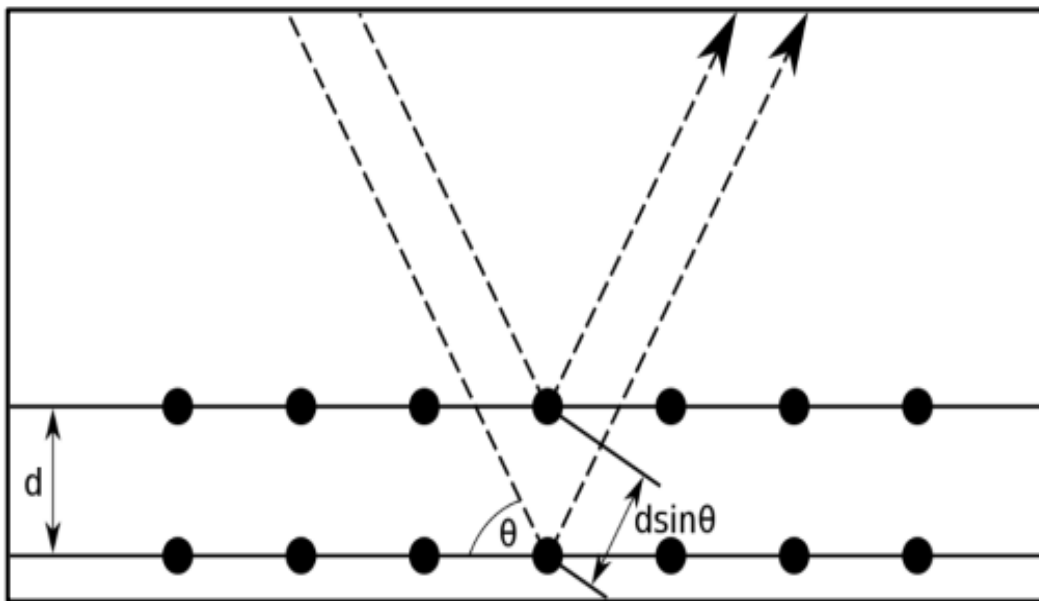


Figure (2-6): Bragg's diffraction. Two beams with identical wavelength and phase approach a crystalline solid and are scattered of two different atoms within it.

This diffraction pattern is used to identify the specimen's crystalline phases and to measure the characteristic of the structure. Diffraction peak positions are accurately measured with XRD, which makes it the best method for characterizing homogeneous and inhomogeneous strains. X-ray diffraction is a powerful technique for determining the crystal structure of crystalline materials. XRD gives information about the composition, crystalline phase, orientation, and lattice parameters of samples. The crystallite size can be estimated using Debye Scherrer's formula [100]:

$$\text{Crystallite size}(D) = \frac{0.9\lambda}{\beta \cos\theta} \dots \dots \dots (2 - 4)$$

Where D is the crystal size, $\lambda = 1.5406 \text{ \AA}$ is the wavelength of X-ray, β is the full width half maximum (FWHM) of the peak in radians, and θ is the Bragg angle.

2-5 Bacterial Strains

They constitute a large domain of prokaryotic microorganisms. Typically, a few micrometers in length, bacteria strains have a number of shapes, ranging from spheres to rods and spirals. Bacteria strains were among the first life forms to appear on Earth, and are present in most of its habitats. Bacteria strains inhabit soil, water, acidic hot springs, radioactive waste [101], and the deep portions of Earth's crust. Bacteria strains also live in symbiotic and parasitic relationships with plants and animals. Most bacteria strains have not been characterized, and only about half of the bacterial strain's phyla have species that can be grown in the laboratory. The study of bacteria strains is known as bacteriology, a branch of microbiology. There are typically 40 million bacterial cells in a gram of soil and a million bacterial cells in a milliliter of fresh water [101].

2-6 Antibacterial Activity of Nanoparticles

Nanobiotechnology is an expression assembles biotechnology and nanotechnology. Nanobiotechnology means building tiny instruments have changed natural structure atom by atom and utilizing it for different biomedical applications [102]. Antibacterial materials can be classified to two kinds: organic and inorganic agents. Organic antibacterial one has been utilized as bactericides for quite a while. However, their antibacterial characteristics will decrease because of high temperatures manufacturing

methodology, in addition to its toxicity the human body. Hence, the interest in inorganic antibacterial one is rising due to their thermal stability, safety and good activity against the microorganisms [103]. Growing of resistance microbes against antibiotics can lead to dangerous health issues. These issues induce researchers to develop new antimicrobial agents, which can successfully inhibit the growth of these microbes. Over the previous years, different nanosized antibacterial agents for example metal oxide nanoparticles had been successfully used. Several kinds of metal oxide nanoparticles, for example, titanium dioxide (TiO₂), zinc oxide (ZnO), calcium oxide (CaO), magnesium oxide (MgO), and copper oxide (CuO) had been recorded to have antimicrobial action. Carbon-based nanoparticles also show powerful antimicrobial action. Size and high surface area of carbon-based nanomaterials are effective factors influencing the antibacterial action. Expanding surface area of nanoparticles by lowering their size results in enhancing NPs interaction within bacteria. Antibacterial action of NPs relies upon modification of their surface, composition, their intrinsic properties, and the kind of microorganisms. Before biomedical use of the carbon-based nanostructures, some vital issues associated with their toxicity should be illustrated [104].

2-7 Structure of the Bacterial Cell Walls

Most of bacteria have a wall surrounding its cell that keeps up cell shape and saves it from the lysis. There are two general kinds of bacterial walls, which first distinguished by Hans Christian Gram relying upon their different retention ability of crystal-violet dye; they are Gram's negative or Gram's positive [105]. Figure (2-7) demonstrates the difference between the two bacterial strains wall types.

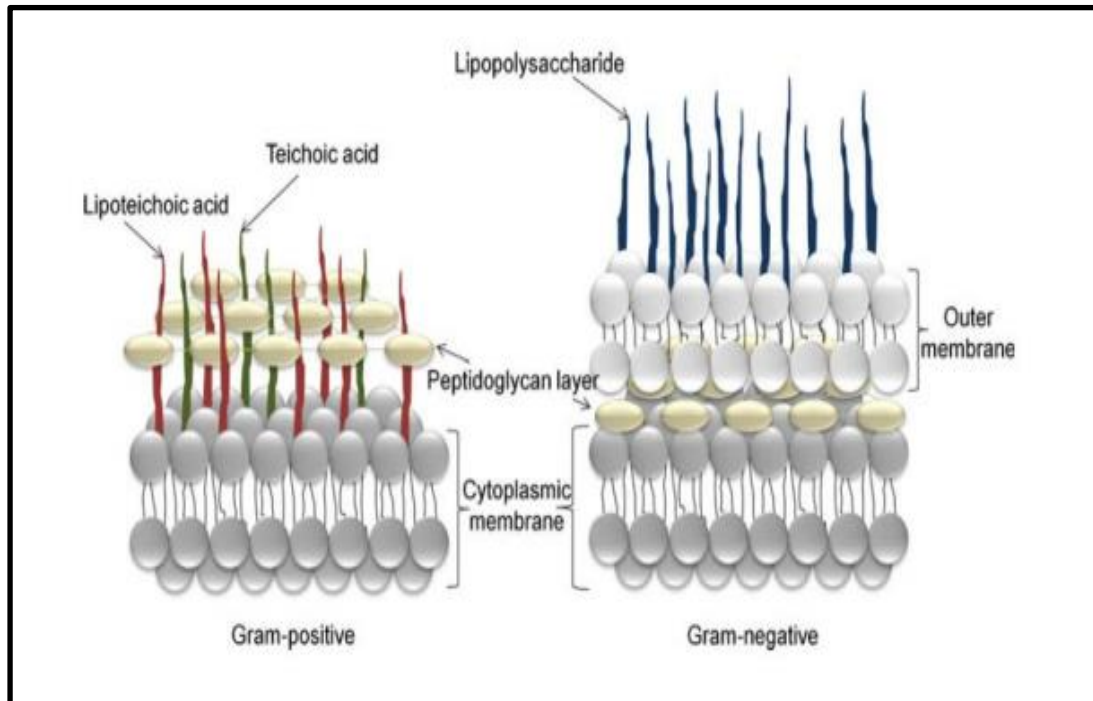


Figure (2-7): Structural distinguishes between Gram's positive and the Gram's negative bacterial cell wall [106].

The basic distinction depends on the peptidoglycan arrangement, which is the key part in the structure of membrane. Wall of Gram's negative bacteria displays a very thin layer of peptidoglycan (around 2–3 nm) between the cytoplasmic layer and the outer cell wall. The peptidoglycan and outer membrane are linked with each other by lipoproteins [107]. While Gram's positive bacteria wall shows a thick layer (around 20–50 nm) of peptidoglycan which is linked to teichoic acids that are unique in Gram's positive bacteria wall [108]. Gram's negative wall have additional outer layer composes of lipopolysaccharides (LPS). This layer is toxic and can be the reason for making gram's negative more dangerous than Gram's positive.

2-8 Bacterial Types

2-8-1 *Pseudomonas aeruginosa* (*P. aeruginosa*)

Pseudomonas aeruginosa is a Gram-negative, rod-shaped, sporogenous, and monoflagellated bacterium. It has a pearlescent appearance and grape like or tortilla-like odor as shown in figure (2-7) [109]. *P. aeruginosa* grows well at (25°C) to (37°C), and its ability to grow at (42°C) helps distinguish it from many other pseudomonas species. *P. aeruginosa* is a ubiquitous microorganism that can survive under a variety of environmental conditions. It not only causes disease in plants and animals but also in humans, causing serious infections in immunocompromised patients with cancer and patients suffering from severe burns and cystic fibrosis [110].

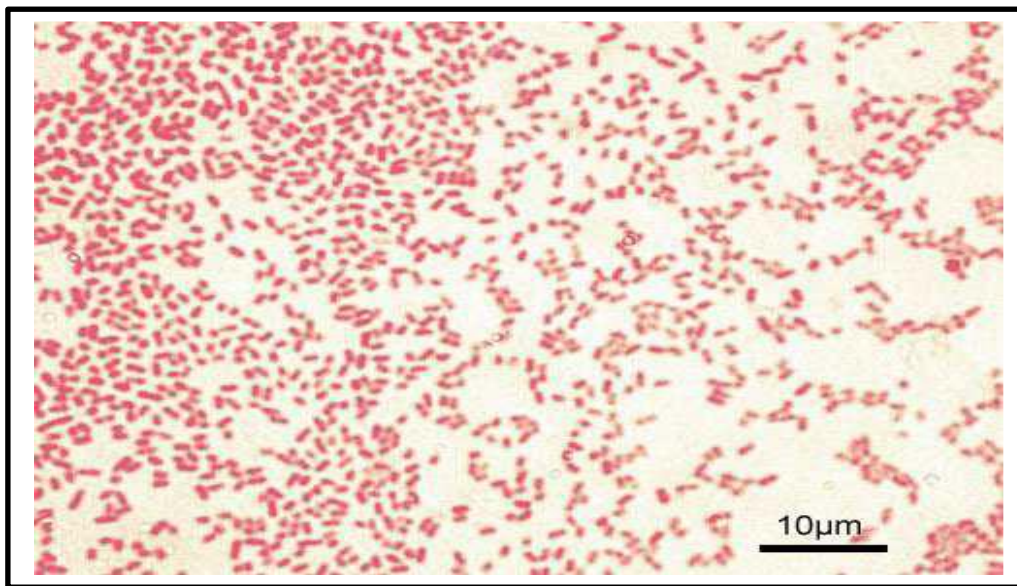


Figure (2-8): The Image for *P.aerruinos*a bacteria [110].

2-8-2 *Bacillus* SPP.

Bacillus species are rod-shaped, endospore-forming aerobic or facultatively anaerobic, Gram-positive bacteria; in some species cultures may turn Gram-negative with age. The many species of the genus exhibit a wide range of physiologic abilities that allow them to live in every natural environment. Only one endospore is formed per cell. The spores are

resistant to heat, cold, radiation, desiccation, and disinfectants. *Bacillus anthracis* needs oxygen to sporulate; this constraint has important consequences for epidemiology and control [111]. In vivo, *B. anthracis* produces a polypeptide (polyglutamic acid) capsule that protects it from phagocytosis. The genera *Bacillus* and *Clostridium* constitute the family Bacillaceae. Species are identified by using morphologic and biochemical criteria [112]. Figure (2-9) shows the image of *Bacillus Spp.* bacteria.

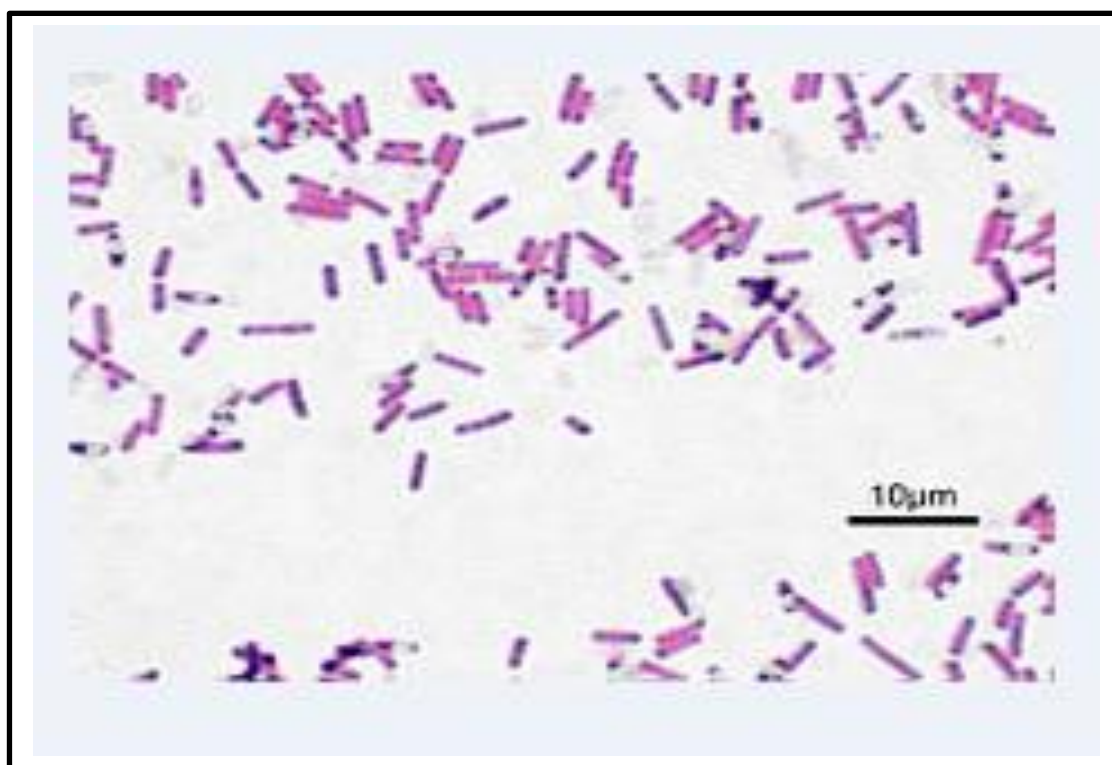


Figure (2-9): The image for *Bacillus Spp.* bacteria [112].

2-9 Interactions between Bacteria and Nanoparticles

The antibacterial agents can be either bactericidal, that kills the bacteria, or bacteriostatic, that slows down the growth of bacteria. Consequently, because of the reality, these bacteria promoted resistance against numerous normal antibacterial agents, the infection diseases keep on being one of the greatest challenges of the health around the world. Disadvantages for traditional antibacterial agents are not just the improvement of various

resistances to drug, but additionally have some side effect. This has developed other different systems to treat bacterial infections. Among these systems, nano-scale system that are have promoted as novel antimicrobial agents [108]. The size of bacterial cell normally in the range of micron and have membranes that contain pores in the range of nanometer. Therefore, the synthesized nanomaterials should be in size range less than the size of membranes pores of bacteria and thus they can cross the bacteria membrane with no impediment [113]. The mechanisms of the antibacterial activity of nanoparticles against bacteria are not clearly understood. NPs may bend to bacteria membranes by electrostatic interaction and deactivate the integrity of bacterial membranes. The overall charge of bacteria surface is negative because of the excessive, which under the dissociation creates the negative charge of the cell surface. The opposite charge of nanoparticles and bacteria is the reason behind their adhesion and bioactivity according to the electrostatic forces [107]. Therefore, parameters that affect antibacterial characteristics of nanoparticles list as follows: (1) Composition of nanoparticles, (2) Size and concentration of nanoparticles, (3) The morphology of nanoparticles, (4) surface modification of nanoparticles, and (5) The types of bacterial species. [108]. It was recommended that when bacteria is treated by nanoparticles, a few changes can happen in the morphology of its membrane and result in an increase in the membrane permeability, so the bacterial cells cannot be able to control the transport through its membrane, resulting into death of the cell. In addition, it was discovered that the creation of reactive oxygen species (ROS) and formation of the oxidative stress in the biological tissues are behind the toxicity mechanism of nanoparticles, which include the damage of DNA, changes in the motility of cell, the cytotoxicity [114]. Figure (2-10) displays the nanoparticles toxicity mechanisms against bacteria. In the cells mitochondria, ROS are by products of cellular oxidative metabolism.

Besides cellular oxidative stress, there are other biological reactions, which can create ROS in tissue. Transition metals such as copper and iron can also participate in the formation of ROS. ROS overproduction may generate oxidative stress, resulting in cells failing functions and leading to cell death and geno-toxic effects. ROS generation and toxicity from the nanomaterials is subject to the nanomaterials physical and chemical characteristics as well as to the cell types. These chemicals and physical determinants of nano-sized materials include size, shape, oxidation states, surface coating, solubility, and aggregation and agglomeration degree [114].

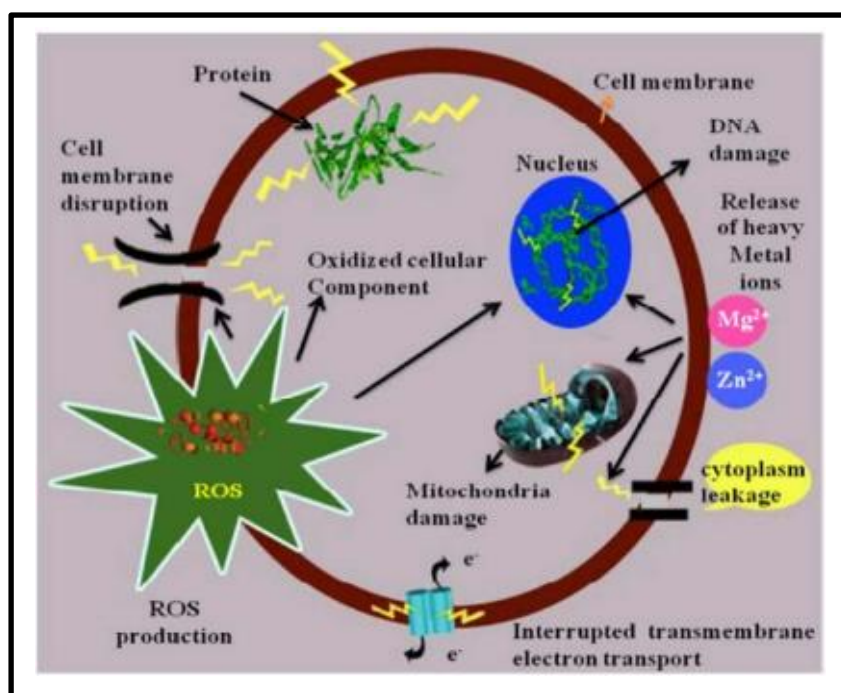


Figure (2-10): Mechanism of antibacterial activity of nanoparticles [115]

2-10 Mechanism of Antimicrobial Activity of Carbon Nanotubes

CNTs are nano-sized hollow cylindrical form of carbon which has been synthesized by Lijima in 1991[116]. Since then, CNTs have been applied in many fields of science and technology. Kang et al. (2007) provided the

first document that showed SWCNTs had strong antimicrobial activity on *Escherichia coli* (*E. coli*). They demonstrated that SWCNTs could cause severe membrane damage and subsequent cell death [117].

In other study (2008) they presented the first evidence that the size of carbon nanotubes was an important factor affecting their antibacterial activity. They prepared SWCNTs and multi-walled carbon nanotubes (MWCNTs) and investigated their antibacterial effect against *E. coli*. Their results indicated that SWCNTs were much more toxic to bacteria than MWCNTs.

The authors also reported that, direct cell contact with CNTs influenced the cellular membrane integrity, metabolism processes and morphology of *E. coli*. According to the authors, SWCNTs could penetrate into the cell wall better than MWCNTs due to their smaller nanotube diameter. Furthermore, the superior surface area of SWCNTs initiated better interaction with the cell surface [118].

Arias and Yang (2009) investigated the antimicrobial activities of SWCNTs and MWCNTs with different surface groups towards rod-shaped or round-shaped Gram-negative and Gram-positive bacteria. According to their results, SWCNTs with surface groups of -OH and -COOH indicated improved antimicrobial activity to both Gram-positive and Gram-negative bacteria while MWCNTs with the same surface groups did not exhibit any significant antimicrobial effect. Their results showed that, formation of cell-CNTs aggregates caused to damage the cell wall of bacteria and then release of their DNA content [119].

In a study by Yang et al. (2010), the effect of SWCNTs length on their antimicrobial activity was investigated. Upon their findings the longer SWCNTs indicated stronger antimicrobial activity due to their improved aggregation with bacterial cells [120].

Dong et al. (2012) investigated the antibacterial properties of SWCNTs dispersed in different surfactant solutions (sodium holate, sodium dodecyl benzenesulfonate, and sodium dodecyl sulfate) against *Salmonella enteric* (*S. enteric*), *E. coli*, and *Enterococcus faecium*. According to their results, SWCNTs exhibited antibacterial activity against both *S. enterica* and *E. coli* which was improved with the increase of nanotube concentrations. The combination of SWCNTs with surfactant solutions was also found to be low toxic to 1321N1 human astrocytoma cells, so they can be employed in biomedical applications especially for drug-resistant and multidrug-resistant microorganisms [121]. Figure (2-11) shows the schematic mechanism of antimicrobial activity of carbon nanotubes [122].

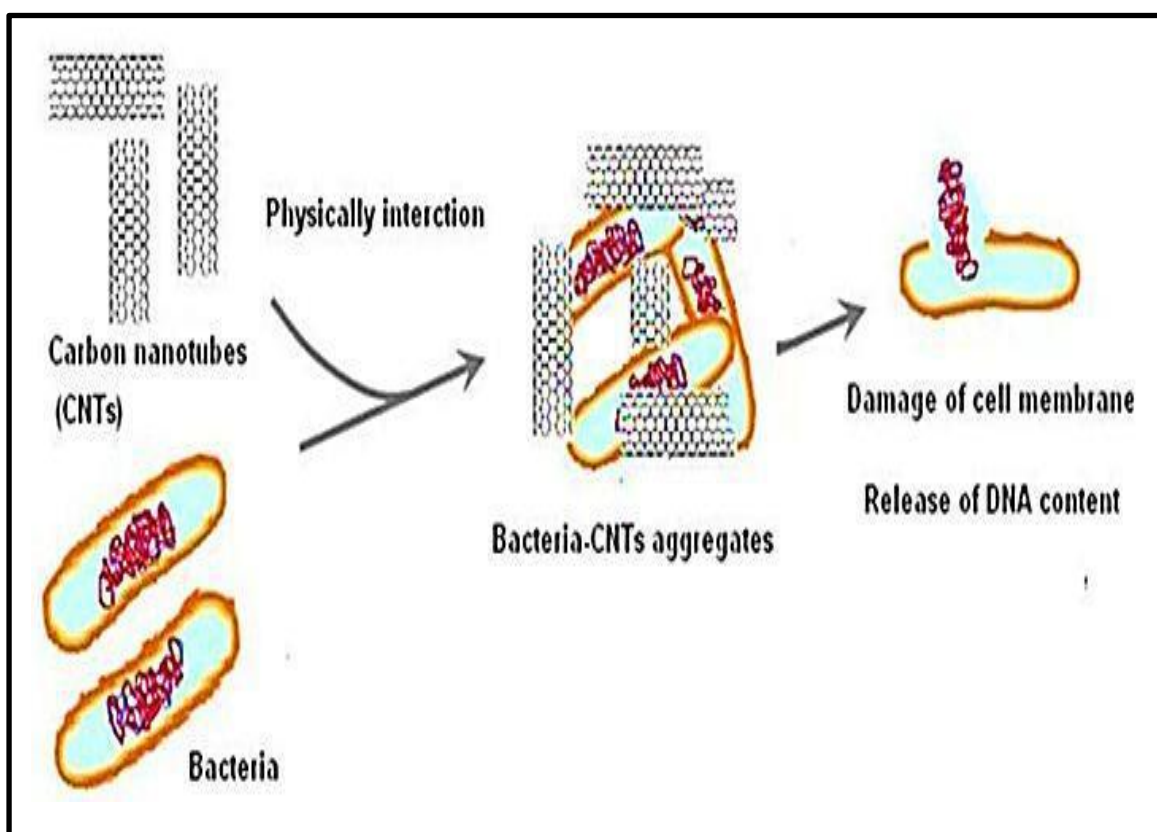


Figure (2-11): Mechanism of antimicrobial activity of carbon nanotubes [122].

Carbon nanostructures, fullerenes, SWCNTs and GO nanoparticles and their derivatives were found to be more efficient as antibacterial agents. The probable mechanisms of their antibacterial activity were proposed as follow: inhibition of bacterial growth by impairing the respiratory chain; inhibition of energy metabolism; physical interaction with cell membrane; formation of cell-CNTs/ cell-GO aggregates; induction the cell membrane disruption. In order to biological and medicinal applications, carbon nanostructures should be purified and functionalized. Their solubility should also be enhanced in physiological media. Finally, application of carbon nanocomposites composed of carbon nanostructures and metal nanoparticles could be considered as a hopeful approach for disinfection purposes [122].

2-11 Core -Shell Particles

Core-shell particles form a novel class of nanocomposite materials in which a thin layer of nanometer size is coated on another material by some specialized procedure. The core can be just a nanoparticle (few nanometers to tens of nanometers) with a nanometer thick coating or it can be a large core (few tens to hundreds of nanometer diameter) with nanometer thick coating as schematically shown in figure (2-12). The properties of core-shell particles are different from core or shell material [123].

Their properties depend usually upon core to shell ratio. These particles are synthesized for a variety of purposes like providing chemical stability to colloids, enhancing luminescent properties, engineering band structures, sensors, drug delivery etc. These materials can be of economic interest also as precious materials can be [123].

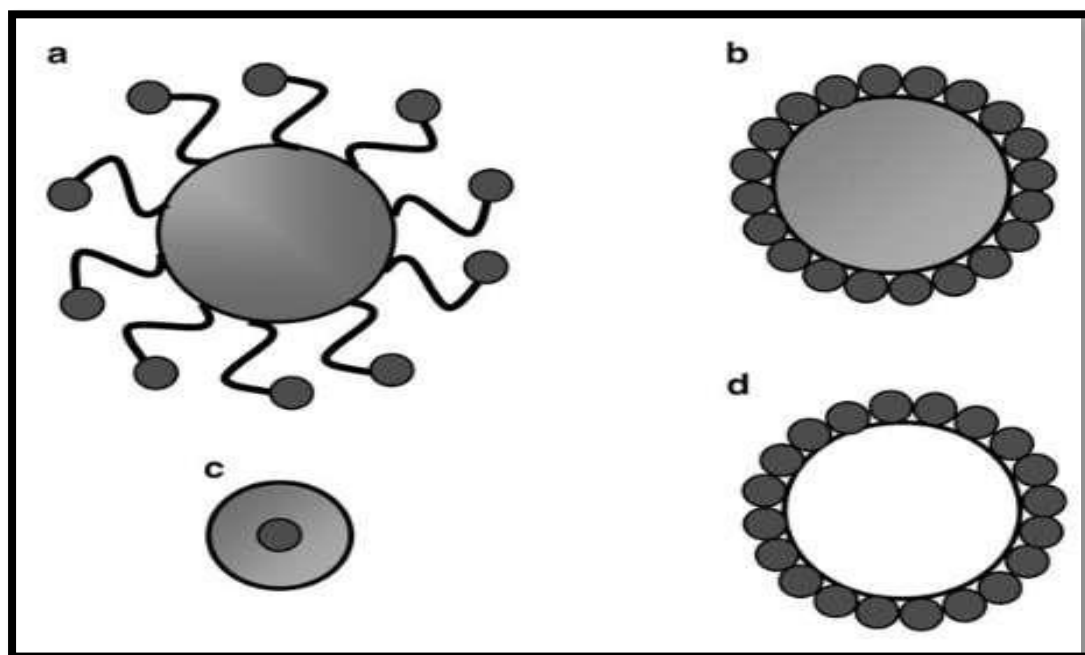


Figure (2-12): Variety of core-shell particles: (a) Surface modified core particles anchored with shell particles. (b) Smooth coating of dielectric core with shell. (c) Encapsulation of very small particles with dielectric material and (d) Quantum bubble deposited on inexpensive cores [123].

Core particles of different morphologies such as rods, wires, tubes, rings, cubes etc. also can be coated with thin shell to get desired morphology in core shell structures. Core-shell materials can be synthesized practically with all the materials, like semiconductors, metals and insulators. Dielectric materials such as silica and polystyrene are popular materials to use as core because they are soluble in water and hence can be useful in biological applications. Core-shell particles can be synthesized using variety of combinations such as dielectric-metal, dielectric-semiconductor, dielectric-dielectric, semiconductor-metal, metal-metal, semiconductor-semiconductor, semiconductor-dielectric, metal-dielectric, dydielectric, dielectric-biomolecules etc. Although core shell particles have novel properties, these can be further assembled and utilized for creation of another class of novel materials like colloidal crystal

or quantum bubbles (i.e. hollow spheres with thin shells). It is indeed possible to create novel core shell structures having multishells and tuning optical properties from visible to infrared region of the electromagnetic spectrum. Synthesis of core-shell particles requires highly controlled and sensitive synthesis protocols to ensure complete coverage of core particles with shell. There are various methods to fabricate core-shell structures which involve precipitation, polymerization, micro emulsion, reverse micelle sol-gel condensation etc. Although these methods themselves may appear to be simple, it is rather difficult to control the thickness and homogeneity of the coating. If reaction is not controlled properly, eventually it leads to aggregation of core particles, formation of separate particles of shell material or incomplete coverage.

2-12 Cancer

Cancer is defined as abnormal and uncontrolled cell growth due to an accumulation of specific genetic and epigenetic defects, which are either environmental or hereditary in origin [124]. The unregulated cell growth leads to the formation of a tumor mass that over time becomes independent of normal homeostatic checks and balances [125]. As the cancer progresses, the tumor begins to spread beyond the site of origin and metastasizes to other body organs and systems, making it incurable [124]. More than 200 distinct forms of cancer exist which include lung, prostate, breast, ovarian, hematologic, skin, and colon cancer, and leukemia etc [126]. Some cancers like stomach and cervical cancer are strongly associated with bacterial and viral infections, respectively [127].

Chemotherapy plays a vital role in treating undetectable cancer micro-foci and free cancer cells. Chemotherapy uses chemicals to kill or block the growth of cancer cells [128]. As cancer cells grow faster than healthy

ones, fast-growing cells are the main targets of chemotherapeutics; however, because there are healthy cells which are also fast-growing, the drugs used in chemotherapy also attack those fast-growing healthy cells. This unwanted attack results in the failure of conventional chemotherapy [129].

In addition, multi drug resistance (MDR) is another major obstacle to successful chemotherapy [130-133]. MDR enables the cancer cells to escape the effects of chemotherapeutics by developing resistance against the cytotoxic drugs during or shortly after the therapy. The limitations of conventional chemotherapy have led to the development of smart nanocarrier-based drug delivery systems, which are also known as Smart Drug Delivery Systems (SDDSs). SDDSs promise to apply drugs to specific and targeted sites [134]. Although, the magic bullet concept of Paul Ehrlich is the cornerstone of the relationship between drug delivery and nanoparticles, the well-controlled release of drugs using a bead polymerization technique was reported first by Speiser et al. [134,135].

Nanocarriers are the base of SDDSs. Unfortunately, not all types of nanocarriers are reliable as drugs carriers in SDDSs. To qualify as an ideal nanocarrier in SDDSs, a nanocarrier should meet some basic criteria, discussed in detail in the subsequent sections, review emphasizes the eight (8) most reported nanocarriers: (i) liposomes, (ii) micelles, (iii) dendrimers, (iv) meso-porous silica nanoparticles (MSNs), (v) gold nanoparticles (GNPs), (vi) super paramagnetic iron oxide nanoparticles (SPIONs), (vii) carbon nanotubes (CNTs), and (viii) quantum dots (QDs) in the context of their structures, classification, synthesis and degree of smartness. The schematic representation of these 8 nanocarriers is shown in figure (2-13). Choosing the right strategies to identify cancer cells follows the selection of a suitable nanocarrier type. SDDS utilizes the physiochemical differences between cancer cells and healthy cells to identify cancer sites.

To exactly identify the cancer cell site, there are two major approaches: passive targeting and active targeting. Passive targeting utilizes the Enhanced Permeability and Retention (EPR) effect to specify the cancer site indirectly. Active targeting uses overexpressed cell surface receptors of cancer cells to target cancer cells directly like a guided missile [136,137]. Releasing drugs at the specific location at a precise concentration is the subsequent step. Drugs could be released from the nanocarriers by external or internal stimuli, depending on the type of nanocarriers and their smartness [138].

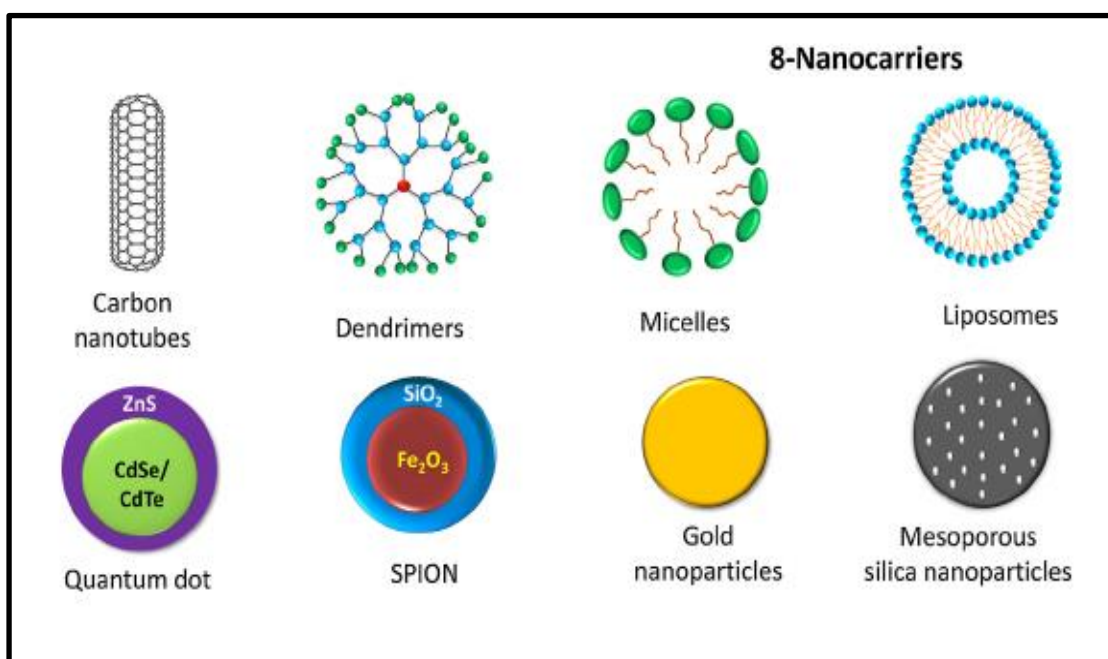


Figure (2-13): Schematic representation of the nanocarriers used in smart drug delivery systems [138].

In clinical diagnosis of cancer, detecting tumor biomarkers at the early stage enables early diagnosis of cancer and receives great deal of attentions. Among various cancer biomarker detections, quantified detection of serum biomarkers plays a critical role not only in detecting disease at the early stage, but also in tracking disease development after medical treatment.

Recently, varieties of immunoassays and immunosensors are devoted to the detection of a single cancer biomarker [139]. Although they achieved low detection limits, a majority of cancers have more than one biomarker that correlated with their incidence, and some cancer biomarkers are nonspecific to a special cancer, such as α -fetoprotein (AFP) and carcinoembryonic antigen (CEA), CEA and AFP are related to many kinds of cancer, including liver cancer, colorectal cancer, lung cancer, ovarian carcinoma, breast cancer and pancreatic cancer. Moreover, due to biological diversity of man, only one biomarker detection may generate false positive, which is unreliable [140,141]. Therefore, the detection of a single cancer biomarker is inadequate in diagnosing a special cancer. Comparing with the single biomarker test, multiplex immunoassays of cancer biomarkers can promote the screening and diagnosis of some cancer-related illness [142-144].

2-13 Mechanism of NPs action against tumor

A carcinoma is a series of diseases, make different pathology and metabolism changes in the environment of cells. It is progressing by different coding mechanisms which include cell unlimited generation, metastasis, and angiogenesis [145]. Cancer-cells possess abnormal metabolic effectiveness in mitochondrial-DNA. The chemical and physical therapies of carcinoma are limited at various stages, and they represented as a drug and radiation [146]. There are different mechanisms of NPs actions against cancer. Some mechanisms deal with specific receptors in neoplastic cells so they designing the surface of nanoparticles like folic acid [147]. Other mechanism designing NPs as antibody-mediated against some types of cancer antigen [148]. Also, some time, by targeting the angiogenesis of the cancer cells, where NPs is warp up via targeting the receptors of VEGF, which VEGF responsible of supplied a tumor by

oxygen, where nanoparticles target VEGF, consequently, a defect occurs in the oxygen supply to cancer cells. [149]. Furthermore, NPs genotoxicity is propped via the obstetrics of DNA double-stranded breakdown along with the instability of chromosomes, which controls the apoptotic execution initiations [150]. This expressible mechanism suggests that NPs could be mutually related to major many antitumor drugs which DNA-targeting figure (2-14). In an active and a passive way could NPs target cancer-cells. The passive deals with the drug accumulation around the tumor area with leaky vasculature, it has also known as the effect of EPR (the enhanced permeation and retention). While, the active way refers to certain interactive in the drug-drug carriers and target-cells, commonly via interactions of specific ligand-receptor, for the drug localization in intracellular figure (2-15) [151]. Both mechanisms of NPs acting shown an increase in drug concentration in the tumor tissues. In addition, they have been shown in different researches to be further efficient in the accumulation of drugs in cancer cells and therefore play a significant function in cancer chemotherapy and herbal medicines [152].

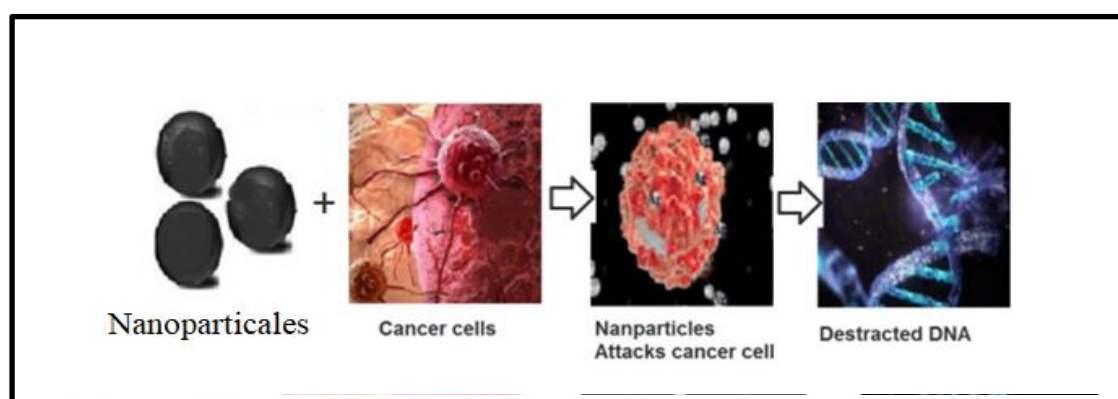


Figure (2-14): The Mechanism of action of nanoparticles against Tumor-cells [152].

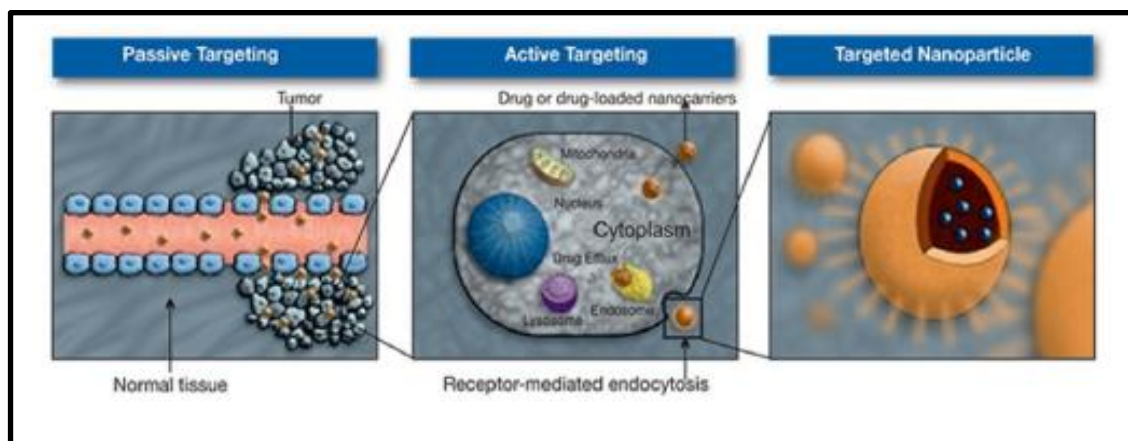


Figure (2-15): The active and passive targets of nanoparticles [148].

2-14 Cell Lines

Cell culture refers to the removal of cells from an animal or plant and their subsequent growth in a favorable artificial environment [153]. Primary culture refers to the stage of the culture after the cells are isolated from the tissue and proliferated under the appropriate conditions until they occupy all of the available substrate (i.e., reach confluence) [154]. Cell lines comprise cells that are able to multiply for extended periods in vitro and can therefore be maintained by serial subculture. They can be subdivided into finite cell lines, continuous cell lines and stem cell lines [155]. Cell lines are an appropriate experimental model for mechanistic studies, because they are simpler than a complete organism [156]. Subculturing, is the removal of the medium and transfer of cells from a previous culture into fresh growth medium, a procedure that enables the further propagation of the cell line or cell strain. The growth of cells in culture proceeds from the lag phase following seeding to the log phase, Cells in culture can be divided in to three basic categories based on their shape and appearance (i.e., morphology) [157].

❖ **Fibroblastic** (or fibroblast-like).

- ❖ **Epithelial-like** cells are polygonal in shape with more regular dimensions.
- ❖ **Lymphoblast-like** cells are spherical in shape.

2-14-1 AMJ13 Cell Line

Breast cancer is a very heterogeneous disease that includes several genetically and epigenetically different diseases with a wide range of clinical characteristics [158]. Given that breast cancer cell lines could supply a limitless source of homogenous self-replicating materials utilizing simple yet standard media and techniques, a substantial percentage of existing knowledge on breast carcinomas is generated from in vivo and in vitro investigations using breast cancer cell lines [159]. Therefore, AMJ13 is a newly developed breast cancer cell line derived from an Iraqi breast cancer patient. It's the first time happened to an Iraqi populace. The AMJ13 cell line was created from the primary tumor of a 70-year-old Iraqi woman who had to infiltrate ductal carcinoma on histology, discovered by [160].

2-14-2 Hep-G2 Cell line

Cell line history Hep-G2 is a human liver cancer cell line that was derived from the liver tissue of a 15-year-old Caucasian male with a hepatocellular carcinoma. In 2013 liver cancer was diagnosed in more than 350,000 people and there were over 160,000 deaths after diagnosis; hepatocellular carcinoma is the fifth most common cancer worldwide. The cells secrete a variety of major plasma proteins, for example transferrin and plasminogen. These cells have been successfully grown in large scale cultivation systems [161].

2-14-3 RD Cell Line

RD was derived directly from biopsy specimens of a 7-year-old female with a pelvic RMS previously treated with cyclophosphamide and radiation and found to have refractory disease. It has an embryonal histology based on histologic appearance of the tumor biopsies and the cultured cells, and 51-hyperdiploid chromosomes. RD has been shown to have amplification of the MYC oncogene, Q61H mutation of NRAS, and homozygous mutation of TP53. Houghton et al. studied tumor size following injections of various chemotherapy agents and found that RD demonstrated growth inhibition to vincristine and cyclophosphamide, but no other agents tested. RD was also used to test tolfenamic acid, and showed decreased tumor size, decreased cell migration, and decreased expression of Sp specificity transcription factors after treatment. The cell line TE671, which was originally thought to be a medulloblastoma line, was later shown through cytogenetic analysis and DNA fingerprinting to likely be a subclone of RD cells. RD cells are one of the most commonly used cell lines in RMS research, can be obtained from ATCC, and are grown in Eagle's medium with 10% FBS [162].

2-15 Nanoparticles for Drug Delivery

The delivery of drugs and other therapeutic agents via the use of nanoparticles seeks to accomplish several primary goals which overlap with targeted drug delivery in general and include [163]:

- 1- More specific drug targeting and delivery.
- 2- Reduction in toxicity while maintaining efficacy.
- 3- Increased biocompatibility.
- 4- Faster development of new therapeutic strategies.

In order to properly and effectively design a novel nanoparticle-based targeted drug delivery platform there are basic prerequisites that must be taken into consideration including knowledge on [163]:

- 1- Drug incorporation and release.
- 2- Nanoparticle/drug complex formulation stability and shelf-life.
- 3- Biocompatibility.
- 4- Biodistribution and targeting efficiency.
- 5- Functionality.

Table (2-1) shows the different types of nanoparticle-based system for drug delivery [163].

Table (2-1): The different types of nanoparticle-based system for drug delivery [163].

Synthetic Polymer-Based Nanoparticles	Synthetic Metal-Based Nanoparticles	Natural Material-Based Nanoparticles
Polyethylene Glycol (PEG)	Iron Oxide	Liposomes
Poly(D,L-lactic-co-glycolic) Acid (PLGA)	Fullerenes	Liposomal Nanoparticles and Targeting Inflammation
Poly(lactic Acid) (PLA)	Buckyballs (C60)	Chitosan
Polycaprolactone (PCL)	Buckysomes	Gelatin
Polyacrylate (PACA)	Carbon Nanotubes (CNTs)	Albumin
Dendrimers	-	-

2-16 CNTs in Drug Delivery

Chemotherapeutic agents have some limitations due to their toxic side effects. There is a niche in the pharmaceutical market for drug delivery that does not elicit such toxicity, whilst still having high therapeutic efficacy. Thus, there is an unmet need to develop cell-targeting drug formulations with a wide therapeutic index. CNTs have shown great promise as nano scaled vehicles for targeted drug delivery [164,165]. One of the main advantages of the CNT is its ability to deliver drugs directly to cancer cells [166,167]. In the past, there have been numerous experimental studies performed in vitro and in vivo using antibody-functionalized CNTs loaded with chemotherapeutic agents. Another application of CNTs for drug delivery is intravenous injection. One of the issues with injecting drugs into the body is the risk of blood vessels becoming blocked because of the large size of the drugs, which would lead to tissue toxicity. It has been suggested that CNTs could be used as nanocarriers for delivering drugs into the body via injectable routes [167]. Drugs can either attach to the outer surface of the CNT via functional groups or be loaded inside the CNT. Attachment of the anticancer drug to the outer surface of the CNT can be through either covalent or noncovalent bonding, including hydrophobic, π - π stacking, and electrostatic interactions [168-170]. Filling of the CNT with the anticancer drug is another method of incorporating drugs to CNTs.

2-17 CNT Functionalization Techniques

Despite the advantages of CNTs, there are limitations to their biomedical use. Purification of CNTs is still tedious. CNTs that are commercially available are severely contaminated with metal catalysts and amorphous carbons, and are known to be generally insoluble and not biocompatible. In order to make these materials less toxic and more

biocompatible, a number of procedures have been designed to attach appropriate molecules to the CNT surface. It has been shown that once the CNTs are appropriately functionalized and intravenously injected into mice, they are excreted via the biliary pathway without causing any significant side effects [171]. Generally, CNTs can be either covalently or noncovalently functionalized with different chemical groups [172]. In terms of CNT reactivity with functional groups, researchers have divided CNTs into two zones, ie, the tips and the side walls. It has been shown that CNT tips have a higher affinity for binding functional groups than do the side walls [173].

2-17-1 Noncovalent Functionalization

Noncovalent functionalization involves Van der Waals interactions, π - π interactions, and hydrophobic interactions of biocompatible functional groups with the surface of the CNT. One of the main advantages of this type of bonding is the minimal damage caused to the CNT surface. It has been suggested that noncovalent attachment preserves the aromatic structure and thus the electronic characteristics of CNTs. On the other hand, because noncovalent bonding provides a weak force between the functional group and the CNT, it is not suitable for targeted drug delivery applications [174].

2-17-2 Covalent Functionalization

Covalent binding of biocompatible groups to the surface of the CNT is another method of functionalization. Using this method, the surface of the CNT can be modified by different techniques, creating a suitable platform on the surface of these materials, enabling covalent attachment of biocompatible groups to the surface of CNTs. Oxidation of CNTs using

strong acids is a method commonly used for generating covalent functionalization [175]. Briefly, concentrated nitric acid, concentrated sulphuric acid, and CNTs are sonicated and heated. This process allows for side-wall covalent functionalization, and carboxylic acid groups would be attached, rendering CNTs water-soluble. Figure (2-16) shows a transmission electron microscopic CNT image before and after oxidization using a combination of nitric and sulfuric acid. These modifications would provide a suitable platform for the covalent attachment of biocompatible functional groups to the surface of the CNT, and the presence of a carboxylic group can improve CNT biocompatibility. It has been shown that a highly negative charge, developed as a result of the carboxylic group on the surface of the CNT, increases the hydrophilicity of these materials [176]. Oxidized CNTs can then be further coated with PEG, a hydrophilic substance with the ability to make CNTs more biostable. Covalent binding of a functional group to the CNT can produce a stable functionalized CNT, making it more suitable for use as a vehicle for drug delivery. However, the side wall of the CNT is damaged during this process, resulting in alteration of other properties of the CNT [176]. Hence, CNTs functionalized by covalent bonding should not be used in some applications, including imaging [171].

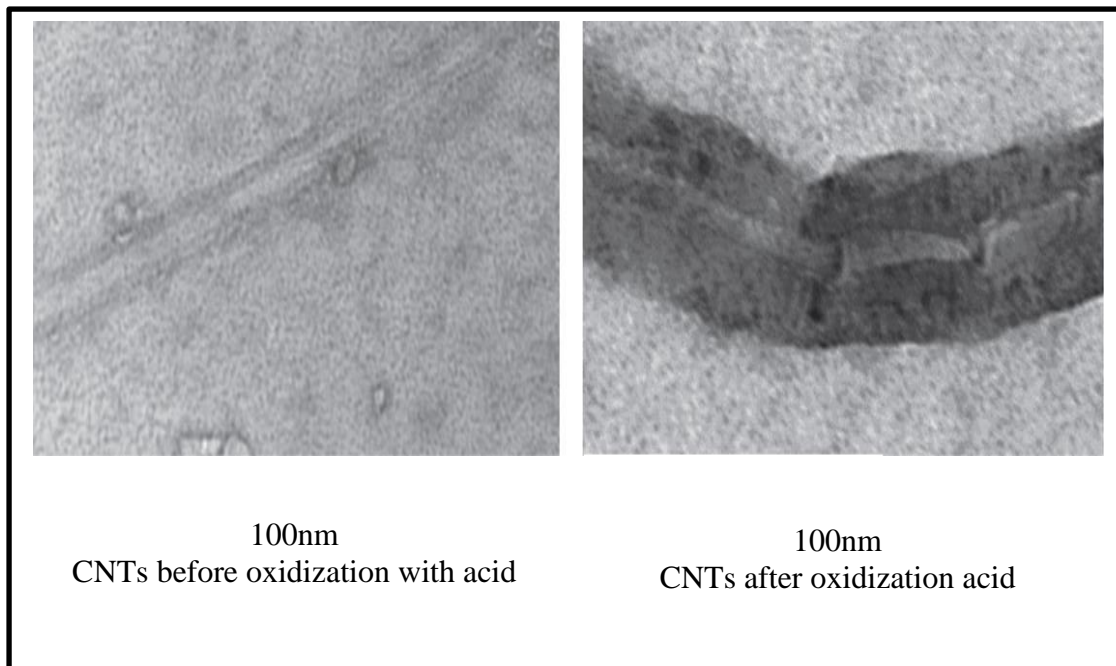


Figure (2-16): Carbon nanotubes (CNT) before and after oxidization using a combination of nitric and sulfuric acid. This method resulted in chemical nanotubes and formation of carboxylate groups on the surface modifications carbon [171].

Chapter Three
Experimental Work

3-1 Introduction

This chapter includes the stages of samples preparation, and testing measurement stages and tools used in the preparation, measurement and bio application.

3-2 Chemical and Biomedical Material Reagents

The table below (3-1) shows the chemical and biomedical of the materials used in the study.

Table (3-1): The Chemical and Biomedical Material Reagents.

No.	Chemical and Biomedical Material	Company	Country
1-	SWCNTs	Cheap Tubes	USA
2-	HCl	CDH	India
3-	EDC Hydrochloride C ₆ H ₁₇ N ₃ -HCl	Sigma-Aldrich	Germany
4-	N-Hydroxy succinimide (NHS)	Sigma-Aldrich	Germany
5-	PEG 4000	HI Media	India
6-	Ethanol C ₅ H ₆ OH	Scharlab	
7-	NaOH	Dae-Jung	
8-	H ₂ SO ₄	LOBA Chemie, Maharashtra	India
9-	HNO ₃	LOBA Chemie, Maharashtra	India
10-	PEI	Sigma-Aldrich	Germany
11-	Trypsin/EDTA	Capricorn	Germany
12-	DMSO	Santacruz Biotechnology	USA
13-	RPMI 1640	Capricorn	Germany
14-	MTT Stain	Bio-World	USA
15-	Fetal Bovine Serum	Capricorn	Germany
16-	CO ₂ Incubator	Cypress Diagnostics	Belgium
17-	Microtiter Reader	Gennex Lab	USA
18-	Laminar Flow Hood	K & K Scientific Supplier	Korea
19-	Micropipette	Cypress Diagnostics	Belgium
20-	Cell Culture Plates	Santa Cruz Biotechnology	USA
21-	CUR	Nanochemazone	Canada

Figure (3-1) Shows a schematic diagram of laboratory experiments carried of the completed tests in this study.

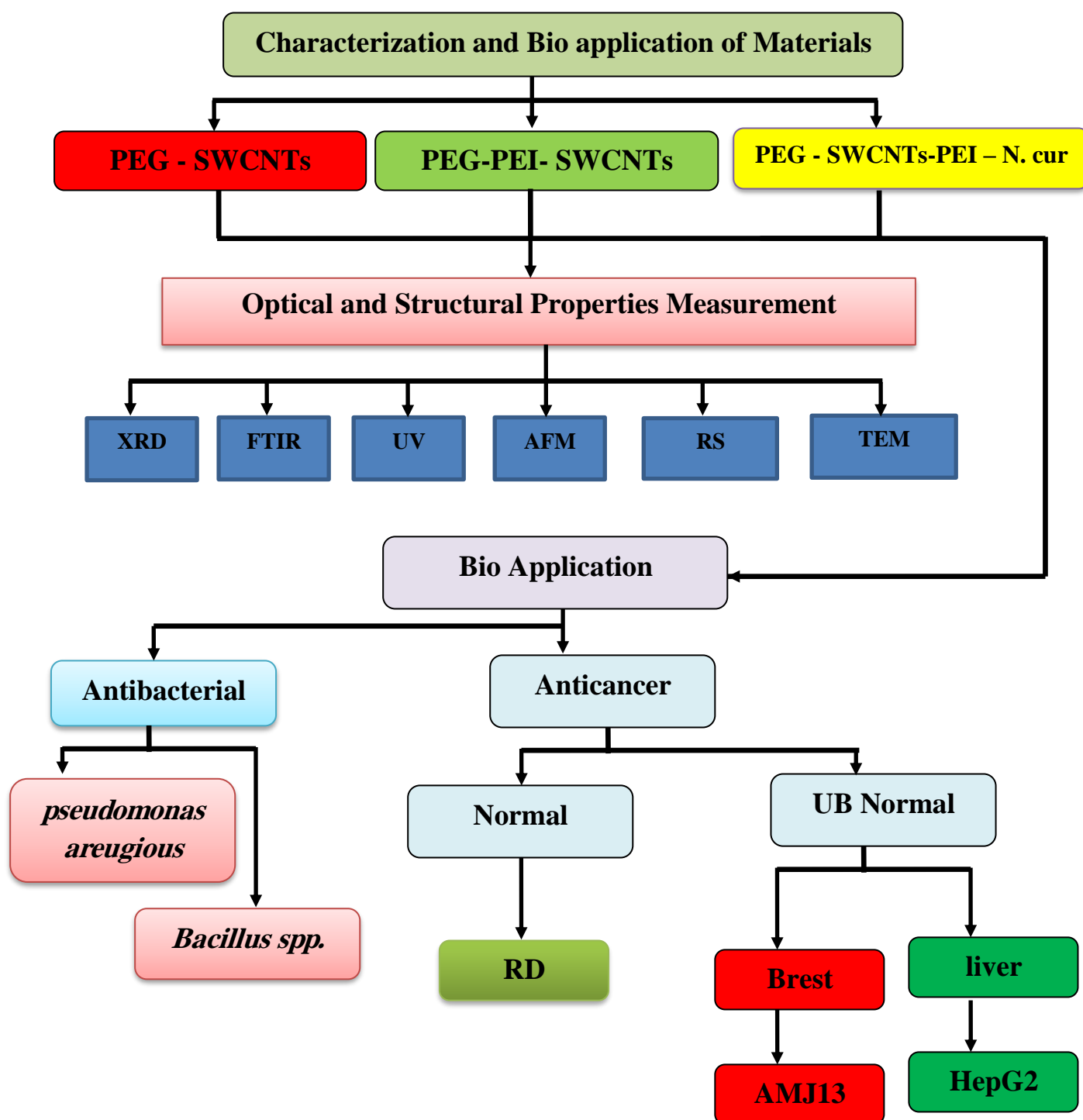


Figure (3-1): Schematic diagram laboratory experiments carried out to achieve the aim of the present study.

3-3 Preparation of Material

3-3-1 Functionalization of SWCNTs by PEG

In the first beaker, (0.004g) of single-walled carbon nanotube (SWCNTs) inserted into (40ml) of deionized water and (0.24g) of sodium hydroxide (NaOH) were inserted into (40ml) deionized water in another beaker, and after it dissolves fully, we add it to the first beaker. Following that, the first beaker was placed in which each of (SWCNTs + NaOH) was placed on the ultrasonic cleaner device for an hour before transferring it to the magnetic stirrer for three hours without heat only. After three hours, the beaker was placed in the ultrasonic cleaner and adds six milliliters of hydraulic acid (HCl) for ten minutes, then remove the solution. The material was then placed in an electronic centrifuge and spun for half an hour at a speed of (4000) revolutions per minute (rpm). The surplus water was removed after separating the material and place it on the filter paper, which we then wash with deionized water (20-30ml). After that, we add (0.8gm) of (EDC) and (0.48g) of (NHS) and leave it on the magnetic stirrer for three hours, then (3g) of (PEG) was added and leave it on the mixer for (21 hours). After that, we put the material in an electronic centrifuge for half an hour at a speed of (4000) revolutions per minute (rpm) to separate it from the water before drying it in a drying oven to obtain powder.

3-3-2 Functionalization of SWCNTs with PEG and PEI mixture

On the electromagnetic mixer, we put (0.4 g) of (SWCNTs) in a (1:1) mixture of sulfuric and nitric acid for two hours without heat. The product was filtered using filter paper and washed with deionized water and methanol after two hours of mixing, and then it was precipitated to yield the powder. Then we poured (120ml) of deionized water in another beaker,

added (6.2gm) of EDC-HCl and (3.5g) of NHS material, and set it on the electromagnetic mixer for half an hour to dissolve the substance in the deionized water; after half an hour, (SWCNTs) added in the stage (SWCNTs -COOH). The solution is then put into a Petri shower and set in an electric oven at a temperature of (80 °C) to dry after adding (96g) of PEG-4000 and (8g) of PEI progressively and churning on the electromagnetic mixer for (24 hours). We receive a paste-like substance with a sticky texture, meaning it has a high viscosity, and keep it in a glass box until we need it.

3-3-3 Loading Nanocurcumin on PEG-PEI-SWCNTs

For loading Cur on PEG-PEI-SWCNTs (2.250 mL) of the Cur solution (3.33 mg/ml) was added to aqueous (7ml) PEG-PEI-SWCNTs suspension (4.28 mg/mL) and stirred for overnight. Cur rate in compare to PEG-PEI-SWCNTs was about (1:4). The suspension was centrifuged (12000 rpm, 25 °C) for (150 minutes) and dried for (48 hours) at (40 °C) in the oven to obtain the final sample which is called curcumin bonded PEG-PEI-SWCNTs (PEG-PEI-SWCNTs-N. Cur).

3-4 Measurement of Optical Properties

The spectra of absorbance for materials have been recorded for the wavelengths (190-1100) nm by using the UV-Visible 1800 double beam spectrophotometer provided by Shimadzu, Japanese company.

3-5 Structural Properties and Surface Morphology Measurements

3-5-1 X-Ray Diffraction

X-ray diffraction (XRD) analysis is used to investigate the crystal structure of SWCNTs, PEG-SWCNTs, PEG-PEI-SWCNTs, PEG-PEI-SWCNTs-N.Cur and N.Cur. When incident (X-ray) beam of mono wavelength diffracts on materials surface this will exhibit peaks on specific angles for each material because of Bragg's reflection on parallel crystalline surface. The X-ray diffraction instrument used in this study (Shimadzu 6000) having the following properties:

1. Source: Cu k_{α} radiation of $\lambda=1.5406 \text{ \AA}$.
2. Current: 30 mA.
3. High voltage: 40 kV.
4. Speed: 5 deg / min.
5. Incident angle from 20 to 80 degrees.

3-5-2 Atomic Force Microscopy (AFM) Measurements

Surface morphological measurements for SWCNTs, PEG-SWCNTs, PEG-PEI-SWCNTs, PEG-PEI-SWCNTs-N.Cur and N.Cur are made by SPM-AA3000 contact mode spectrometer, Angstrom Advanced Inc. 2008, USA.

3-5-3 Transmission Electron Microscopy (TEM)

Transmission Electron Microscope (TEM) was employed. This test relies on producing an electron beam with high energy to be passed through

the targets to investigate the material microstructure. The electron beam is then focused, quickened at a few hundred kilovolts and at wavelengths shorter than wavelengths of the visible range of light; the definitive pictures are accomplished by a digital camera. The analysis was done in School of Electrical and Computer Engineering / University of Tehran, Iran.

3-6 Chemical Properties

3-6-1 Fourier Transform Infrared (FTIR) Spectroscopy

The IR transmission spectra were recorded by double beam Fourier transform infrared spectroscopy using IR Affinty-1 CE (FTIR) spectrophotometer provided by Shimadzu, Japanese company, The technique operates in the wave number range of (4000-400 cm^{-1}) with resolution of (0.5 cm^{-1}).

3-6-2 Raman Measurement

Raman spectroscopy is a type of spectroscopy that is used to observe rotational, vibrational, and other low-frequency modes. Raman spectroscopy is used to examine the structural fingerprint of molecules in order to identify them. (Bruker Senterra Raman microscope) was used to measure the samples using (532 nm) line, argon laser, incident laser power (5mW), and automatic software switching of excitation wavelength with intensity calculation.

3-7 Bioactivity

A-Antibacterial Activity

1- Isolation and Identification of Bacteria from UTI.

Twenty out samples of urine were collected from patients with suspicious clinical symptoms like dysuria, loin pain, fever, frequent urination, and need to urinate with an empty bladder; patients were visited Ibn Al-Nafees Hospital/ Baghdad and asked about taken antibiotic prior visiting the hospital during last seven days. The ethical committee approved the study of the University. All urine samples were cultured over blood agar, Mac Conkey agar, and mannitol salt agar. Bacterial characters were identified using Gram stain, urease test, oxidase, catalase, hemolysis of RBCs, and Indole Methyl red Vokes Proskauer (IMVC).

2- Antibacterial Activity of Aqueous Herbal Extracts

Agar well diffusion approach on Mueller-Hinton agar was once used in imitation of the search for antibacterial activity. Bacterial cultures were crashed out from the nutrient agar plate and were suspended in sterilized peptone water. Turbidity was evaluated and compared with McFarland standard tube number 1, which equivalents approximately to (1×10^8) CFU/mL. The cotton swab was immersed in bacterial suspension and spread over Muller Hinton agar, which let for (10 minutes) to ensure bacterial adherence. Meanwhile, the borer applicator was sterilized by flame, cooled, and pressed on the top of seeded Muller Hinton agar to make well with a (6 mm) radius, let distance about (15 mm) between wells the aspect of the plate. Each well was filled with (25, 50, 75, and 100 $\mu\text{g/ml}$), plates were stand for (10 minutes) and were incubated for (24 h) at

(37 °C). Four replicas of each plate were prepared, and the diameter of the inhibition zone was recorded from the edge of the well.

B- Anticancer Activity

1- Maintenance of Cell Cultures

AMJ13 and HepG2 cells were maintained in RPMI-1640 supplemented with (10%) fetal bovine serum, (100 units/mL) penicillin, and (100 µg/mL) streptomycin. Cells were passaged using Trypsin-EDTA reseeded at (80%) confluence twice a week, and incubated at (37 °C).

2- Cytotoxicity Assays

To determine the cytotoxic effect of (CNTs, PEG-CNTs, PEG-CNTs-CUR, PEG-PEI-CNTs, PEG-PEI-CUR), the MTT assay was done using (96-well) plates. Cell line were seeded at (1×10^4 cells/well). After (24 h) or a confluent monolayer was achieved, cells were treated with tested compounds at different concentration. Cell viability was measured after (72 h) of treatment by removing the medium, adding (28 µL) of (2 µg/MI) solution of MTT and incubating the cells for (2.5 h) at (37 °C). After removing the MTT solution, the crystals remaining in the wells were solubilized by the addition of (130 µL) of DMSO (Dimethyl Sulphoxide) followed by (37 °C) incubation for (15 min) with shaking. The absorbency was determined on a microplate reader at (492 nm); the assay was performed in triplicate. The inhibition rate of cell growth (the percentage of cytotoxicity) was calculated as the following equation:

$$\text{Inhibition rate} = A - \frac{B}{A} \times 100 \dots\dots\dots (3-1)$$

where A is the optical density of control, and B is the optical density of the samples.

To visualize the shape of the cells under an inverted microscope, the cell was seeded into 24-well micro-titration plates at a density of (1×10^5) cells mL^{-1} and incubated for (24 h) at (37 °C). Then, cells were exposed to (CNTs, PEG-CNTs, PEG-CNTs-CUR, PEG-PEI-CNTs, PEG-PEI-CUR) at IC (50) for (24hr). After the exposure time, the plates were stained with crystal violet stain and incubated at (37 °C) for (10–15 min). The stain was washed off gently with tap water until the dye was completely removed. The cells were observed under an inverted microscope at 40× magnification and the images were captured with a digital camera attached to the microscope.

3- Statistical Analysis:

The obtained data were statically analyzed using an unpaired t-test with GraphPad Prism (6). The values were presented as the mean \pm SD of triplicate measurements.

Chapter Four
Results and Discussion

4-1 Introduction

This chapter includes the results and discussions optical, chemical, structural and morphological properties of the functionalization SWCNTs by PEG, SWCNTs with PEG and PEI mixture. It will also discuss the effect of loading the nano curcumin on PEG-PEI-SWCNTs and study its bio applications on bacteria inhibition and anticancer activity.

4-2 Optical Properties

Figure (4-1) shows the spectra of SWCNTs and (SWCNTs – PEG), the black line indicates the SWCNTs spectra at (291nm) which represent the absorptions bands that related to electronic transition $n - \pi^*$ for C=O in the SCWNTs. The red line represents the (SWCNTs – PEG) that shifted to (289 nm), confirming the synthesis of (SWCNTs – PEG). Also, it was shown that decreasing the intensity of the absorbance peak for (SWCNTs) is due to the color of SWCNTs changing from black to gray because of link (SWCNTs-PEG).

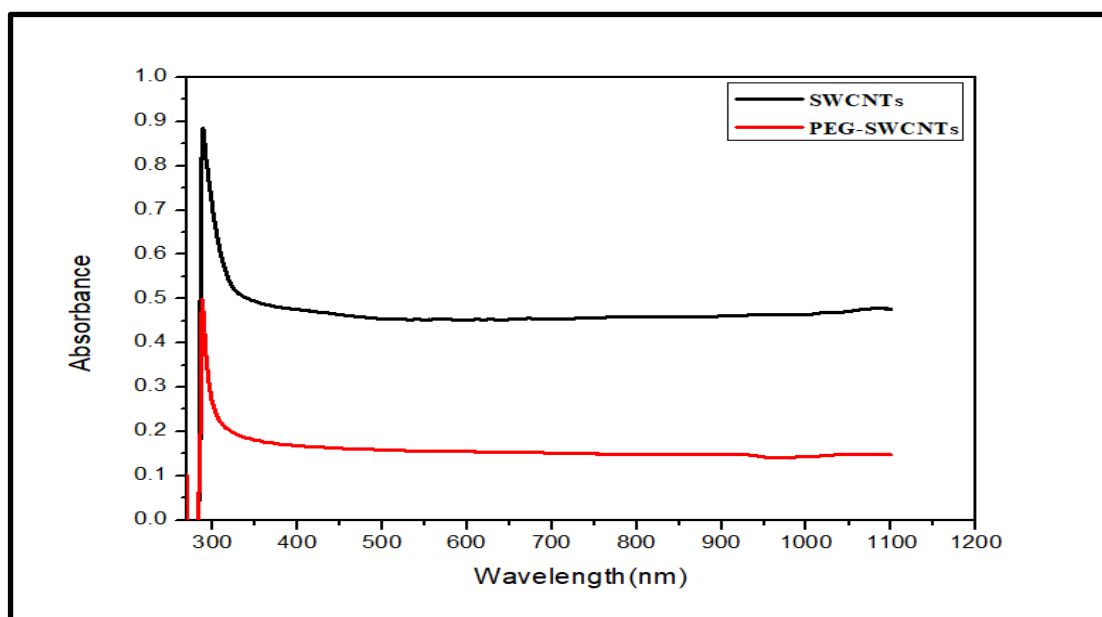


Figure (4-1): The absorbance of SWCNTs and PEG-SWCNTs as a function of wavelength

In the UV-vis spectra of SWCNTs and PEG-PEI-SWCNTs (figures 4-1-a,b), the black line at (289 nm) represents the absorption bands that relate to the $\pi-\pi^*$ electronic transition for C-C (aromatic rings) and $n-\pi^*$ transition for C=O in the SWCNTs. The green line at (300.98 nm) indicates a shift of these transitions, which confirms the synthesis of PEG-PEI-SWCNTs. The blue line illustrates the spectra of N.Cur and the orange line represented PEG-PEI-SWCNT-N. Cur. The Cur spectrum includes two peaks at (275 nm) and (425 nm). In UV-Vis spectra, the highest absorption peak for Cur is (420–430 nm); in our data, an absorption peak at (431 nm) occurs in the UV-Vis spectra, which is typical of Cur, implying binding of Cur to PEG-PEI-SWCNTs. When compared to Cur suspension, the most plausible explanation is $\pi-\pi^*$ interaction between Cur and PEG-PEI-SWCNTs; in addition, the change in curcumin maximum absorption might be potentially related to its interaction with the more soluble co-polymer.

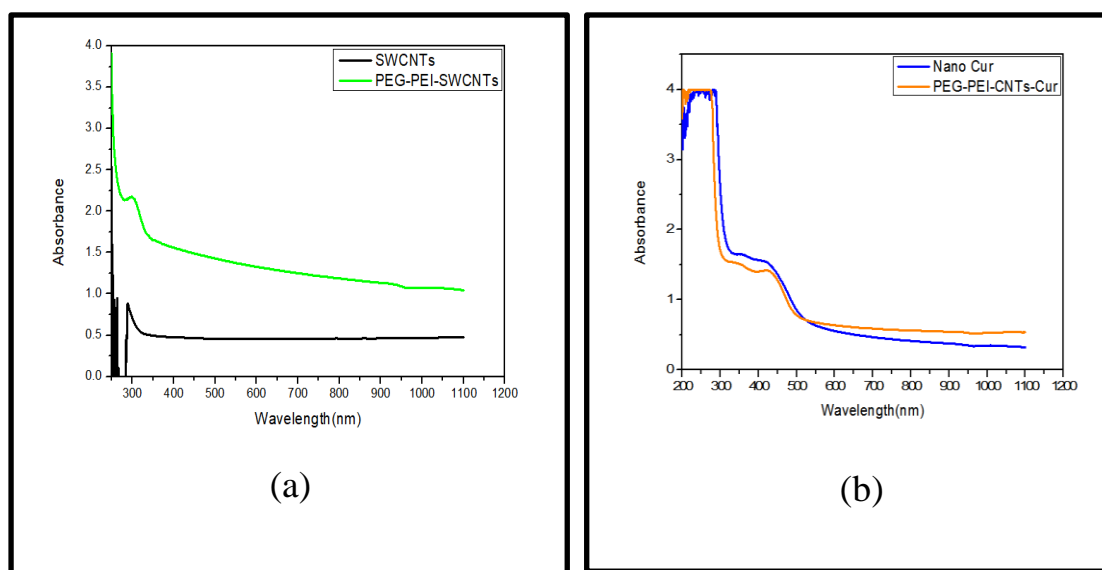


Figure (4-1): The absorbance of (a) SWCNTs and PEG-PEI-SWCNTs, (b) Nano Cur and PEG-PEI-SWCNTs-N. Cur as a function of wavelength.

4-3 Chemical Properties

4-3-A-Fourier Transform Infrared (FTIR)

In FTIR spectrums of SWCNT, SWCNTs-PEG, SWCNTs-PEG-PEI and (PEG-PEI-SWCNTs-Cur), in figure (4-2-a) black line represents the SWCNTS sample, the peaks at (3431 cm^{-1}) is stretching related to OH, while (2897 and 1636 cm^{-1}) are C-H groups and C=O group carboxyl. While in the case of (PEG – SWCNTs) as shown in figure (4-2-b), the peak at (3431 cm^{-1}) shifted to (3438 cm^{-1}), with the appearance of C-H at (2875 cm^{-1}) proving that SWCNTs are associated with PEG, as well as the appearance of C=C at ($1952, 1472\text{ cm}^{-1}$), C-O and C=O at ($1100, 1648\text{ cm}^{-1}$) was also identified, while in case of (PEG-PEI-SWCNTs) as shown in figure (4-2-c) the peak at (3431 cm^{-1}) shifted to (3432 cm^{-1}) also appearance of C-H at (2883 cm^{-1}) which proved that SWCNTs conjunction to PEG-PEI, also the appearance of C=C at (1468 cm^{-1}) and C=O at (1716 cm^{-1}) was also identified, the peak at (1616 cm^{-1}) is related to N-H and peaks at (1344 cm^{-1}) is related to C-N. The FTIR pattern of N. Cur extract was shown in figure (4-2-d), which shows a broad and strong band at approximately (3368 cm^{-1}) which represented the stretching vibration of O-H in the hydroxyl groups of hydrogen bonds and peak at (1378 cm^{-1}) is related O-H bending vibration alcohol. The region between (1281 cm^{-1}) and (1117 cm^{-1}) may be assigned to C-O stretching vibrations. The small bands at ($619, 573, 470$ and 446 cm^{-1}) were attributed to stretching vibrations of C-O in the ester. The peak at (2924 cm^{-1}) is related to C-H stretch (Alkane), peak at (1456 cm^{-1}) is related to C-H bending methyl group, peak at (767 cm^{-1}) is related to C-H bending and peak at (710 cm^{-1}) is related to C-H bending vibrations of the aromatic ring. Another absorption peak noticed at (1631 cm^{-1}) might be due to the (C=C) stretching and peak at (840 cm^{-1}) is related to C=C bending vibrations. Then peak at

(1324 cm^{-1}) represents the C-N stretching in aromatic amine. The other peak at (1028 cm^{-1}) attributed for C-O-C groups and peak at (1531 cm^{-1}) is assigned to the C=O. The orange line in figure (4-2-e) illustrates the loading drug PEG-PEI-SWCNTs-N.Cur, The OH stretching of PEG-PEI-SWCNTs-N.Cur is shifted to (3735,3850 cm^{-1} and peak at 1359 cm^{-1}) is related O-H bending vibration alcohol while the peaks (2889 cm^{-1}) C-H stretch (Alkane) and peak at (1474 cm^{-1}) is related to C-H bending methyl group. The peak at (1646 cm^{-1}) is related to N-H bending amine and peak at (849 cm^{-1}) is related to C=C bending vibrations, peak at (1359 cm^{-1}) is related to C-N stretching aromatic amine. The peak at (1115 cm^{-1}) is related to C-O stretching vibrations while the peak at (598 cm^{-1}) is assigned to C-O stretching vibrations (ester). These results demonstrated that the conjugation PEG-PEI-SWCNTs-N. Cur had been successfully synthesized. Table (4-1) shown the FTIR Peaks Assignments of all sample.

Table (4-1): The FTIR Peaks Assignments of SWCNTs, PEG-SWCNTs, PEG-PEI-SWCNTs, N. Cur and PEG-PEI-SWCNTs-N.Cur.

Band assignments	Wavenumber (cm^{-1})				
	SWCNTs	PEG-SWCNTs	PEG-PEI-SWCNTs	N. Cur	PEG-PEI-SWCNTs-N. Cur
O-H	3431	3438	3432	3365 1378	1359 3735 3850
C-H	2897	2875	2883	710 767 1456 2956	1474 2889
C=C		1472 1952	1468	840 1631	849
C-O		1100		446 470 573 619 1117 1281	598 1115
C=O		1648	1716	1531	
N-H			1616		1646
C-N			1344	1324	1359
C-O-C				1028	

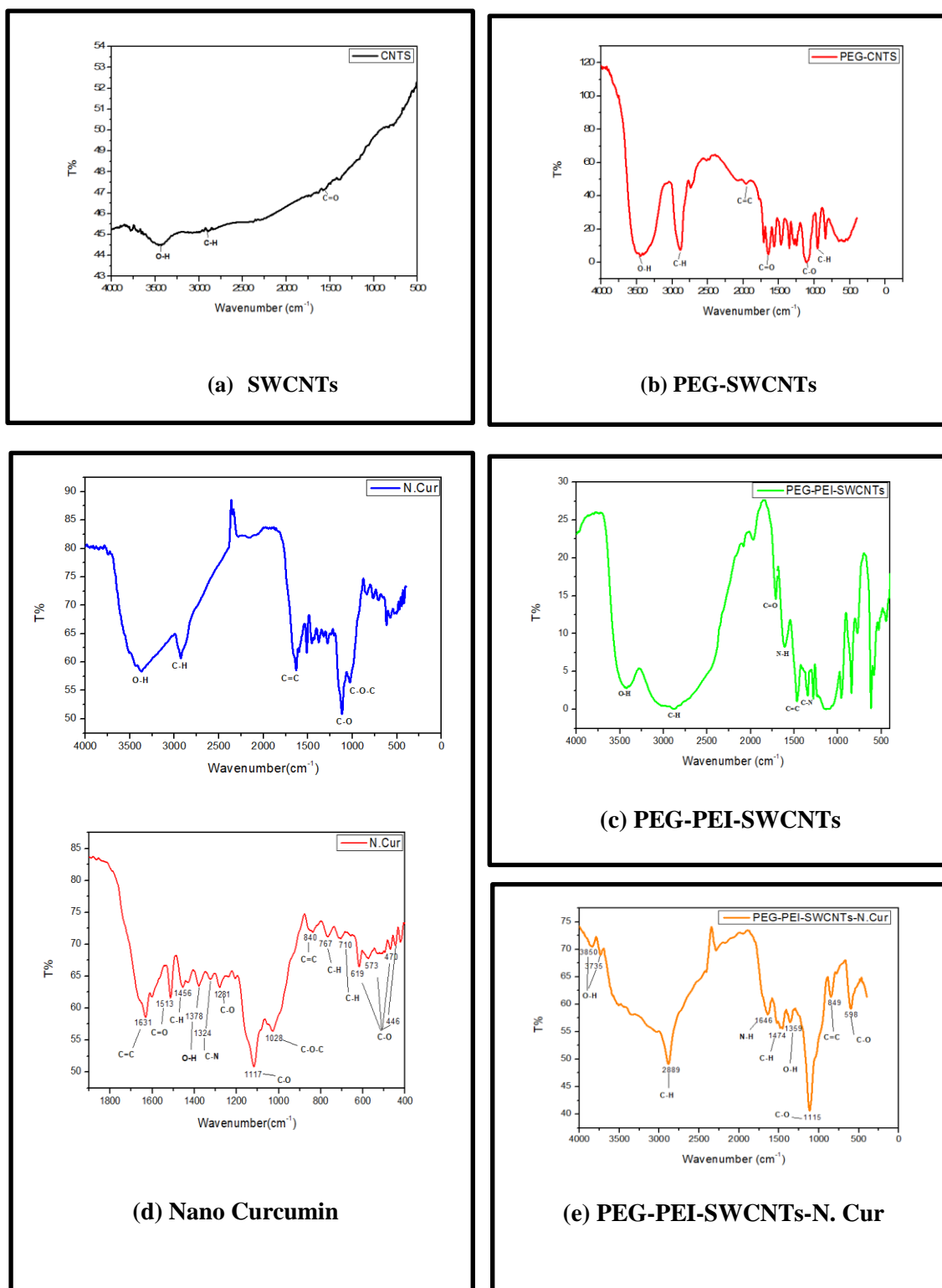


Figure (4-2): FTIR spectrum of (a) SWCNTs, (b) PEG-SWCNTs, (c) PEG-PEI-SWCNTs, (d) Nano Curcumin and (e) PEG-PEI-SWCNTs-N. Cur.

4-3-B Raman Spectroscopy (RS)

Figure (4-3 a, b and c) shows the Raman spectra of SWCNTs and (SWCNTs – PEG). The black line in figure (4-3-a) indicates the SWCNTs spectra which show four significant features namely: (1) the radial breathing mode (RBM) band ($(150.89, 255.91) \text{ cm}^{-1}$), which is caused by Raman modes in which all of the tube's atoms vibrate in phase; (2) the D band (1291.60 cm^{-1}), also called the “disorder” band, that is related to the breathing motions of the sp^2 carbon atoms in the rings and can be activated by the presence of defects on the nanotube surface; (3) the G band (1572.65 cm^{-1}), known as the "tangential" mode, is made up of two sub-bands G^+ and G^2 which correspond to axial and circumferential in-plane vibrations in semiconducting nanotubes, respectively. (4) the overtone of the D band (2D band), which is a fingerprint of the graphitic structure and observed between (2566 cm^{-1}). The intensity changes of D and G bands, as well as their broadening, gives a measure of the functionalization extent, mostly because the presence of organic fragments along the SWCNTs side walls increase the structural disorder due to the introduction of a very high number of defects. Figure (4-3-b) shows Raman spectroscopy of (PEG-SWCNTs) where ($(844, 1138, 1469) \text{ cm}^{-1}$) indicate to PEG, D band and G band in PEG-SWCNTs shifting to ($1287.53 \text{ cm}^{-1}, 1581.12 \text{ cm}^{-1}$) respectively. ID/IG. For the mixture of PEG- SWCNTs/SWCNTs, the ID/IG ratio of SWCNT is (0.82) before adding PEG- -SWCNTs but decreases to (0.81) upon absorbing PEG-SWCNTs.

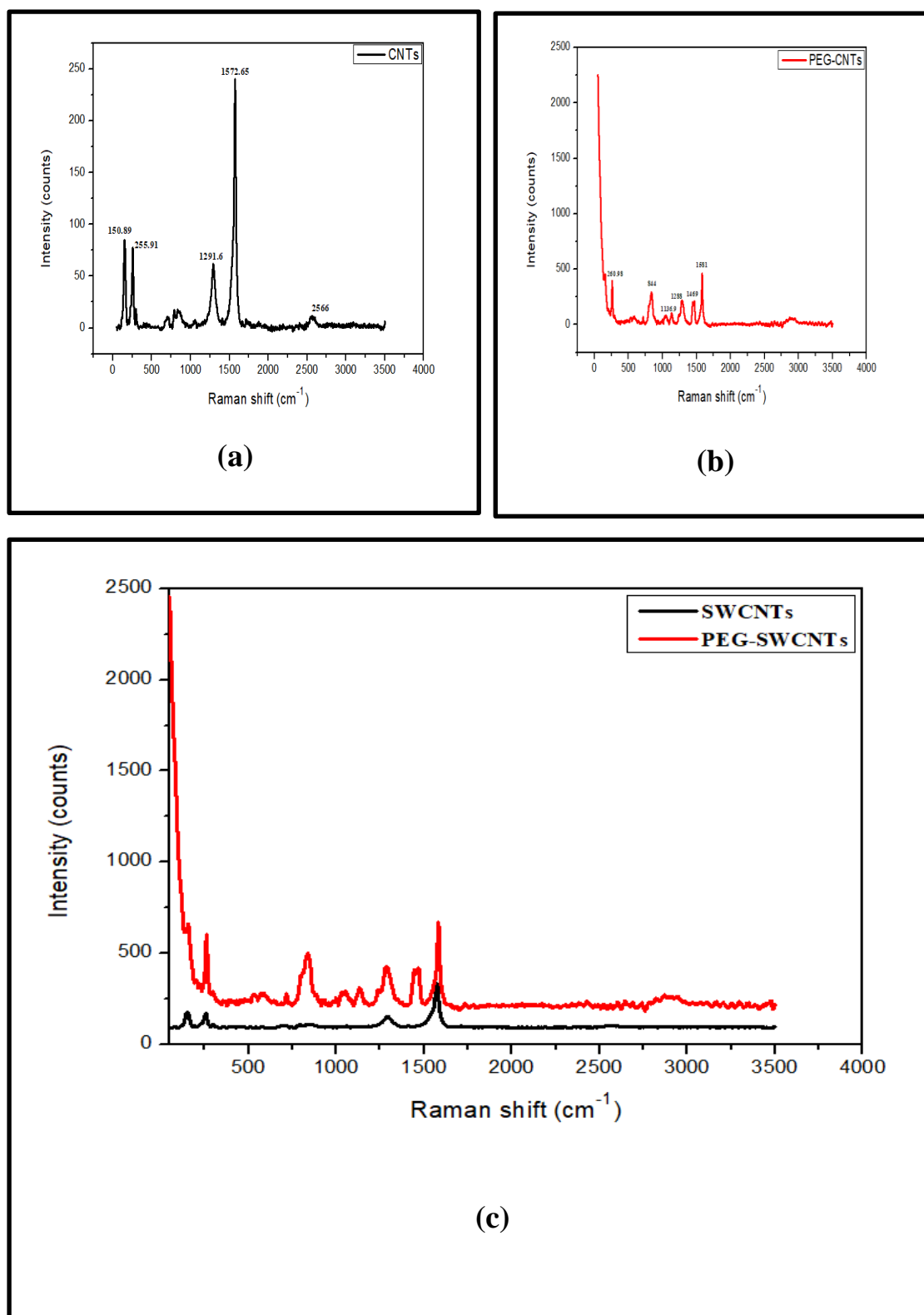


Figure (4-3): Raman Spectroscopy (a) SWCNTs, (b) PEG- SWCNTs and (c) SWCNTs and PEG-SWCNTs together.

Figure (4-4-b) shows Raman spectroscopy of (PEG-PEI-SWCNTs) where (2935,1292,1586 and (156,257) cm^{-1}) indicate to overtone of the D band (2D band), D band, G band and RBM respectively. A quantitative determination of the functionalization extent is provided by the ratio between the intensity of such bands, I_D/I_G . For the mixture of PEG-PEI-SWCNTs/SWCNTs, the I_D/I_G ratio of SWCNT is (0.82) before adding PEG-PEI-SWCNTs but decreases to (0.81) upon absorbing PEG-PEI-SWCNTs, a decrease in the Raman yield over the whole frequency range is observed when passing from pristine SWCNTs to PEG-PEI-SWCNTs. This trend is an indication of a Raman activity weakening in case of functionalized materials. From the fitting procedure, we calculated an I_D/I_G ratio which decreases in passing from pristine SWCNTs to functionalized materials. This behavior is also accompanied by a broadening of the G band. This increase is indicative of the breakage of the graphene sheet symmetry that in the present case can be associated with the introduction of functionalities onto the nanotube surface. Such trends are in very good agreement with other PEGylated-PEI systems. As the frequency of RBM is inversely proportional to the reciprocal of the diameter, it can be used to determine nanotube diameter. The RBM also provides information on chirality and thus, the electronic properties of the nanotube. Because single excitation energy was used in our experiment, only nanotubes resonant with this particular energy will demonstrate a peak at the RBM frequency. The nanotube diameter can be determined by $V_{\text{RBM}} = 248/\omega$, where V_{RBM} is Raman frequency shift of the RBM in cm^{-1} . From measured RBM, calculated SWCNTs diameter is (1.3).

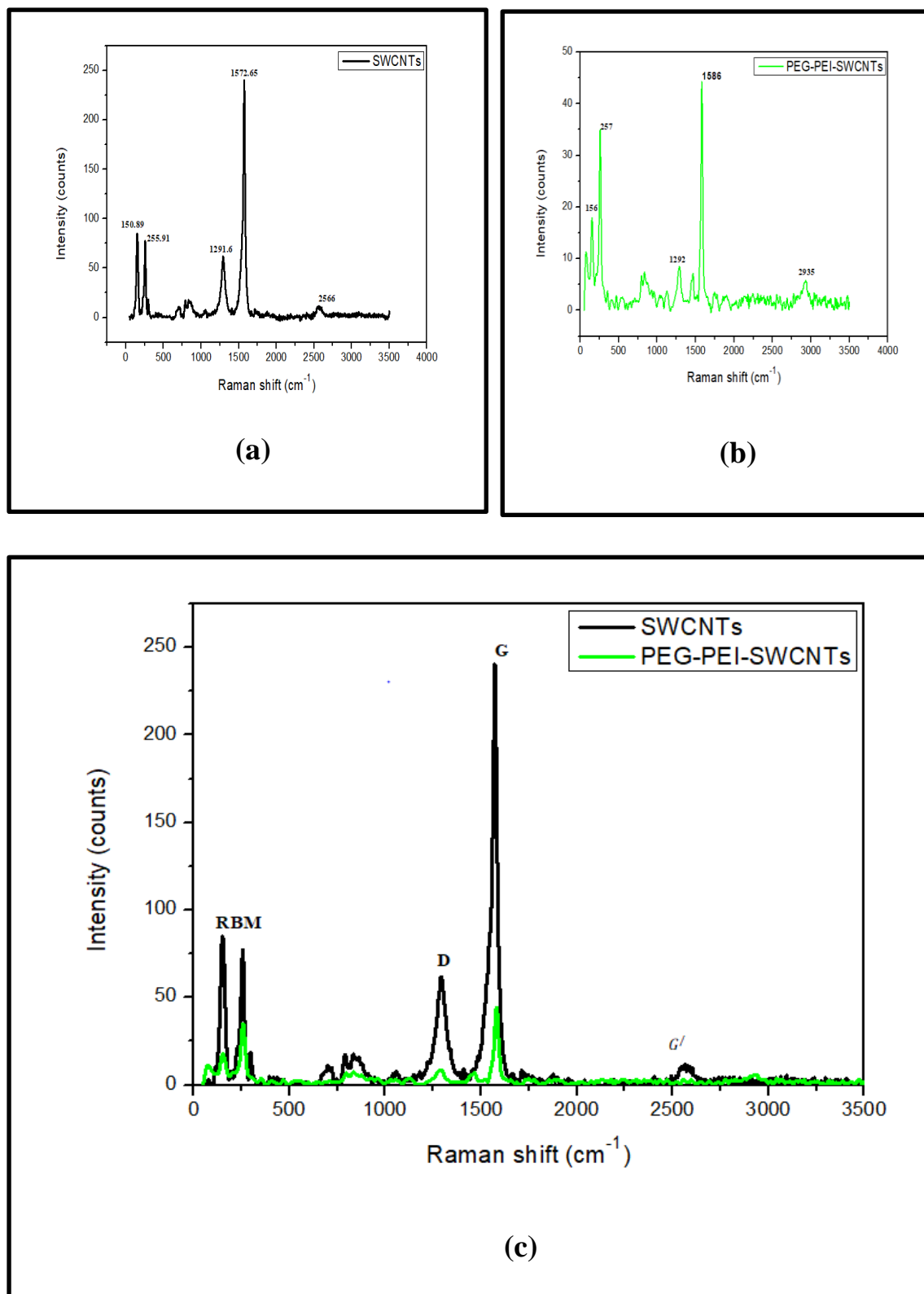


Figure (4-4): Raman Spectroscopy (a) SWCNTs, (b) PEG-PEI-SWCNTs and (c) SWCNTs and PEG-PEI-SWCNTs together.

The Raman vibrational modes of the nanocurcumin are located from (593 cm^{-1}) to (1700 cm^{-1}) as shown in figure (4-5-a), the peak at (593 cm^{-1}) was characteristic peak of methoxy group (R-OCH₃). The peaks at (754 and 794 cm^{-1}) seen in figure (4-5-b) stem from out-of-plane C-C-H bending vibration. The peak at 958 cm^{-1} originates from in-plane C-C-H bending vibration. While two form of nanocurcumin structures are defined by the peak at (1249-1250 cm^{-1}), the keto-enol form of nanocurcumin was obtained at (1249 cm^{-1}). The peak at (1319 cm^{-1}) originates from in-plane C-O-H bending vibrations. The peak at (1428 cm^{-1}) was the characteristic peak of phenol C-O. The strong peak between (1600 and 1630 cm^{-1}) was attributed to the mixed $\nu(\text{C}=\text{C})$ and $\nu(\text{C}=\text{O})$ vibration mode. They were observed at (1601 cm^{-1}) (aromatic C=C) and (1629 cm^{-1}) (carbonyl C=O). The Raman spectra for PEG-PEI-SWCNTs-N. Cur as shown in figure (4-5-b), the radial breathing mode (RBM) band, the disorder band (D band), the tangential mode (G band) and the overtone of the D band (2D band) shifting to ((171,264),1283, 1593 and 2131 cm^{-1})) respectively. The peaks for the nanocurcumin around (958, 1183 and 1428) cm^{-1} experienced shift to (939, 1168 and 1470) cm^{-1} in the drug loaded sample due to nano-encapsulation and indicates successful drug loading. The lines at (716 and 853) cm^{-1} can be assigned to the C-N stretching vibrations. The Raman spectral result indicates the nanocurcumin and SWCNTs is conjugated by the PEG-PEI polymer in the PEG-PEI-SWCNTs-N. Cur composites which could be useful for biomedical applications.

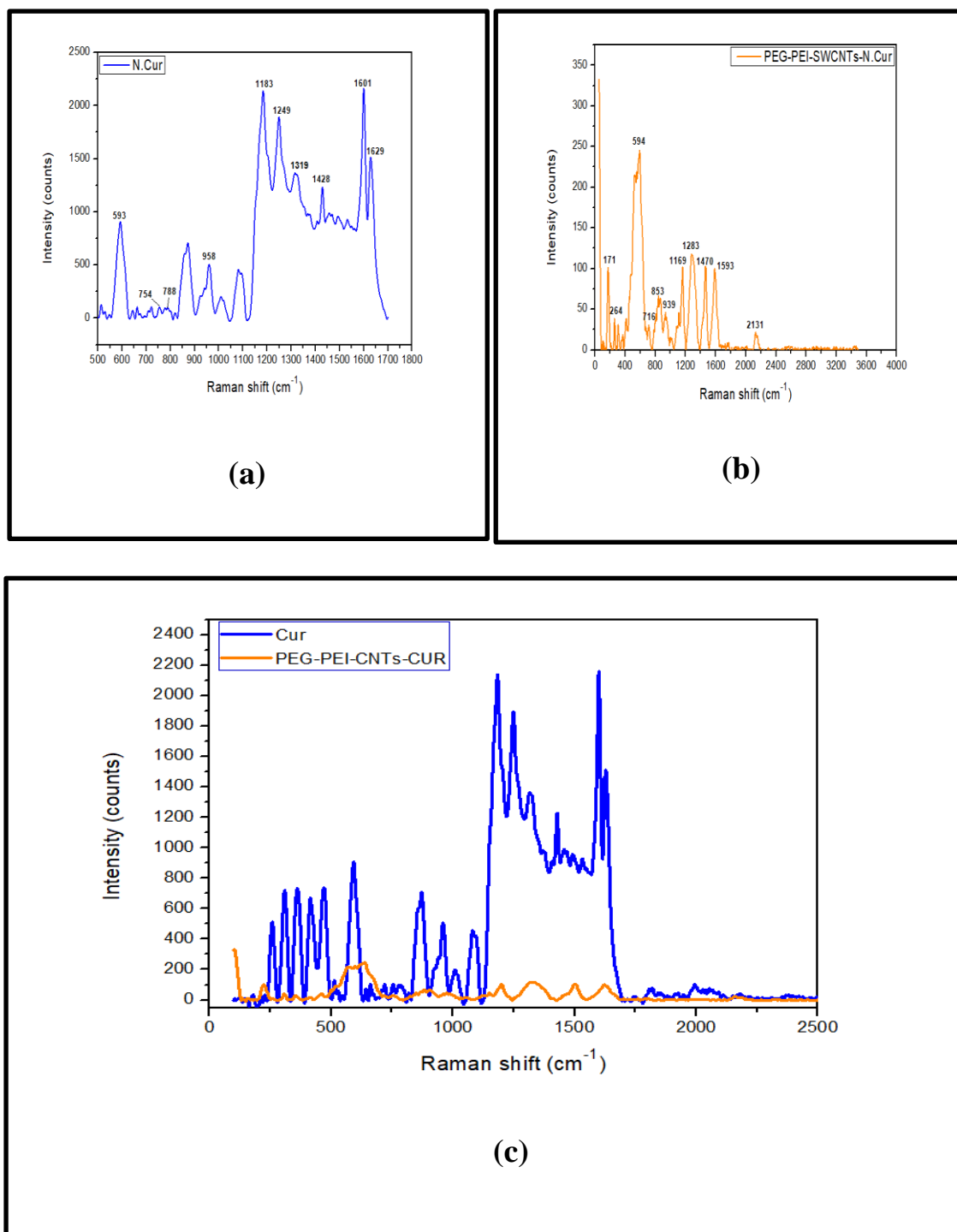


Figure (4-5): Raman Spectroscopy (a) N. Cur, (b) PEG-PEI-SWCNTs-N. Cur and (c) N. Cur and PEG-PEI-SWCNTs-N. Cur together.

4-4 Morphological Properties

4-4-1 Atomic Force Microscopy (AFM) Analysis

The AFM analysis of SWCNTs and SWCNTs – PEG4000 is shown in figure (4-6). The SWCNTs image shows a carbon nano tube with a grain size of (60 nm). SWCNTs – PEG4000 demonstrates aggregation of SWCNTs with PEG4000, with grain sizes increasing to (83.60 nm) with functionalization.

Images in figure (4-7) Shows the AFM analysis of PEG-PEI-SWCNTs, N.Cur and PEG-PEI-SWCNTs-N.Cur. Images of PEG-PEI-SWCNTs illustrated aggregation of carbon nanotube with PEG-PEI. The grain size increases with functionalizing to (80.68 nm). As a result of the extraction nanocurcumin the grain size is (129.96 nm), when adding the nanocurcumin to PEG-PEI-SWCNTs grain size equal (79.6 nm). The morphology of the different nanocarriers was observed using AFM. The raw SWCNTs exhibit large bundles of aggregates, and many long tubes stay close together, which is consistent with TEM images. Compared with the raw SWCNTs (figure 4-6-a), SWCNTs and PEG-PEI-SWCNTs samples are evenly dispersed exhibiting tubular structures (figures 4-6-a and 4-7-a), confirming their good dispersion. Moreover, their length is much shorter than that of the raw SWCNTs, also being consistent with the TEM observations. The above results prove that the raw SWCNTs were shortened by the acid treatment, together with an improvement of the dispersion state. Thus, highly stable dispersions of individual SWCNTs can be obtained by acidification and functionalization. All the above results demonstrate that the raw SWCNTs are shortened and functionalized while retaining their spectroscopically properties. The carbonylated and the functionalized SWCNTs are individually dispersed in aqueous solution, suitable for further biological studies. The result of surface roughness, root

mean square (RMS) and grain size of SWCNTs, PEG-SWCNTs, PEG-PEI-SWCNTs, N. Cur and PEG-PEI-SWCNTs-N. Cur are shown in table (4-2).

Table (4-2): Surface roughness, root mean square (RMS) and grain size of (SWCNTs, PEG-SWCNTs, PEG-PEI-SWCNTs, N. Cur and PEG-PEI-SWCNTs-N. Cur)

Sample	Surface roughness (nm)	RMS (nm)	Grain Size (nm)
SWCNTs	12.1	14.2	60.00
PEG-SWCNTs	6.84	7.9	83.60
PEG-PEI-SWCNTs	86.3	99.8	80.68
N. Cur	1.54	1.77	129.96
PEG-PEI-SWCNTs-N. Cur	51	59.3	79.60

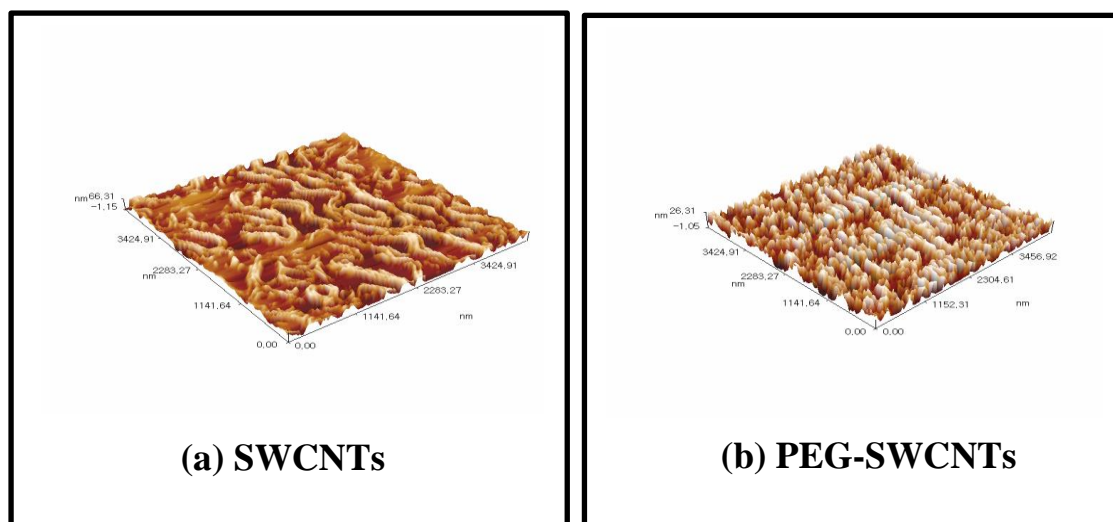


Figure (4-6): Surface images by AFM for (a) SWCNTs and (b) SWCNTs – PEG4000.

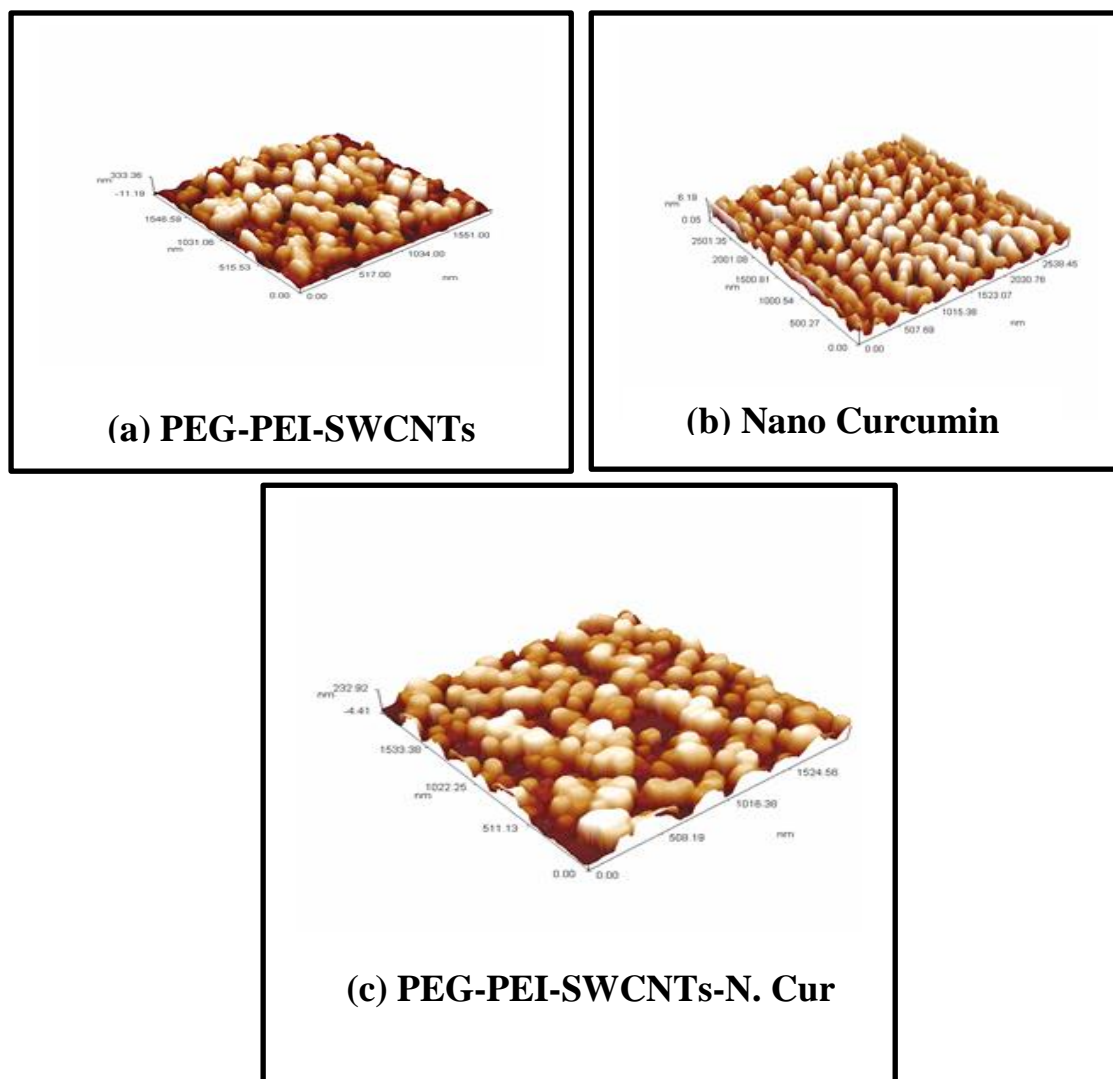


Figure (4-7): Surface images by AFM for (a) PEG-PEI-SWCNTs (b) Nanocurcumin (N. Cur) and (c) PEG-PEI-SWCNTs-N. Cur.

4-4-2 Transmission Electron Microscopy (TEM) Analysis

TEM was used to examine the morphology of SWCNTs and PEG-PEI-SWCNTs, TEM images of shortened and of functionalized SWCNTs are shown in figure (4-8). TEM images show that the raw SWCNTs are long curved aggregates, which appear to be a bundle of inhomogeneous aggregates consisting of many tubes (figure 4-8-a). The length and dispersion state of raw and of acid treated SWCNTs are quite different. After acid treatment, short SWCNTs exhibit a smaller tube length and a tubular structure with a hollow lumen, which is beneficial for the endocytosis of nanotubes. CNTs-COOH produced using different acid solutions, are all dispersed into single tubes with smooth surface without aggregation, and no obvious difference in the morphological characteristics is observed. The tubular structure of PEG-PEI-SWCNTs was rough, and some particles appear to be attached and distributed along the SWCNTs sidewalls, maybe indicating that PEG and PEI groups are conjugated onto nanotubes (figure 4-8-b). The N. Cur as shown in (4-8-c) confirms an average size of (30 nm) for the nanoparticles along with spherical morphology and low polydispersity while the designed drug of PEG-PEI-SWCNTs-N. Cur in figure (4-8-d) showed conjugated polymer with N. Cur.

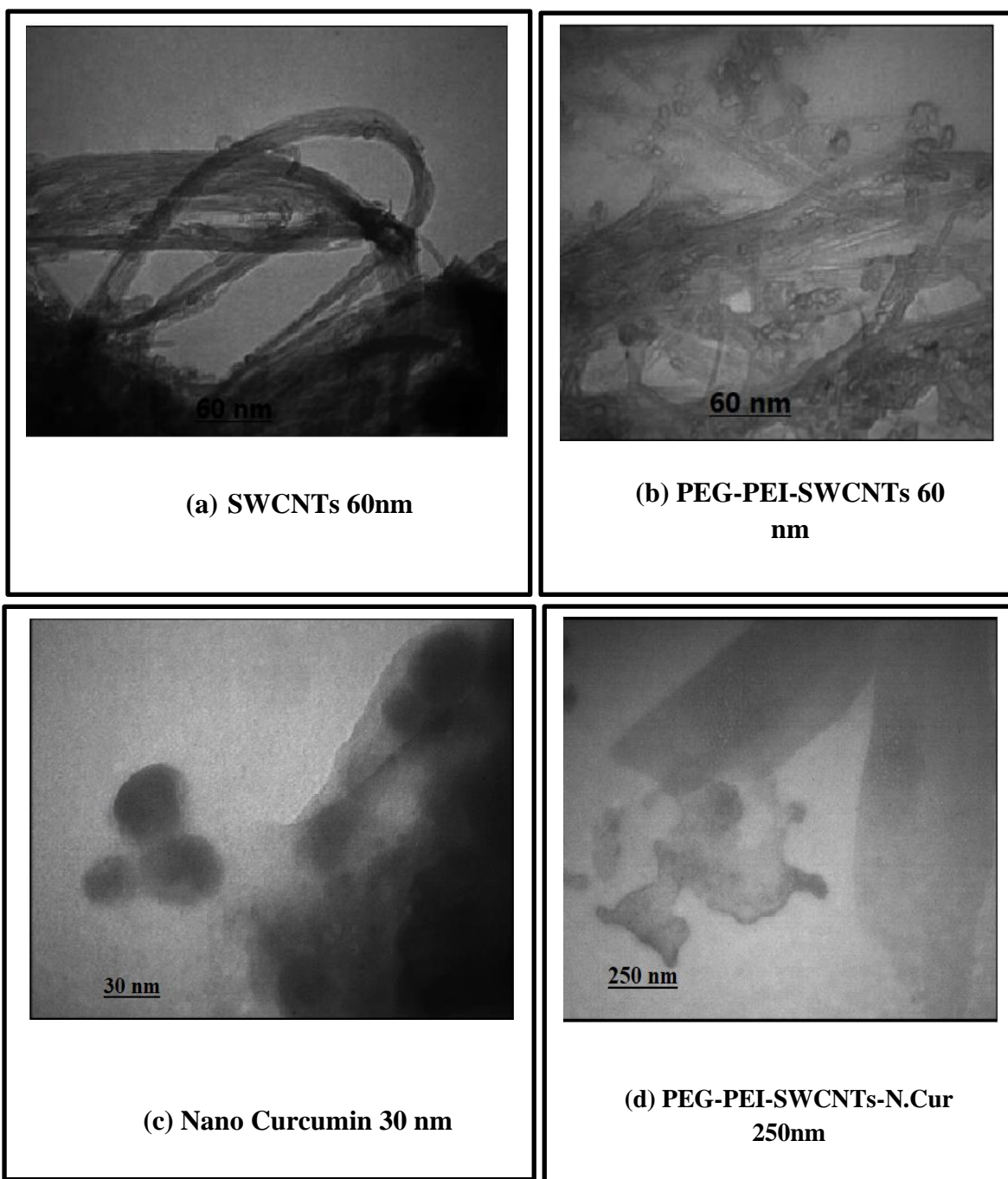


Figure (4-8): TEM images of (a)SWCNTs, (b) PEG-PEI-SWCNTs, (c) N. Cur and (d) PEG-PEI-SWCNTs-N. Cur.

4-5 Structural Properties

4-5-1 X-Ray Diffraction Analysis

The black line in figure (4-9-a) depicted the XRD pattern of SWCNTs, with a sharp peak at $2\theta = 25.6299^\circ$ that corresponds to (002) with d – spacing (3.4729 \AA) and conforms to the hexagonal structure of single wall carbon nanotube, while the red line in figure (4-9-b) depicted the functionalization of SWCNTs – PEG 4000, with a broad peak at $2\theta = 23.4473^\circ$ with d – spacing (3.8447 \AA) that is the result of d. The peak of SWCNTs disappear because SWCNTs has an effect on the structure of the PEG molecular chain in the crystal lattice, disturbing the order of its crystallization. This reduces the crystallinity of PEG and allows for effective ester bonding of PEG to SWCNTs. The orientation (002) is determined by a combination of a high score and a program. SWCNTs and SWCNTs-PEG have crystalline sizes of (3 and 7.7) nanometers, respectively. The green line in figure (4-9-c) indicates the functionalization of PEG-PEI-SWCNTs, which have a broad peak at $2\theta = 23.51^\circ$ with d – spacing (3.7816 \AA) and is the result of functionalization, presents a disrupted crystallization order. This reduces the crystallinity of PEG, allowing for efficient ester bonding of PEG-PEI to SWCNTs nanotubes. The orientation (002) is determined by the High Score Plus program. The values of crystalline size for SWCNT and PEG-PEI-SWCNTs equals (3 and 8.48) nm, respectively. while the orange line in figure (4-9-e) indicted to functionalization of PEG-PEI-SWCNTs-N.Cur with broad peak at $2\theta = 23.33^\circ$ with d – spacing (4.63888 \AA) which results from functionalized while the peak of SWCNTs disappears because SWCNTs have an effect on the structure of the PEG and PEI molecular chain in the crystal lattice ,

disturbing the order of its crystallization. This decreases the crystallinity of PEG-PEI and result in an effective conjugation of PEG-PEI to SWCNTs by ester bonding. Figure (4-9-d) as shown exhibited a mainly amorphous character. The values of crystallite size for SWCNTs and PEG-PEI-SWCNTs- N. Cur equals (3 nm) and (7.58 nm), respectively.

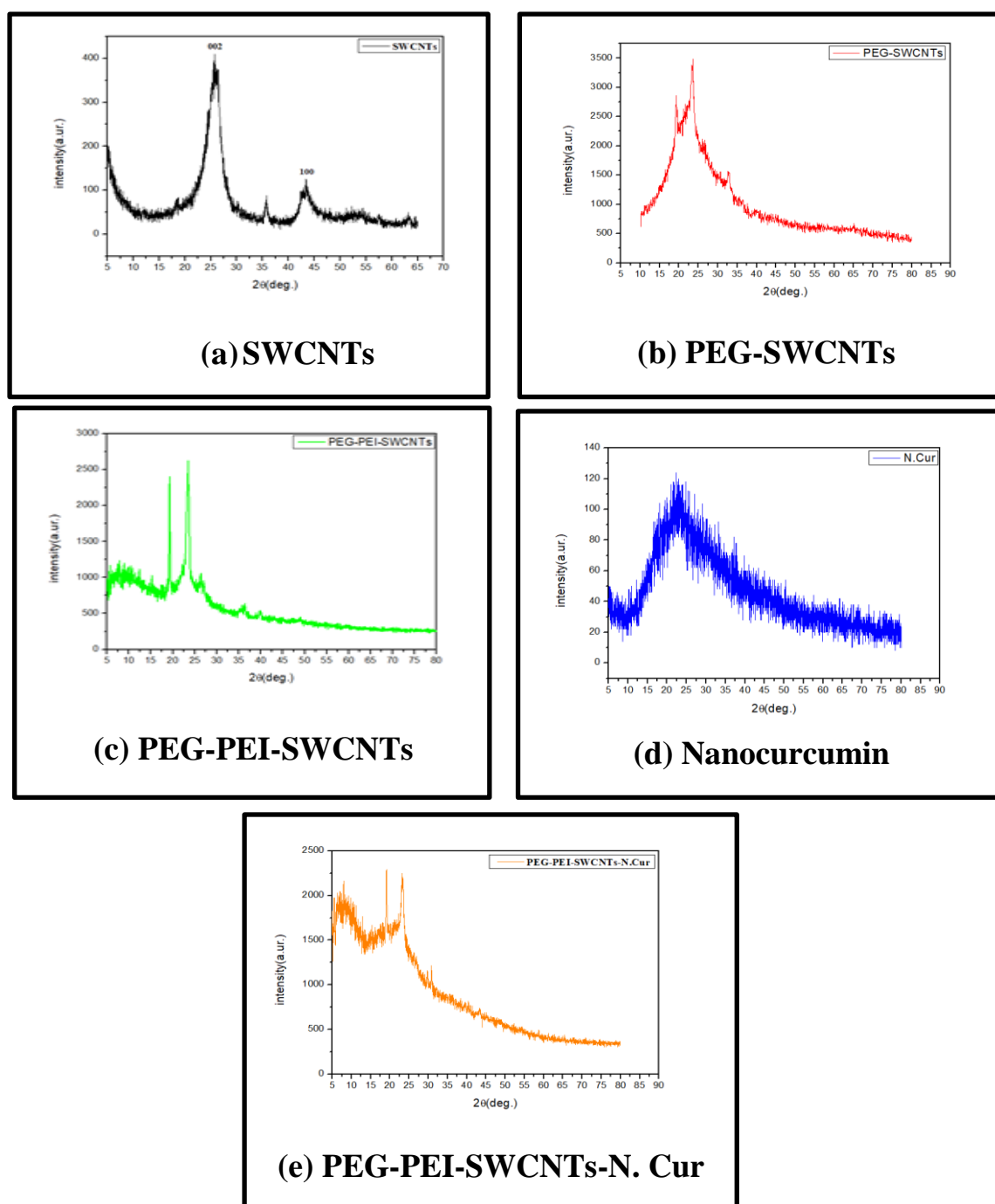


Figure (4-9): The XRD pattern for (a) SWCNTs, (b) PEG-SWCNTs, (c) PEG-PEI-SWCNTs, (d) N. Cur and (e) PEG-PEI-SWCNTs- N. Cur.

4-6 Biomedical Application Results

4-6-1 Antibacterial Activity

Bacillus Spp. and *Pseudomonas aeruginosa* were studied for the antibacterial activity of SWCNTs and PEG-SWCNTs by different volumetric ratios (25,50,75,100) $\mu\text{g/ml}$ expressed in figures (4-10 and 4-11). The inhibition zones were measured and reported. In general, the inhibition zone and the effect of PEG-SWCNTs on two types of antibacterial were greater than SWCNTs. This means the membrane of bacteria becomes weaker when SWCNTs was chemical modification and functionalization by PEG, where functionalization of SWCNTs could also increase SWCNTs dispersibility. This higher dispersibility may contribute enhanced antibacterial activity. The addition of PEG could effectively reduce the toxicity of SWCNTs to human cell and reduce bacterial adhesion [177]. SWCNTs -OH and -COOH functional groups develop more antibacterial action toward both Gram-positive and Gram-negative species. Functionalized carbon nanotubes form cell-SWCNTs collections which caused damage to cell walls due to which bacterial DNA releases from the cell [178]. Some studies show that single walled carbon nanotube (SWCNTs) cause severe cell damage and consequent cell death [179]. It happens because SWCNTs given their large surface areas and damaging capabilities of cell membrane through oxidation, hold disinfection efficiency [180]. Single wall carbon nanotube has higher thermal stability, the last was recorded besides that the large surface area of SWCNTs proved to enhance bacterial inactivation efficiency [181], the microbes removal activity by SWCNTs in that interaction by direct contact with bacterial cell membrane led to inactivation [182]. The mechanism of single wall carbon nanotube against bacterial strains is related to the fact that the cell membrane of the bacteria is composed of lipopolysaccharides which act as

a barrier, where its structural integrity can be degraded when exposed to carbon based nanomaterials, this has been established to be due to the oxidative toxicity of SWCNTs which causes oxidative stress in microbial cell that will lead to inactivation [183], surface area plays a major role in bacterial inactivation by inhibiting the vital metabolic functions of bacteria [184], bacterial deactivation occurred by adsorption on to nisin [185], SWCNTs prevent the bacterial cell division and their capability to multiply by penetrating the cell and disturbing its intracellular network [186], the impact of SWCNTs length on their antimicrobial action was explored they discovered that longer SWCNTs established stronger antimicrobial action because of their improved aggregation with bacterial cell [187], the longer SWCNTs may cause antimicrobial action by covering the bacterial [188], carbon nanostructures are reported to cause bacterial cell lysis by physical excoriation and disrupting cell walls and membranes of bacteria ultimately to cell death [189], direct contact between cells and carbon nano partial which thus lead to cell demise, carbon nanotubes damage the bacteria via phospholipid peroxidation or oxidative stress and SWCNTs oxidize the bacterial cell which leads towards oxidation resulting in cell death [190,191]. Single well carbon nanotube efficiency in microbial removal is affected by several operational condition such as temperature, pH, retention time, solute and solvent composition [192].

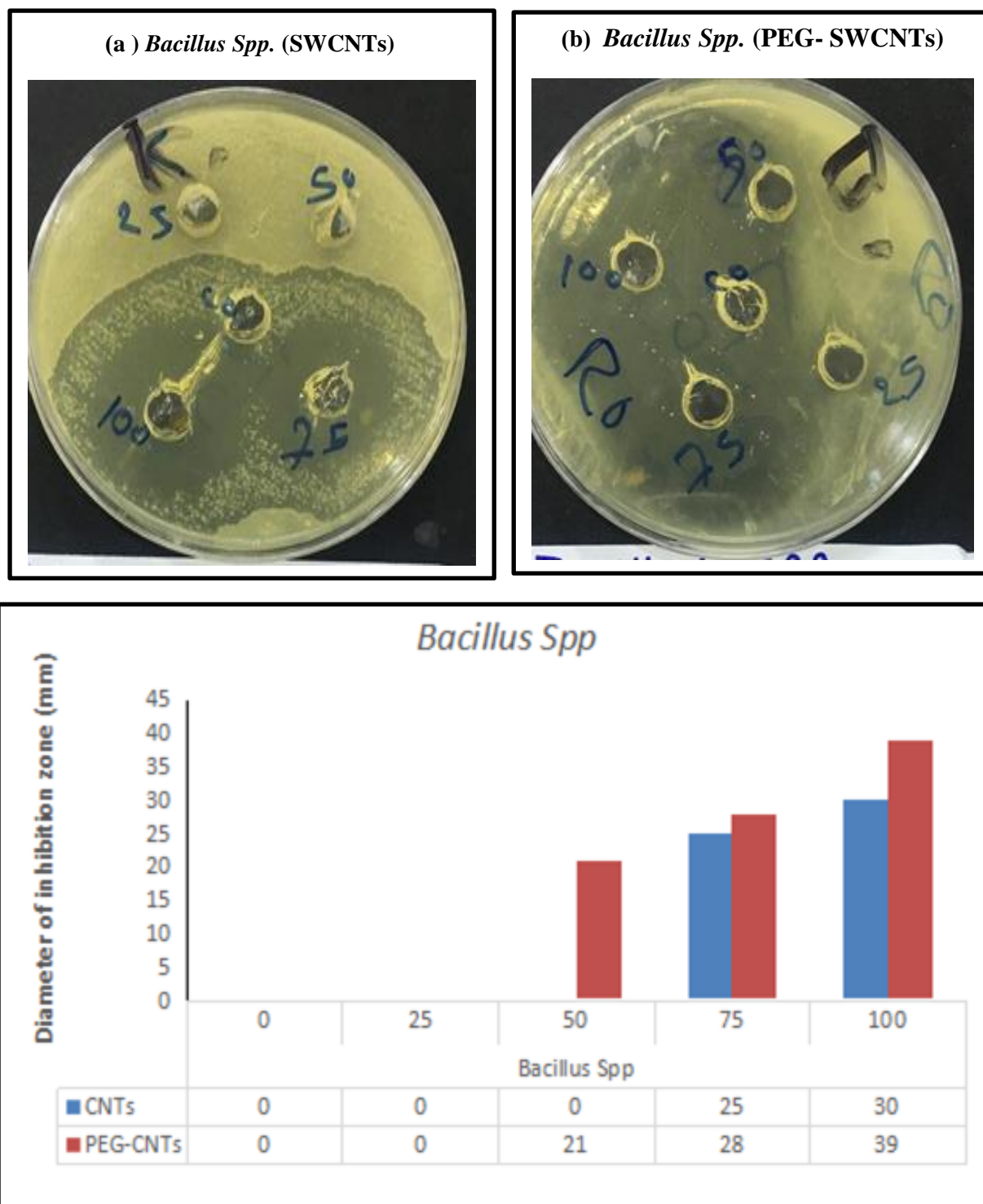


Figure (4-10): Anti-bacterial activity of (a) SWCNTs, (b) PEG- SWCNTs *Bacillus SPP.*, the inhibited zones of bacterial growth for both strains are illustrated when exposed to variety concentrations as follows; (1): 25µg/ mL, (2): 50 µg/ mL, (3): 75 µg/ mL, (4): 100 µg/ mL.

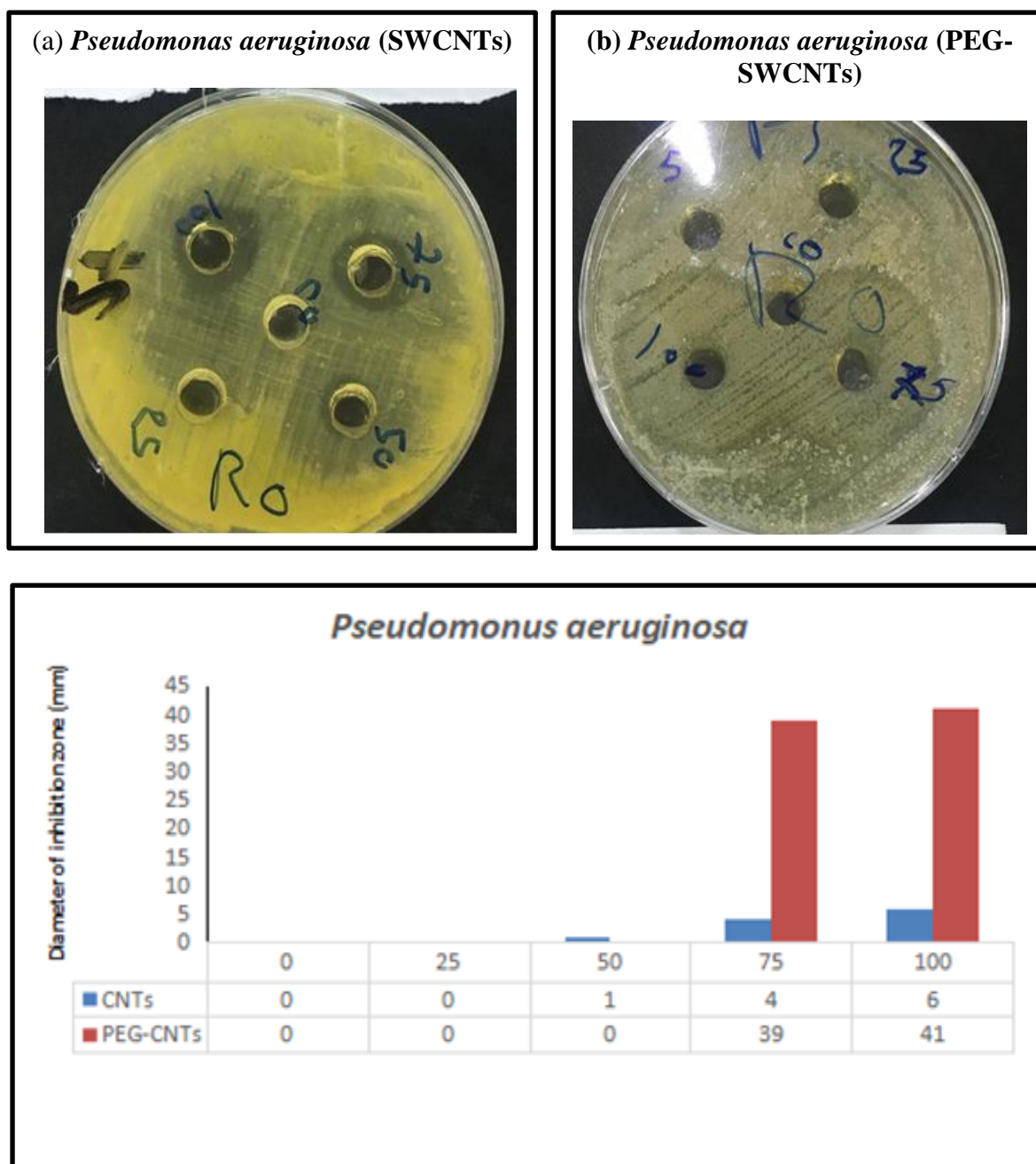


Figure (4-11): Anti-bacterial activity of (a)SWCNTs, (b) PEG-SWCNTs, *Pseudomonas aeruginosa*, the inhibited zones of bacterial growth for both strains are illustrated when exposed to variety concentrations as follows: (1) 25 $\mu\text{g}/\text{mL}$, (2): 50 $\mu\text{g}/\text{mL}$, (3): 75 $\mu\text{g}/\text{mL}$, (4): 100 $\mu\text{g}/\text{mL}$.

4-6-2 Anti-Proliferative Activity Against Cancer Cell Line

4-6-2-A Anti-Proliferative Activity of (SWCNTs) Against Cancer Cell Line

The cytotoxic effect of SWCNTs against Hep G2 and AMJ13 cells was studied to show the effectiveness of these substances in killing infected cells at a range of concentrations ranging between (6.26–100 $\mu\text{g/ml}$), as shown in figures (4-12-a and 4-12-b). These substances show killing activity for the cells under study, with effectiveness increasing with increased concentration of the SWCNTs based on figures (4-12-a), we note that (60%) of the AMJ13 cells were killed with a concentration of (100 $\mu\text{g/ml}$) of SWCNTs. Figure (4-12-b) shows that (55%) of the Hep G2 cells was killed at a concentration of (100 $\mu\text{g/ml}$) of SWCNTs. The apoptosis features were also examined through morphological changes in Hep G2 and AMJ13 cell lines. The treated cells retained their original morphological forms, as shown by the control cells. However, both cell lines showed morphological alterations when treated with SWCNTs. Figure (4-13) shows that those treated with the SWCNTs had lower toxicity, owing to a decrease in the number of HepG2 and AMJ13 cell colonies, indicating significant cell-killing activity [193,194]. The differences in morphology, loss of contact with surrounding cells, and a decrease in the number of cells as concentrations increase during treatment may be due to the synergistic effect of nanoparticles at high concentrations, so their effect is greater than that at lower concentrations [195], biocompatible of single wall carbon tubes, the peculiar features of SWCNTs, such as broad surface area, high aspect ratio, and strong stability enables them to utilize in drug-delivery systems. The characteristics of SWCNTs make them efficient to load drugs in them or to attach drugs with their surfaces, respectively. Due to their distinctive properties, they can be a potent nano-carrier for the deliverance of drug, biomolecule, gene, DNA/RNA, enzymes/proteins to a targeted organ, cell or tissue [196].

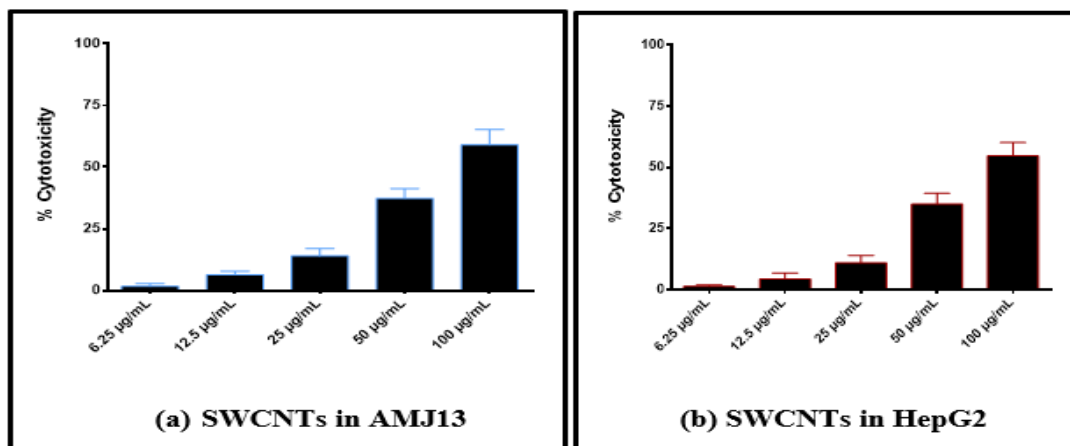


Figure (4-12): Cytotoxic effect of (a) SWCNTs in AMJ13 cell, (b) SWCNTs in HepG2 cells.

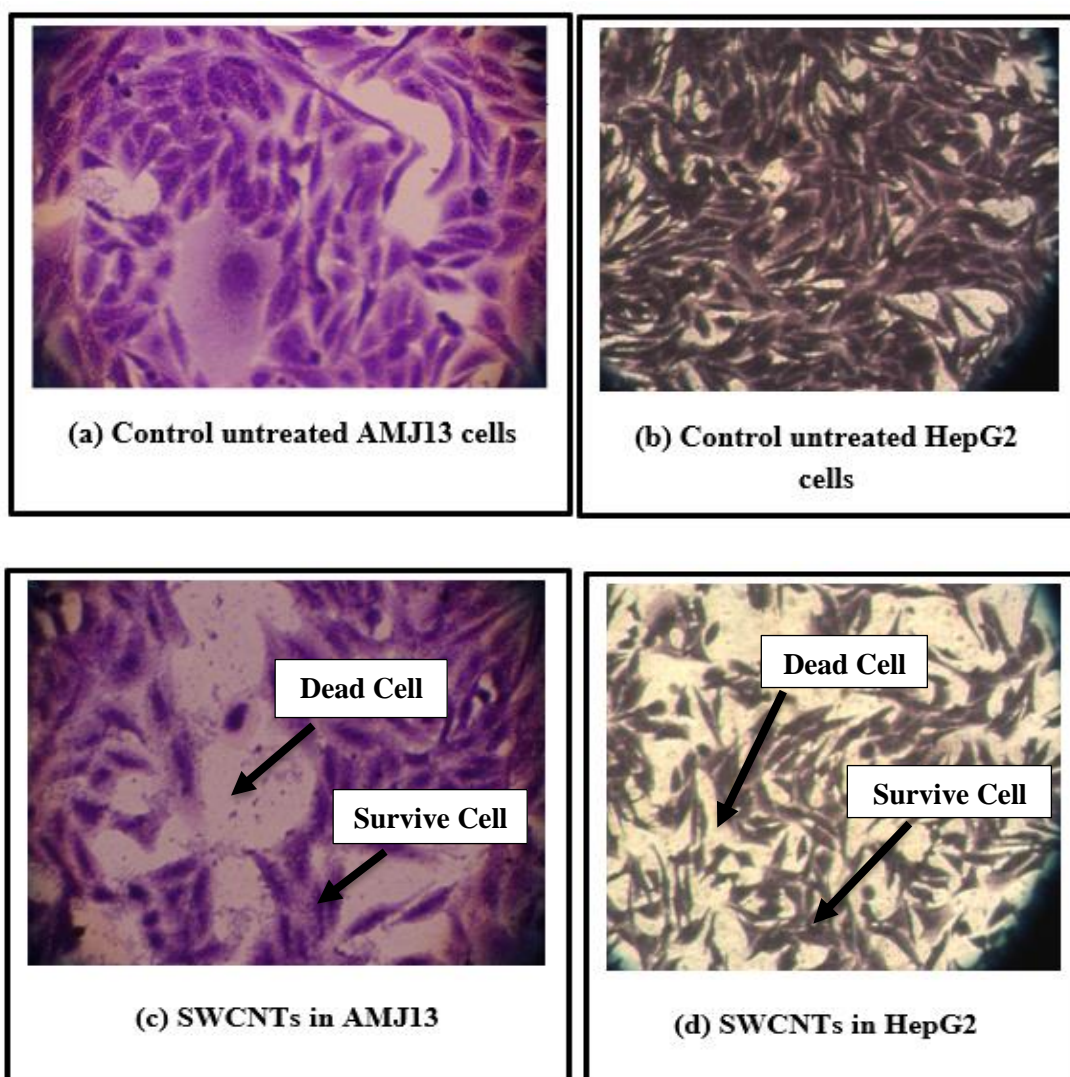


Figure (4-13): Morphological changes in (AMJ13, HepG2) Cells after treated with SWCNTs.

4-6-2-B Anti-Proliferative Activity of (PEG-SWCNTs) Against Cancer Cell Line

The cytotoxic effect of PEG- SWCNTs against Hep G2 and AMJ13 cells was studied to show the effectiveness of these substances in killing infected cells at a range of concentrations ranging between (6.26–100 mg/ml), as shown in figures (4-14-a and 4-14-b). These substances show killing activity for the cells under study, with effectiveness increasing with increased concentration of the PEG-SWCNTs based on figures (4-14-a), we note that (74%) of the AMJ13 cells were killed with a concentration of (100 μ g/ml) of PEG-SWCNTs. Figure (4-14-b) shows that (70%) of the Hep G2 cells was killed at a concentration of (100 μ g/ml) of PEG-SWCNTs. The apoptosis features were also examined through morphological changes in Hep G2 and AMJ13 cell lines. The treated cells retained their original morphological forms, as shown by the control cells. However, both cell lines showed morphological alterations when treated with PEG- SWCNTs. figure (4-15) show that those treated with the PEG-SWCNTs had lower toxicity, owing to a decrease in the number of HepG2 and AMJ13 cell colonies, indicating significant cell-killing activity [193,194]. We notice from figures (4-14-a and 4-14-b) that the rate of cell killing using (PEG-SWCNTs) for both types of cancer cells (AMJ13, HepG2) is greater if compared to (SWCNTs) only. This could be due to the grafting of PEG onto the SWCNTs, resulting in the formation of an effective electrostatic layer in solution, or it could be due to the improvement of dispersal (SWCNTs) by PEG. The anti-static force between the SWCNTs overcomes gravity and van der Waals interactions, resulting in increased water solubility. This finding demonstrates that using PEG to modify the surface of SWCNTs increases their biocompatibility. This could be due to the fact that PEG is non-toxic, non-antigenic, and non-immunogenic, as well as having unique physicochemical features and

strong biocompatibility. As a result, when it's employed to modify SWCNTs as a functional group [197].

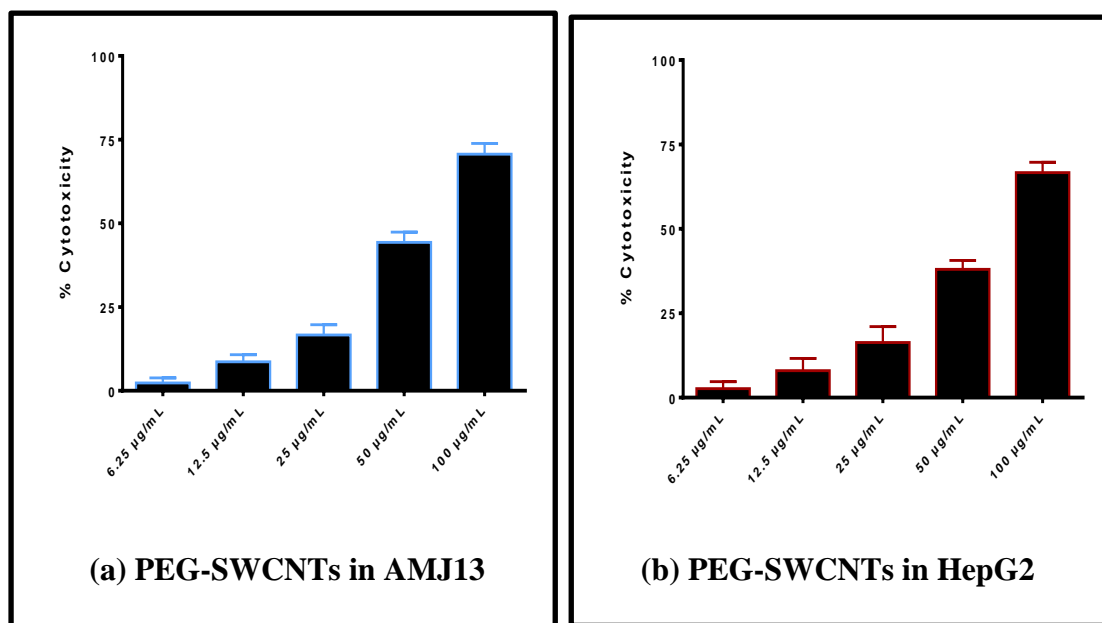


Figure (4-14): Cytotoxic effect of (a)PEG-SWCNTs in AMJ13 cell, (b) PEG- SWCNTs in HepG2 cells.

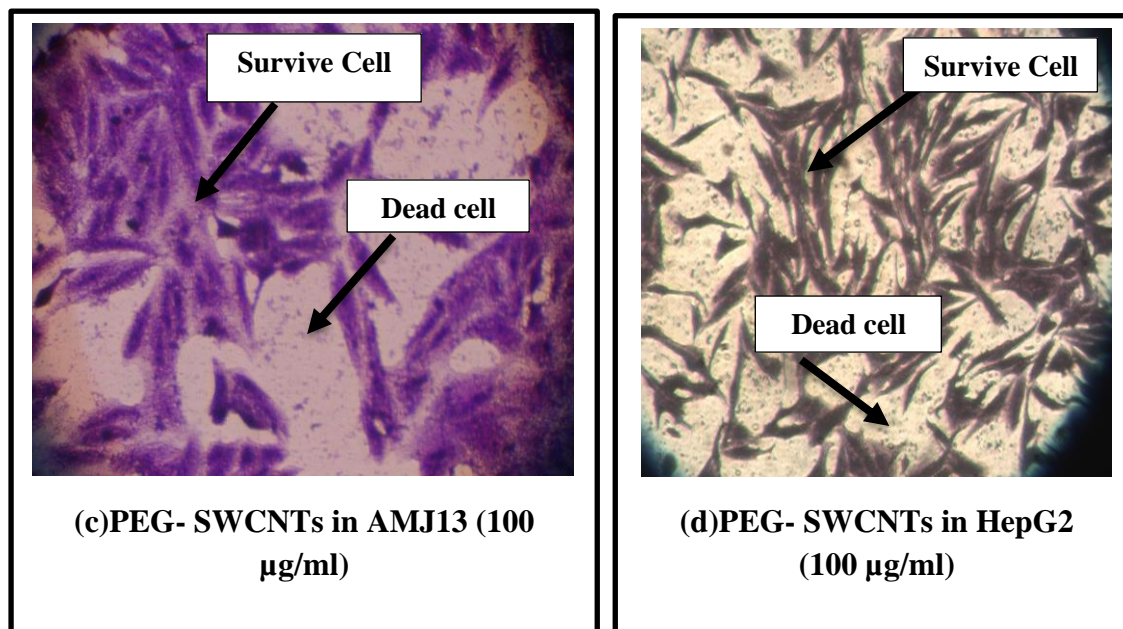


Figure (4-15): Morphological changes in (AMJ13, HepG2) Cells after treated with PEG- SWCNTs.

4-6-2-C Anti-Proliferative Activity of (PEG-PEI-SWCNTs) Against Cancer Cell Line

The cytotoxic effect of PEG-PEI- SWCNTs against Hep G2 and AMJ13 cells was studied to show the effectiveness of these substances in killing infected cells at a range of concentrations ranging between (6.26–100 $\mu\text{g/ml}$), as shown in figures (4-16-a and 4-16-b). These substances show killing activity for the cells under study, with effectiveness increasing with increased concentration of the PEG-SWCNTs based on figure (4-16-a), we note that (75%) of the AMJ13 cells were killed with a concentration of (100 $\mu\text{g/ml}$) of PEG-SWCNTs. Figure (4-16-b) shows that (74%) of the Hep G2 cells was killed at a concentration of (100 $\mu\text{g/ml}$) of PEG-PEI-SWCNTs. The apoptosis features were also examined through morphological changes in Hep G2 and AMJ13 cell lines. The treated cells retained their original morphological forms, as shown by the control cells. However, both cell lines showed morphological alterations when treated with PEG-PEI- SWCNTs. Figure (4-17) shows that those treated with the PEG-PEI- SWCNTs had lower toxicity, owing to a decrease in the number of HepG2 and AMJ13 cell colonies, indicating significant cell-killing activity [193,194]. We notice from figures (4-16-a and 4-16-b) that the rate of cell killing using (PEG-PEI-SWCNTs) for both types of cancer cells (AMJ13, HepG2) is greater if compared to (SWCNTs) only, this may be because PEI can be chemically modified to alter SWCNTs' surface charges and cytotoxicity, thereby significantly improving the biocompatibility of the materials for a variety of biomedical applications [198]; this change is due to PEI polymers' high positive charge density due to the presence of ammonium (NH_4^+) ions. PEI polymers have been widely used as a coating material for inorganic nanoparticles as well as polymeric carriers for gene delivery due to their strong electrostatic affinity for polynucleic acids. They also display an endosomal escape capability via the "proton sponge"

effect after intracellular uptake [199], SWCNTs conjugated with PEG and polyethylenimine (PEI), which contains amino groups, were synthesized (CNTs-PEG-PEI). The length of the SWCNTs was first shortened by ultrasonic scission in different strong acid solutions for improving the dispersion in water. Afterwards, PEG and PEI were grafted onto the CNTs. This functionalization was supposed to attenuate the premature removal and loss of nanocarriers, and also to improve the targeting to the tumor site [200], the high number of positively charged amino groups on their surface, which leads to higher toxicity, the carboxylated and functionalized CNTs are more biocompatible [201]. This is attributed to the fact that PEGylation and amino functionalization could be significant in facilitating the dispersion of nanotubes and decreasing their aggregation, which protects the CNT carriers from interaction with plasma protein components. This result indicates that acidification treatment and the resulting enhancement of water dispersion yields more biocompatible SWCNTs nanocarriers with low cytotoxicity [202].

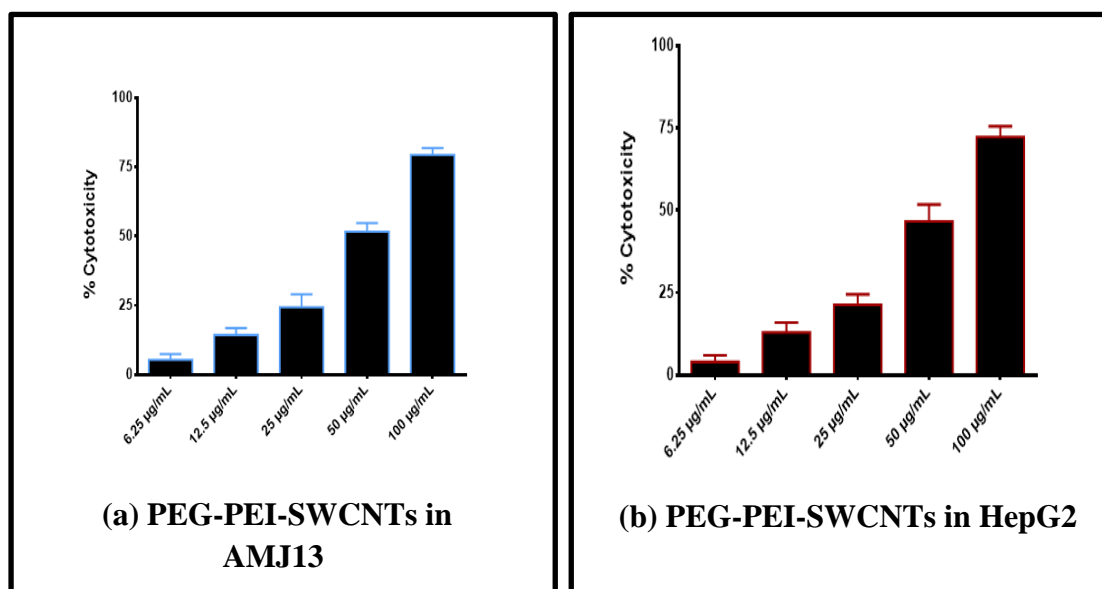


Figure (4-16): Cytotoxic effect of (a) PEG-PEI-SWCNTs in AMJ13 cell, (b) PEG-PEI-SWCNTs in HepG2 cells.

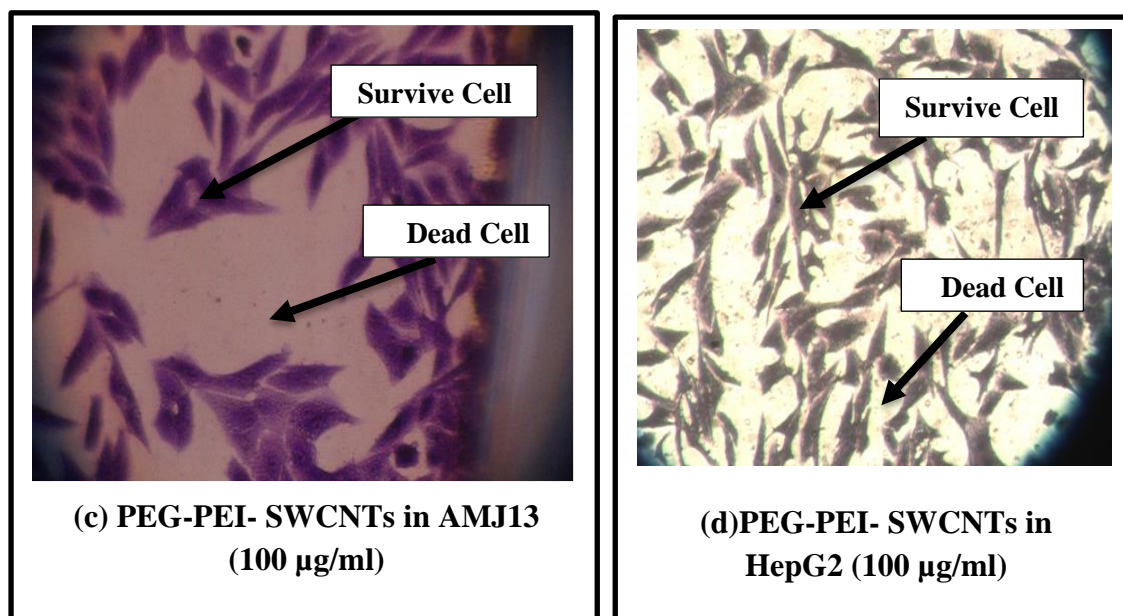


Figure (4-17): Morphological changes in (AMJ13, HepG2) Cells after treated with PEG-PEI- SWCNTs.

4-6-2-D Anti-Proliferative Activity of (PEG-PEI-SWCNTs-N. Cur) Against Cancer Cell Line

The cytotoxic effect of PEG-PEI- SWCNTs-N.Cur against Hep G2 and AMJ13 cells was studied to show the effectiveness of these substances in killing infected cells at a range of concentrations ranging between (6.26–100 µg/ml), as shown in Figure (4-18-a and 4-18-b). These substances show killing activity for the cells under study, with effectiveness increasing with increased concentration of the PEG-PEI-SWCNTs-N.Cur based on figure (4-18-a), we note that (90%) of the AMJ13 cells were killed with a concentration of (100 µg/ml) of PEG-PEI-SWCNTs-N.Cur. Figure (4-18-b) shows that (85%) of the Hep G2 cells was killed at a concentration of (100 µg/ml) of PEG-PEI-SWCNTs-N,Cur. The apoptosis features were also examined through morphological changes in Hep G2 and AMJ13 cell lines. The treated cells retained their original morphological forms, as shown by the control cells. However, both cell lines showed morphological alterations when treated with PEG-PEI- SWCNTs-N.Cur. Figure (4-19)

shows that those treated with the PEG-PEI- SWCNTs-N.Cur had lower toxicity, owing to a decrease in the number of HepG2 and AMJ13 cell colonies, indicating significant cell-killing activity, this may be because loading nano curcumin on SWCNTs where the functionalized CNTs using poly ethylene glycol (PEG) and polyethylenimine (PEI) helped in the modification of CNTs surface with different functional groups such as terminal amine and carboxyl groups. These functional groups enhanced the dispersibility of the SWCNT in the aqueous phase, facilitated binding of an anticancer drug, N. Cur, increased the circulation time, and enhanced permeability and retention effects in the tumor cells [193,194], and curcumin has a toxic effect on cancerous cells but is cytoprotective to healthy cells. Along with substantial antioxidative capacity [195], curcumin is an ideal chemo preventive agent, with properties such as inhibition of cell proliferation and reactive oxidative species, promotion of apoptosis by inhibiting different intracellular transcription factors [203]. These findings suggest that anticancer herbal drugs, when delivered through nanocarrier based approaches, results in high drug loading and therefore it can be a useful therapy for cancer, with minimal side effects. However, selective targeting is still a challenge regarding specificity, bioavailability, toxicity, which could be overcome by carbon nanotubes (SWCNTs). The unique physicochemical properties of SWCNTs are such that they can cross many biological membranes, which has proved useful in both in vivo and in vitro studies [204], without any immunogenic or toxic effect. Suitable functionalization of SWCNTs by the peptide, targeting ligand or attachment of a functional group helps in achievement of site-specific delivery of a drug by site-specific recognition of the carrier [205].

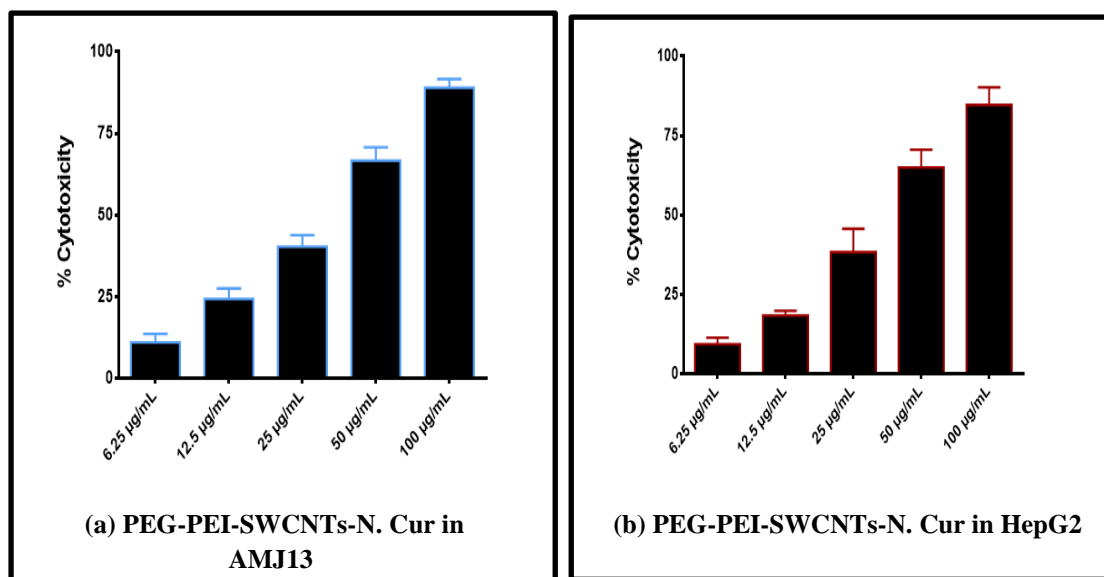


Figure (4-18): Cytotoxic effect of (a)-PEG-PEI-SWCNTs-N. Cur in AMJ13 cell, (b)- PEG-PEI- SWCNTs-N. Cur in HepG2 cells.

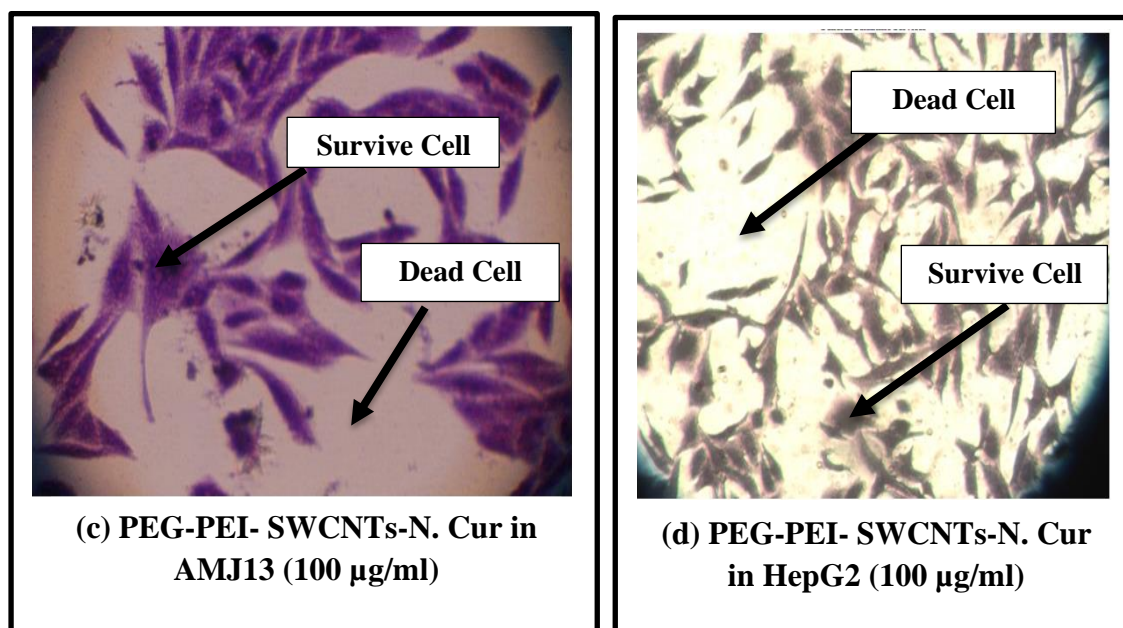


Figure (4-19): Morphological changes in (AMJ13, HepG2) Cells after treated with PEG-PEI- SWCNTs-N.Cur.

4-6-3 Anti-Proliferative Activity of Normal Cancer Cell Line

4-6-3-A Effect of SWCNTs on Normal Cell Line (RD)

The cytotoxic effect of SWCNTs on normal cell line (RD) was studied to show the effectiveness of these substances in killing infected cells at a range of concentrations ranging between (6.26–100 $\mu\text{g/ml}$), as shown in figure (4-20). These substances show killing activity for the cells under study, with effectiveness increasing with increased concentration of the SWCNTs based on figures (4-20), we note that (42.61%) of the (RD) cells were killed with a concentration of (100 $\mu\text{g/ml}$) of SWCNTs, this result shown is in table (4-3).

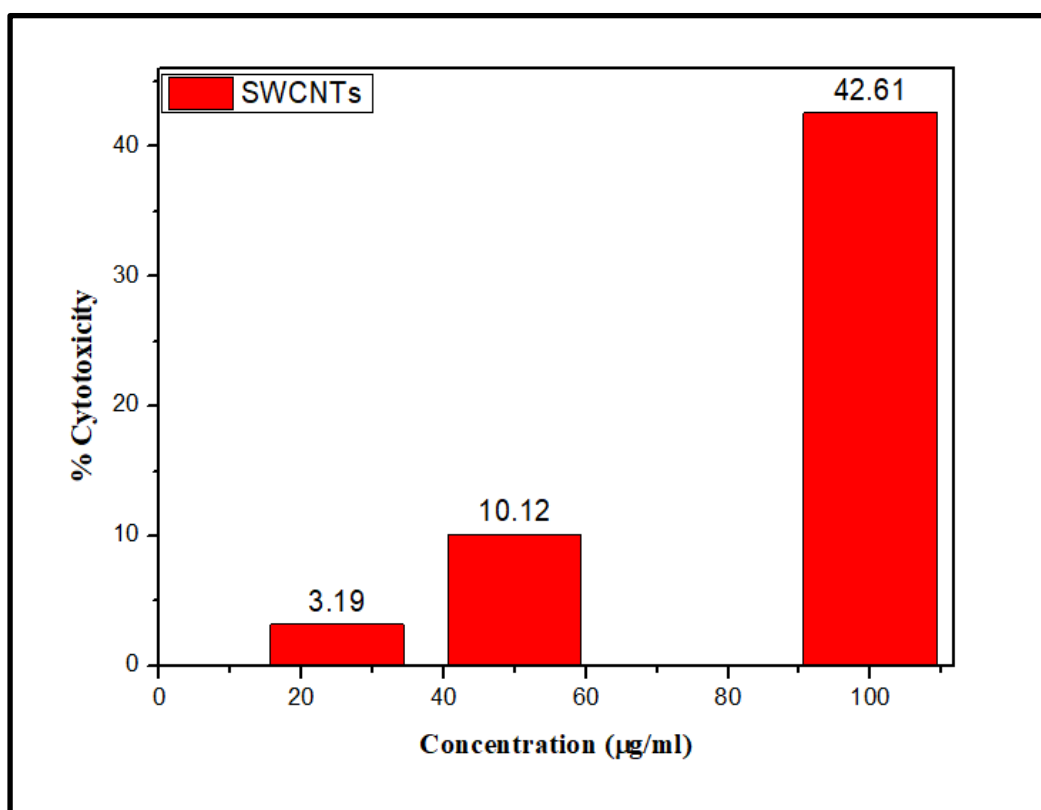


Figure (4--20): Cytotoxic effect of of SWCNTs on normal cell line (RD).

Table (4-3): Inhibition rates in the normal cell line RD by the effect of different concentrations of CNT for an exposure period of (72 hours) and a temperature of (37 ° C).

Concentration (µg/ml)	Ratio Inhibition ± Standard Deviation
6.25	0 c
12.5	0 c
25	3.19 c ± 1.0
50	10.12 b ± 1.1
100	42.61 a ± 1.3

The different letters in the same column indicate that there are statistical differences at the level of $0.05 \geq P$.

The inverted microscope images showed the effect of SWCNTs on the normal cell line (RD) at (6.25 µg/ml) concentration and (100 µg/ml) concentration shown in figures (4-21-a,b).

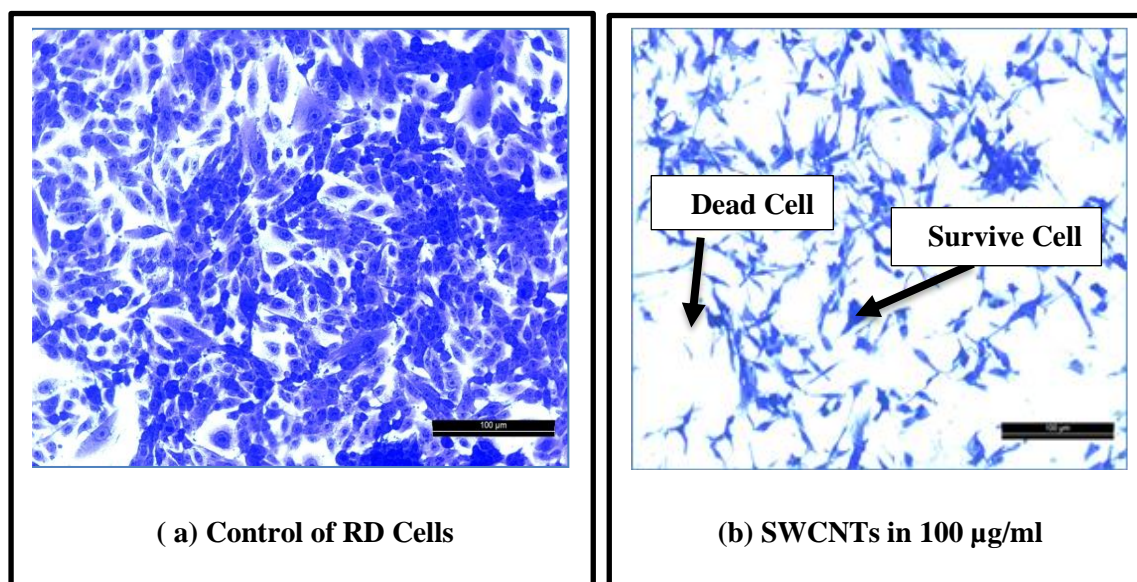


Figure (4-21): Inverted microscope image showing effect of different concentrations of SWCNTs.

4-6-3-B Effect of PEG-PEI-SWCNTs on Normal Cell Line (RD)

The cytotoxic effect of SWCNTs on normal cell line (RD) was studied to show the effectiveness of these substances in killing infected cells at a range of concentrations ranging between (6.26–100 $\mu\text{g/ml}$), as shown in figure (4-22). These substances show killing activity for the cells under study, with effectiveness increasing with increased concentration of the SWCNTs based on figure (4-22), we note that (29.21%) of the (RD) cells were killed with a concentration of (100 $\mu\text{g/ml}$) of SWCNTs, this result is shown in table (4-4).

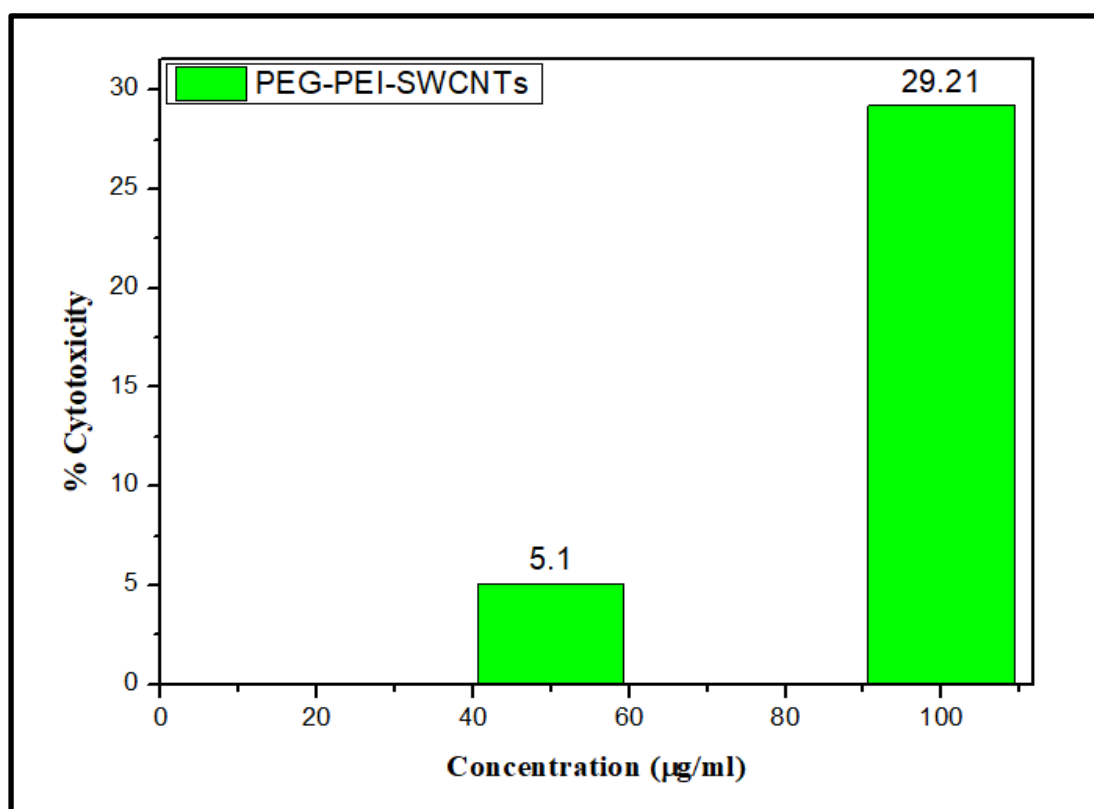


Figure (4-22): Cytotoxic effect of of PEG-PEI- SWCNTs on normal cell line (RD).

Table (4-4): Inhibition rates in the normal cell line RD by the effect of different concentrations of PEG-PEI-SWCNT for an exposure period of (72 hours) and a temperature of (37 ° C).

Concentration (µg/ml)	Ratio Inhibition ± Standard Deviation
6.25	0 c
12.5	0 c
25	0
50	5.10 b ± 1.3
100	29.21 a ± 1.0

The different letters in the same column indicate that there are statistical differences at the level of $0.05 \geq P$.

The inverted microscope images showed the effect of PEG-PEI-SWCNTs on the normal cell line (RD) at (6.25 µg/ml) concentration and (100 µg/ml) concentration shown in figures (4-23-a,b).

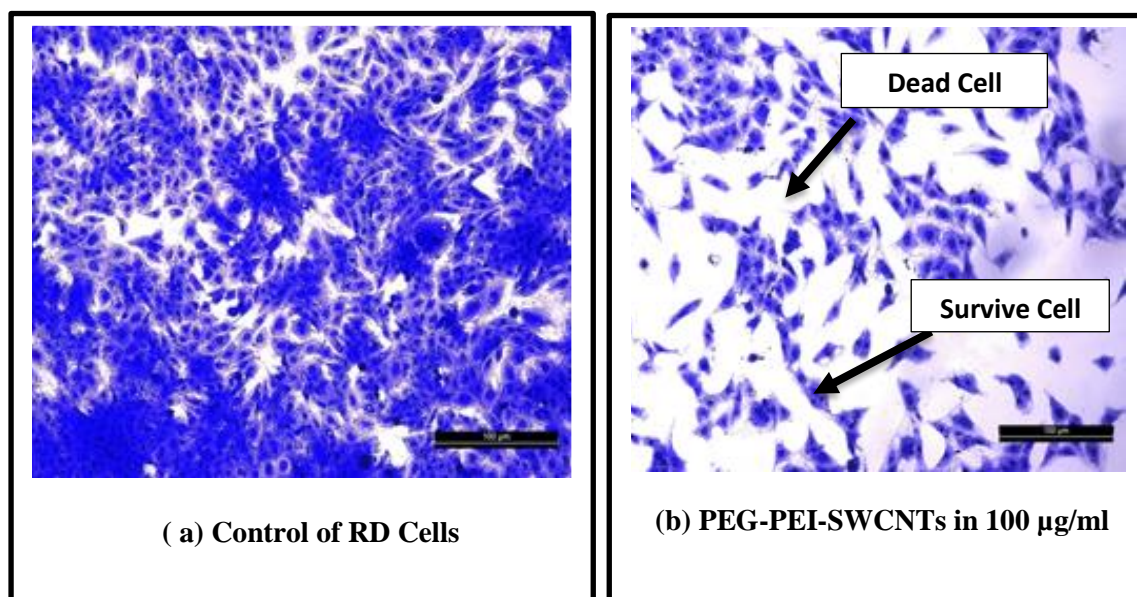


Figure (4-23): Inverted microscope image showing effect of different concentrations of PEG-PEI- SWCNTs.

4-6-3-C Effect of PEG-PEI-SWCNTs-N.Cur on Normal Cell Line (RD)

The cytotoxic effect of SWCNTs on normal cell line (RD) was studied to show the effectiveness of these substances in killing infected cells at a range of concentrations ranging between (6.26–100 $\mu\text{g/ml}$), as shown in figure (4-24). These substances show killing activity for the cells under study, with effectiveness increasing with increased concentration of the SWCNTs based on figures (4-24), we note that (44.61%) of the (RD) cells were killed with a concentration of (100 $\mu\text{g/ml}$) of SWCNTs, this result is shown in table (4-5).

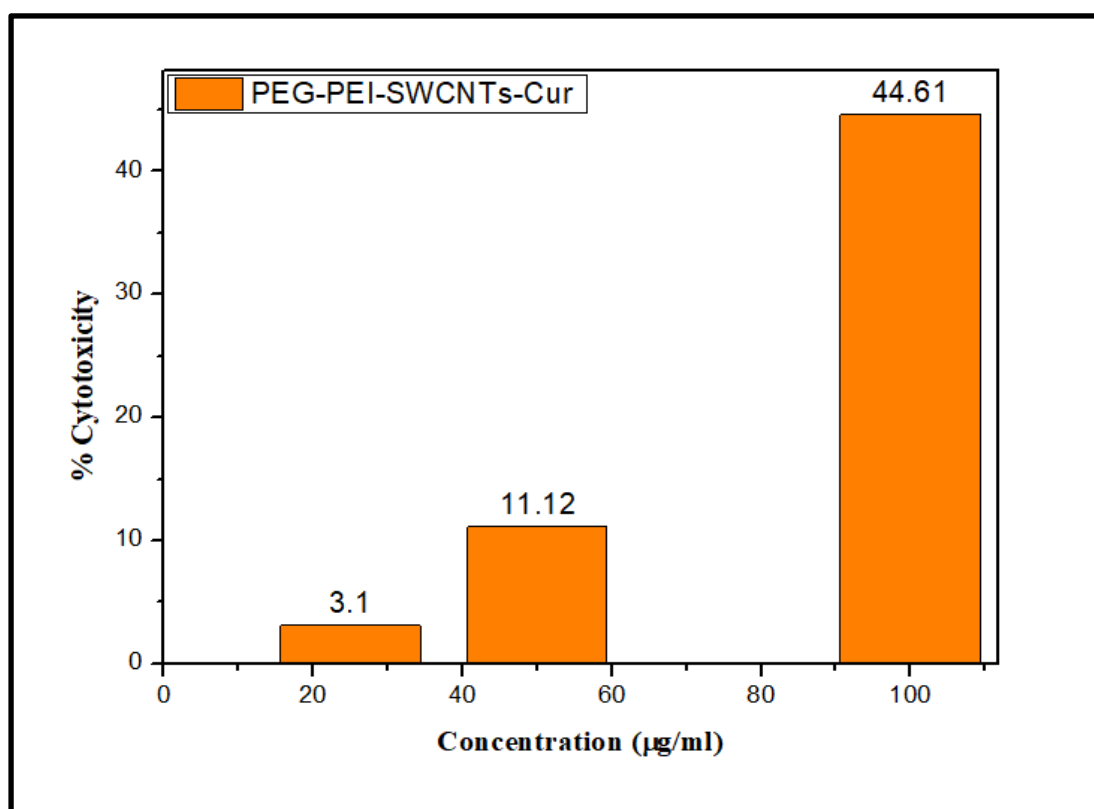


Figure (4-24): Cytotoxic effect of of PEG-PEI- SWCNTs-N. Cur on normal cell line (RD).

Table (4-5): Inhibition rates in the normal cell line RD by the effect of different concentrations of PEG-PEI-SWCNTs-N. Cur for an exposure period of (72 hours) and a temperature of (37 ° C).

Concentration (µg/ml)	Ratio Inhibition ± Standard Deviation
6.25	0 c
12.5	0 c
25	3.10b ±1.3
50	11.12 b ± 1.5
100	44.61 a ± 1.0

The different letters in the same column indicate that there are statistical differences at the level of $0.05 \geq P$.

The inverted microscope images showed the effect of PEG-PEI-SWCNTs-N. Cur on the normal cell line (RD) at (6.25 µg/ml) concentration and (100 µg/ml) concentration shown in figures (4-25-a,b).

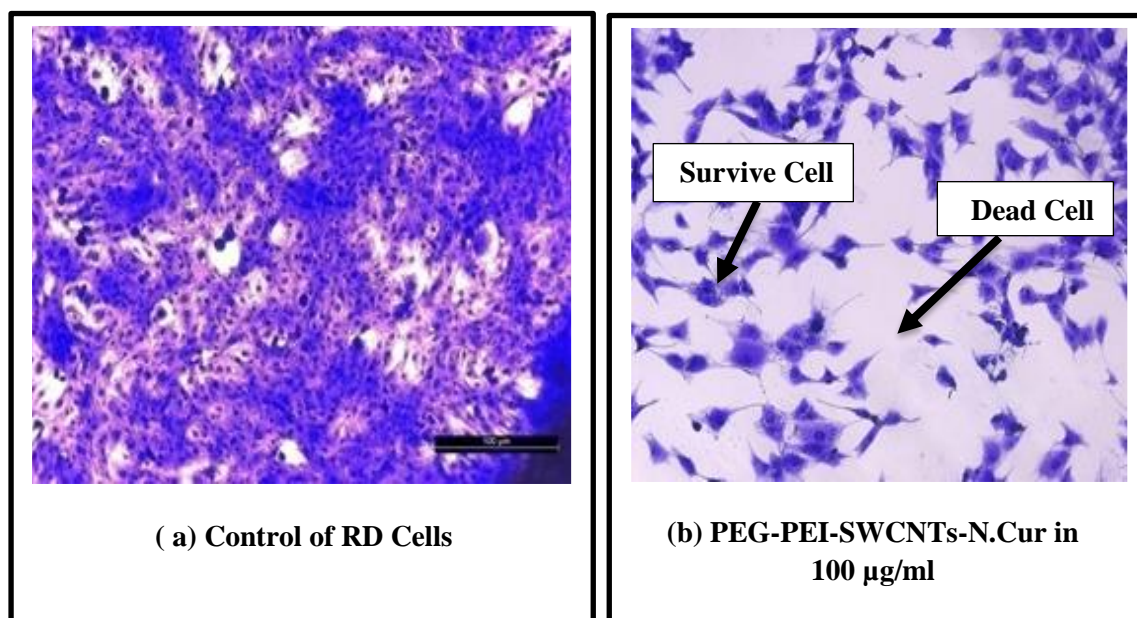


Figure (4-25): Inverted microscope image showing effect of different concentrations of PEG-PEI- SWCNTs -N.Cur.

4-7 Conclusions

In this study, we successfully

- 1- Functionalization SWCNTs by using PEG where the esterification reaction between the SWCNTs carboxylic acid group and the Polyethylene glycol (PEG) hydroxyl group was studied utilizing SWCNTs organic chemical materials as active (CNTs – COOH). PEG4000 was used to conjugate single wall carbon nanotubes (SWCNTs) (medical polymer). XRD, FTIR, UV- Vis, RS, and AFM were used to characterize the composite (PEG – SWCNTs). Gram-negative bacteria *p. aeruginosa* and Gram-positive bacteria *B.spp.* were both inhibited by the (PEG-SWCNTs). Furthermore, promising results were observed against the human AMJ13 breast cancer cell line and the human HepG2 liver cancer cell line (PEG-SWCNTs).
- 2- Functionalization SWCNTs by using PEG-PEI where SWCNTs conjugated with PEG and polyethylenimine (PEI), which contains amino groups, were synthesized (CNTs-PEG-PEI). The length of the SWCNTs was first shortened by ultrasonic scission in different strong acid solutions for improving the dispersion in water. Afterwards, PEG and PEI were grafted onto the SWCNTs. This functionalization was supposed to attenuate the premature removal and loss of nanocarriers, and also to improve the targeting to the tumor site and the results are PEG-PEI–SWCNTs smart drug delivery. The drug-loaded by Nanocurcumin to get PEG-PEI-SWCNTs-N. Curcumin. This study investigated the anticancer activity of functionalized single wall carbon nanotube with PEG-PEI loading Nanocurcumin. From the results the loading drug PEG- PEI-SWCNTs-N. Curcumin showed inhibitory more than SWCNTs and

PEG-PEI-SWCNTs. The nanoparticles exhibited more activity in AMJ13 breast cancer compared to the HepG2 liver cancer. Our study demonstrated that the preparation and characterization of the SWCNTs, functionalized nanoparticles PEG-PEI-SWCNTs, and drug PEG-PEI-SWCNTs-N. Cur was successful and demonstrated a potential anticancer activity against both AMJ13 breast cancer and HepG2 liver cancer.

- 3- After study effect of (SWCNTs, PEG-PEI-SWCNTs and PEG-PEI-SWCNTs-N.Cur) on normal cell line (RD), we found few effect for these material on normal cell line and it was within the normal range of effect at (50 μ g/ml).

4-8 Future Recommendations

- 1- Use SWCNTs after chemical modification on the other normal cell lines to detect its toxicity, and also on the cancer cell lines as a comparative study.
- 2- Study of effect all material prepared in this study on animals with cancer in vivo.
- 3- Using other plant extracts such as apricot fruit kernels and loading them on carbon nanotubes after chemical modification and studying their effect on cancer and normal cell lines and comparing the results with commercial chemotherapy.
- 4- Use specific chemical coating materials at the SWCNTs to reduce its cytotoxic effect.
- 5- Mode of action, mice metabolism, gene therapy, gene expression, apoptosis, caspase, TNF and P₅₃.

References

References

References

- [1] Wang, M., 2004. Bioactive materials and processing. In Biomaterials and tissue engineering (pp. 1-82). Springer, Berlin, Heidelberg.
- [2] Singh, N.E.E.T.U. and Sharma, U.C., 2014. Introduction to Nano-Biomaterials. Nanotechnology Biomaterials, (11), pp.1-12.
- [3] Ratner, B.D., Hoffman, A.S. and McArthur, S.L., 2020. Physicochemical surface modification of materials used in medicine. In Biomaterials science (pp. 487-505). Academic Press.
- [4] Liu, X., Chu, P.K. and Ding, C., 2010. Surface nano-functionalization of biomaterials. Materials Science and Engineering: R: Reports, 70(3-6), pp.275-302.
- [5] Chen, Q., Liang, S. and Thouas, G.A., 2013. Elastomeric biomaterials for tissue engineering. Progress in polymer science, 38(3-4), pp.584-671.
- [6] Yadav, P., Yadav, H., Shah, V.G., Shah, G. and Dhaka, G., 2015. Biomedical biopolymers, their origin and evolution in biomedical sciences: A systematic review. Journal of clinical and diagnostic research: JCDR, 9(9), p.ZE21.
- [7] Babu, R.P., O'connor, K. and Seeram, R., 2013. Current progress on bio-based polymers and their future trends. Progress in biomaterials, 2(1), pp.1-16.
- [8] Pawelec, K.M., Husmann, A., Best, S.M. and Cameron, R.E., 2014. Ice-templated structures for biomedical tissue repair: from physics to final scaffolds. Applied Physics Reviews, 1(2), p.021301.
- [9] Anwunobi, A.P. and Emeje, M.O., 2011. Recent applications of natural polymers in nanodrug delivery. J Nanomed Nanotechnol, 4, pp.2-7.

References

- [10] Prameela, K., Mohan, C.M. and Ramakrishna, C., 2018. Biopolymers for food design: consumer-friendly natural ingredients. In *Biopolymers for food design* (pp. 1-32). Academic Press.
- [11] Li, S., Ge, Y. and Li, H., 2012. *Smart Nanomaterials for Sensor Application*. Bentham Science Publishers.
- [12] Qureshi, D., Nayak, S.K., Anis, A., Ray, S.S., Kim, D., Nguyen, T.T.H. and Pal, K., 2020. Introduction of biopolymers: food and biomedical applications. In *Biopolymer-Based Formulations* (pp. 1-45). Elsevier.
- [13] Wróblewska-Krepsztul, J., Rydzkowski, T., Michalska-Požoga, I. and Thakur, V.K., 2019. Biopolymers for biomedical and pharmaceutical applications: recent advances and overview of alginate electrospinning. *Nanomaterials*, 9(3), p.404.
- [14] Thakur, V.K. and Singha, A.S., 2011. Rapid synthesis, characterization, and physicochemical analysis of biopolymer-based graft copolymers. *International Journal of Polymer Analysis and Characterization*, 16(3), pp.153-164.
- [15] Pandele, A.M., Neacsu, P., Cimpean, A., Staras, A.I., Miculescu, F., Iordache, A., Voicu, S.I., Thakur, V.K. and Toader, O.D., 2018. Cellulose acetate membranes functionalized with resveratrol by covalent immobilization for improved osseointegration. *Applied Surface Science*, 438, pp.2-13.
- [16] Jones, O.G. and McClements, D.J., 2010. Functional biopolymer particles: design, fabrication, and applications. *Comprehensive Reviews in Food Science and Food Safety*, 9(4), pp.374-397.

References

- [17] Agüero, L., Zaldivar-Silva, D., Peña, L. and Dias, M.L., 2017. Alginate microparticles as oral colon drug delivery device: A review. *Carbohydrate Polymers*, 168, pp.32-43.
- [18] Raju, G.S.R., Benton, L., Pavitra, E. and Yu, J.S., 2015. Multifunctional nanoparticles: recent progress in cancer therapeutics. *Chemical communications*, 51(68), pp.13248-13259.
- [19] Sanginario, A., Miccoli, B. and Demarchi, D., 2017. Carbon nanotubes as an effective opportunity for cancer diagnosis and treatment. *Biosensors*, 7(1), p.9.
- [20] Groover, M.P., 2020. *Fundamentals of modern manufacturing: materials, processes, and systems*. John Wiley & Sons.
- [21] Davis, J.R., 2003. Overview of biomaterials and their use in medical devices. *Handbook of materials for medical devices*, pp.1-11.
- [22] Akovali, G. ed., 2001. *Handbook of composite fabrication*. iSmithers Rapra Publishing.
- [23] Sheldon, R.P., 1982. *Composite polymeric materials*.
- [24] Marquis, D.M., Guillaume, E. and Chivas-Joly, C., 2011. Properties of Nanollers in Polymer. *Nanocomposites and polymers with analytical methods*, 261.
- [25] Kelly, A. ed., 2012. *Concise encyclopedia of composite materials*. Elsevier.
- [26] Chen, J., Spear, S.K., Huddleston, J.G. and Rogers, R.D., 2005. Polyethylene glycol and solutions of polyethylene glycol as green reaction media. *Green Chemistry*, 7(2), pp.64-82.

References

- [27] French, A.C., Thompson, A.L. and Davis, B.G., 2009. High-Purity Discrete PEG-Oligomer Crystals Allow Structural Insight. *Angewandte Chemie International Edition*, 48(7), pp.1248-1252.
- [28] Antonietti, L., Aymonier, C., Schlotterbeck, U., Garamus, V.M., Maksimova, T., Richtering, W. and Mecking, S., 2005. Core– shell-structured highly branched poly (ethylenimine amide) s: synthesis and structure. *Macromolecules*, 38(14), pp.5914-5920.
- [29] Reddy, B.R., Eoff, L., Crespo, F. and Lewis, C., 2013, April. Recent advances in organically crosslinked conformance polymer systems. In *SPE International Symposium on Oilfield Chemistry*. OnePetro.
- [30] Reddy, B.R., Eoff, L., Dalrymple, E.D., Black, K., Brown, D. and Rietjens, M., 2003. A natural polymer-based cross-linker system for conformance gel systems. *SPE Journal*, 8(02), pp.99-106.
- [31] Vicennati, P., Giuliano, A., Ortaggi, G. and Masotti, A., 2008. Polyethylenimine in medicinal chemistry. *Current medicinal chemistry*, 15(27), pp.2826-2839.
- [32] Virgen-Ortiz, J.J., Dos Santos, J.C., Berenguer-Murcia, Á., Barbosa, O., Rodrigues, R.C. and Fernandez-Lafuente, R., 2017. Polyethylenimine: A very useful ionic polymer in the design of immobilized enzyme biocatalysts. *Journal of materials chemistry B*, 5(36), pp.7461-7490.
- [33] Vicennati, P., Giuliano, A., Ortaggi, G. and Masotti, A., 2008. Polyethylenimine in medicinal chemistry. *Current medicinal chemistry*, 15(27), pp.2826-2839.
- [34] Ajayan, P.M. and Vajtai, R., 2001. Properties and applications of carbon nanotubes. In *Carbon Filaments and Nanotubes: Common Origins, Differing Applications?* (pp. 315-330). Springer, Dordrecht.

References

- [35] Harris, P.J. and Harris, P.J.F., 2009. Carbon nanotube science: synthesis, properties and applications. Cambridge university press.
- [36] Baughman, R.H., Zakhidov, A.A. and De Heer, W.A., 2002. Carbon nanotubes--the route toward applications. *science*, 297(5582), pp.787-792.
- [37] Paul, R., Maity, A., Mitra, A., Kumbhakar, P. and Mitra, A.K., 2011. Synthesis and study of optical and electrical characteristics of a hybrid structure of single wall carbon nanotubes and silver nanoparticles. *Journal of Nanoparticle Research*, 13(11), pp.5749-5757.
- [38] Karna, S.K. and Holmestad, R., Properties and applications of carbon nanotubes.
- [39] Rahmani, M., Golian, A., Kermanshahi, H. and Bassami, M.R., 2017. Effects of curcumin and nanocurcumin on growth performance, blood gas indices and ascites mortalities of broiler chickens reared under normal and cold stress conditions. *Italian Journal of Animal Science*, 16(3), pp.438-446.
- [40] Ghalandarlaki, N., Alizadeh, A.M. and Ashkani-Esfahani, S., 2014. Nanotechnology-applied curcumin for different diseases therapy. *BioMed research international*, 2014.
- [41] Kurita, T. and Makino, Y., 2013. Novel curcumin oral delivery systems. *Anticancer research*, 33(7), pp.2807-2821.
- [42] Hani, U. and Shivakumar, H.G., 2014. Solubility enhancement and delivery systems of curcumin a herbal medicine: a review. *Current drug delivery*, 11(6), pp.792-804.
- [43] Ma, Z., Shayeganpour, A., Brocks, D.R., Lavasanifar, A. and Samuel, J., 2007. High-performance liquid chromatography analysis of curcumin in

References

rat plasma: application to pharmacokinetics of polymeric micellar formulation of curcumin. *Biomedical Chromatography*, 21(5), pp.546-552.

[44] Song, Z., Feng, R., Sun, M., Guo, C., Gao, Y., Li, L. and Zhai, G., 2011. Curcumin-loaded PLGA-PEG-PLGA triblock copolymeric micelles: Preparation, pharmacokinetics and distribution in vivo. *Journal of colloid and interface science*, 354(1), pp.116-123.

[45] Nelson, K.M., Dahlin, J.L., Bisson, J., Graham, J., Pauli, G.F. and Walters, M.A., 2017. The essential medicinal chemistry of curcumin: miniperspective. *Journal of medicinal chemistry*, 60(5), pp.1620-1637.

[46] Sobh, R.A., Mohamed, W.S., Moustafa, A.B. and Nasr, H.E., 2015. Encapsulation of curcumin and curcumin derivative in polymeric nanospheres. *Polymer-Plastics Technology and Engineering*, 54(14), pp.1457-1467.

[47] Prasad, S., Tyagi, A.K. and Aggarwal, B.B., 2014. Recent developments in delivery, bioavailability, absorption and metabolism of curcumin: the golden pigment from golden spice. *Cancer research and treatment: official journal of Korean Cancer Association*, 46(1), p.2.

[48] Mohamed, S.A., El-Shishtawy, R.M., Al-Bar, O.A. and Al-Najada, A.R., 2017. Chemical modification of curcumin: Solubility and antioxidant capacity. *International Journal of Food Properties*, 20(3), pp.718-724.

[49] Kunwar, A., Barik, A., Pandey, R. and Priyadarsini, K.I., 2006. Transport of liposomal and albumin loaded curcumin to living cells: an absorption and fluorescence spectroscopic study. *Biochimica et Biophysica Acta (BBA)-General Subjects*, 1760(10), pp.1513-1520.

References

[50] Priyadarsini, K.I., 2014. The chemistry of curcumin: from extraction to therapeutic agent. *Molecules*, 19(12), pp.20091-20112.

[51] Gangwar, R.K., Tomar, G.B., Dhumale, V.A., Zinjarde, S., Sharma, R.B. and Datar, S., 2013. Curcumin conjugated silica nanoparticles for improving bioavailability and its anticancer applications. *Journal of agricultural and food chemistry*, 61(40), pp.9632-9637.

[52] Singh, S.P., Sharma, M. and Gupta, P.K., 2014. Enhancement of phototoxicity of curcumin in human oral cancer cells using silica nanoparticles as delivery vehicle. *Lasers in medical science*, 29(2), pp.645-652.

[53] Ma'Mani, L., Nikzad, S., Kheiri-Manjili, H., Al-Musawi, S., Saeedi, M., Askarlou, S., Foroumadi, A. and Shafiee, A., 2014. Curcumin-loaded guanidine functionalized PEGylated I3ad mesoporous silica nanoparticles KIT-6: practical strategy for the breast cancer therapy. *European journal of medicinal chemistry*, 83, pp.646-654.

[54] Moniruzzaman, M. and Min, T., 2020. Curcumin, curcumin nanoparticles and curcumin nanospheres: A review on their pharmacodynamics based on monogastric farm animal, poultry and fish nutrition. *Pharmaceutics*, 12(5), p.447.

[55] Bhirde, A.A., Patel, S., Sousa, A.A., Patel, V., Molinolo, A.A., Ji, Y., Leapman, R.D., Gutkind, J.S. and Rusling, J.F., 2010. Distribution and clearance of PEG-single-walled carbon nanotube cancer drug delivery vehicles in mice. *Nanomedicine*, 5(10), pp.1535-1546.

[56] Hadidi, N., Kobarfard, F., Nafissi-Varcheh, N. and Aboofazeli, R., 2011. Optimization of single-walled carbon nanotube solubility by

References

noncovalent PEGylation using experimental design methods. *International Journal of Nanomedicine*, 6, p.737.

[57] Bhattacharya, D., Samanta, S., Mukherjee, A., Santra, C.R., Ghosh, A.N., Niyogi, S.K. and Karmakar, P., 2012. Antibacterial activities of polyethylene glycol, tween 80 and sodium dodecyl sulphate coated silver nanoparticles in normal and multi-drug resistant bacteria. *Journal of nanoscience and nanotechnology*, 12(3), pp.2513-2521.

[58] Hadidi, N., Shirazi, S.F.H., Kobarfard, F., Nafissi-Varchehd, N. and Aboofazeli, R., 2012. Evaluation of the effect of PEGylated single-walled carbon nanotubes on viability and proliferation of jurkat cells. *Iranian Journal of Pharmaceutical Research: IJPR*, 11(1), p.27.

[59] Khandare, J.J., Jalota-Badhwar, A., Satavalekar, S.D., Bhansali, S.G., Aher, N.D., Kharas, F. and Banerjee, S.S., 2012. PEG-conjugated highly dispersive multifunctional magnetic multi-walled carbon nanotubes for cellular imaging. *Nanoscale*, 4(3), pp.837-844.

[60] Hadidi, N., Kobarfard, F., Nafissi-Varcheh, N. and Aboofazeli, R., 2013. PEGylated single-walled carbon nanotubes as nanocarriers for cyclosporin a delivery. *Aaps Pharmscitech*, 14(2), pp.593-600.

[61] Son, H.L., Trang, N.T., Sinh, D.T. and Anh, M.N., 2013. Effect of nanocurcumin particles prepared by top-down method on CCl⁴-induced hepatic fibrosis mice. *International Journal of Pharmaceutical Sciences and Research*, 4(12), p.4542.

[62] Ravelli, D., Merli, D., Quartarone, E., Profumo, A., Mustarelli, P. and Fagnoni, M., 2013. PEGylated carbon nanotubes: preparation, properties and applications. *RSC advances*, 3(33), pp.13569-13582.

References

- [63] Tan, J.M., Arulselvan, P., Fakurazi, S., Ithnin, H. and Hussein, M.Z., 2014. A review on characterizations and biocompatibility of functionalized carbon nanotubes in drug delivery design. *Journal of Nanomaterials*, 2014.
- [64] Annaraj, J., Dhivya, R., Vigneshwar, M., Dharaniyambigai, K., Kumaresan, G. and Rajasekaran, M., 2014. Studies on the enhanced biological applications of PVA loaded nanocurcumin. *J Nanosci Nanotechnol*, 2(1), pp.490-495.
- [65] Marković, Z.M., Prekodravac, J., Tošić, D., Holclajtner-Antunović, I.D., Milosavljević, M., Dramićanin, M. and Todorović-Marković, B., 2015. Facile synthesis of water-soluble curcumin nanocrystals. *Journal of the Serbian Chemical Society*, 80(1), pp.63-72.
- [66] Dizaj, S.M., Mennati, A., Jafari, S., Khezri, K. and Adibkia, K., 2015. Antimicrobial activity of carbon-based nanoparticles. *Advanced pharmaceutical bulletin*, 5(1), p.19.
- [67] Anbarasu, M., Anandan, M., Chinnasamy, E., Gopinath, V. and Balamurugan, K., 2015. Synthesis and characterization of polyethylene glycol (PEG) coated Fe₃O₄ nanoparticles by chemical co-precipitation method for biomedical applications. *Spectrochimica Acta Part A: Molecular and Biomolecular Spectroscopy*, 135, pp.536-539.
- [68] Malhotra, B.D., Kumar, S. and Pandey, C.M., 2016, April. Nanomaterials based biosensors for cancer biomarker detection. In *Journal of Physics: Conference Series* (Vol. 704, No. 1, p. 012011). IOP Publishing.
- [69] Farvadi, F., Tamaddon, A., Sobhani, Z. and Abolmaali, S.S., 2017. Polyionic complex of single-walled carbon nanotubes and PEG-grafted-hyperbranched polyethyleneimine (PEG-PEI-SWNT) for an improved

References

doxorubicin loading and delivery: development and in vitro characterization. *Artificial cells, nanomedicine, and biotechnology*, 45(5), pp.855-863.

[70] Sun, Y. and Li, Z., 2017. Aqueous dispersion of single walled carbon nanotubes stabilized by PEG modified diperylene bisimide and their application as an antibacterial agent. *RSC advances*, 7(42), pp.26125-26129.

[71] Assali, M., Zaid, A.N., Abdallah, F., Almasri, M. and Khayyat, R., 2017. Single-walled carbon nanotubes-ciprofloxacin nanoantibiotic: strategy to improve ciprofloxacin antibacterial activity. *International Journal of Nanomedicine*, 12, p.6647.

[72] Oskoueian, A., Amin Matori, K., Bayat, S., Oskoueian, E., Ostovan, F. and Toozandehjani, M., 2018. Fabrication, characterization, and functionalization of single-walled carbon nanotube conjugated with tamoxifen and its anticancer potential against human breast cancer cells. *Journal of Nanomaterials*, 2018.

[73] Sireesha, M., Jagadeesh Babu, V., Kranthi Kiran, A.S. and Ramakrishna, S., 2018. A review on carbon nanotubes in biosensor devices and their applications in medicine. *Nanocomposites*, 4(2), pp.36-57.

[74] Sharmeen, S., Rahman, A.M., Lubna, M.M., Salem, K.S., Islam, R. and Khan, M.A., 2018. Polyethylene glycol functionalized carbon nanotubes/gelatin-chitosan nanocomposite: An approach for significant drug release. *Bioactive materials*, 3(3), pp.236-244.

[75] Yu, S., Zhang, Y., Chen, L., Li, Q., Du, J., Gao, Y., Zhang, L. and Yang, Y., 2018. Antitumor effects of carbon nanotube-drug complex

References

against human breast cancer cells. *Experimental and therapeutic medicine*, 16(2), pp.1103-1110.

[76] Joly, A. and Latha, M.S., 2019. Synthesis of Nanocurcumin-Alginate Conjugate and its Characterization by XRD, IR, UV-VIS Andraman Spectroscopy. *Oriental Journal of Chemistry*, 35(2), p.751.

[77] Charmi, J., Nosrati, H., Amjad, J.M., Mohammadkhani, R. and Danafar, H., 2019. Polyethylene glycol (PEG) decorated graphene oxide nanosheets for controlled release curcumin delivery. *Heliyon*, 5(4), p.e01466.

[78] Roy, S. and Kim, J., 2019. Synergistic effect of polydopamine–polyethylenimine copolymer coating on graphene oxide for EVA nanocomposites and high-performance triboelectric nanogenerators. *Nanoscale Advances*, 1(6), pp.2444-2453.

[79] Wang, Y., Sun, G., Gong, Y., Zhang, Y., Liang, X. and Yang, L., 2020. Functionalized folate-modified graphene oxide/PEI siRNA nanocomplexes for targeted ovarian cancer gene therapy. *Nanoscale Research Letters*, 15(1), pp.1-11.

[80] Yang, S., Wang, Z., Ping, Y., Miao, Y., Xiao, Y., Qu, L., Zhang, L., Hu, Y. and Wang, J., 2020. PEG/PEI-functionalized single-walled carbon nanotubes as delivery carriers for doxorubicin: synthesis, characterization, and in vitro evaluation. *Beilstein Journal of Nanotechnology*, 11(1), pp.1728-1741.

[81] Hanna, D.H. and Saad, G.R., 2020. Nanocurcumin: preparation, characterization and cytotoxic effects towards human laryngeal cancer cells. *RSC Advances*, 10(35), pp.20724-20737.

References

- [82] Jihad, M.A., Noori, F., Jabir, M.S., Albukhaty, S., AlMalki, F.A. and Alyamani, A.A., 2021. Polyethylene Glycol Functionalized Graphene Oxide Nanoparticles Loaded with *Nigella sativa* Extract: A Smart Antibacterial Therapeutic Drug Delivery System. *Molecules*, 26(11), p.3067.
- [83] Lakshmanan, A., Akasov, R.A., Sholina, N.V., Demina, P.A., Generalova, A.N., Gangadharan, A., Sardar, D.K., Lankamsetty, K.B., Khochenkov, D.A., Khaydukov, E.V. and Gudkov, S.V., 2021. Nanocurcumin-Loaded UCNPs for Cancer Theranostics: Physicochemical Properties, In Vitro Toxicity, and In Vivo Imaging Studies. *Nanomaterials*, 11(9), p.2234.
- [84] Förster, H., 2004. UV/vis spectroscopy. Characterization I, pp.337-426.
- [85] Larkin, P., 2017. Infrared and Raman spectroscopy: principles and spectral interpretation. Elsevier.
- [86] Lehman J. H., Terrones M., Mansfield E., Hurst K. E. and Meunier, V. , "Evaluating the characteristics of multiwall carbon nanotubes" , *Carbon*, Vol.49, No.8, pp. 2581-2602, 2011.
- [87] Jorio A., Pimenta M. A., Souza Filho A. G., Saito R., Dresselhaus G. and Dresselhaus M. S. , "Characterizing carbon nanotube samples with resonance Raman scattering", *New Journal of Physics*, Vol. 5, No.1, pp.1-17, 2003.
- [88] Davis V., "Investigation of dye-sensitized solar cell performance with single chirality semiconducting carbon nanotubes", Doctoral dissertation, 2015.

References

- [89] Ismail K. and Ismail K. , "Fabrication and characterisation of SERS substrates through photo-deposition of Gold Nanoparticles", CH.1, pp.1-37 , 2015.
- [90] Hodkiewicz J. and Scientific T. F. , "Characterizing carbon materials with Raman spectroscopy", application note, 2010.
- [91] Kataura H., Kumazawa Y., Maniwa Y., Umezu I., Suzuki S., Ohtsuka Y. and Achiba Y., "Optical properties of single-wall carbon nanotubes", *Synthetic metals*, Vol. 103, No.1-3, pp. 2555-2558, 1999.
- [92] Cheng Q., Debnath S., Gregan E. and Byrne H. J. , "Effects of chlorinated aromatic solvents on the dispersion of HiPco SWNTs", *physica status solidi (b)*, Vol.245, No.10, pp. 1947-1950, 2008.
- [93] Nair N., Usrey M. L., Kim W. J., Braatz R. D. and Strano M. S. , "Estimation of the (n, m) concentration distribution of single-walled carbon nanotubes from photoabsorption spectra", *Analytical chemistry*, Vol.78, No.22, pp.7689-7696, 2006 .
- [94] Yu Z . and Brus L. , "Rayleigh and Raman scattering from individual carbon nanotube bundles", *The Journal of Physical Chemistry B*, Vol.105, No.6, pp. 1123-1134, 2001.
- [95] Gohil S. and Ghosh S. , "Surface enhanced Raman scattering from multiwalled carbon nanotubes at low temperatures", *Applied Physics Letters*, Vol. 96, No.14, pp. 143108, 2010.
- [96] Ferrari A. C., Meyer J. C., Scardaci V., Casiraghi C., Lazzeri M., Mauri F. and Geim A. K. , "Raman spectrum of graphene and graphene layers ", *Physical review letters*, Vol.97, No.18, pp. 1-4, 2006.
- [97] Maciel I. O., Anderson N., Pimenta M. A., Hartschuh A., Qian H., Terrones M. and Jorio A. , "Electron and phonon renormalization near

References

charged defects in carbon nanotubes", *Nature materials*, Vol.7, No.11, pp. 878-883, 2008.

[98] Fantini C., Pimenta M. A. and Strano M. S., "Two-phonon combination Raman modes in covalently functionalized single-wall carbon nanotubes", *The Journal of Physical Chemistry C*, Vol.112, No.34, pp. 13150-13155, 2008.

[99] Rao R., Reppert J., Podila R., Zhang X., Rao A. M., Talapatra S. and Maruyama B. , " Double resonance Raman study of disorder in CVD-grown single-walled carbon nanotubes", *Carbon*, Vol.49, No.4, pp.1318-1325 , 2011.

[100] Kumar, V., Dwivedi, D.K. and Agrawal, P., 2013. Optical, structural and electrical properties of nanosized zinc oxide sintered films for photovoltaic applications. *Science of Sintering*, 45(1), pp.13-19.

[101] Fredrickson JK, Zachara JM, Balkwill DL, Kennedy D, Li SM, Kostandarithes HM, Daly MJ, Romine MF, Brockman FJ, "Geomicrobiology of high-level nuclear waste-contaminated vadose sediments at the Hanford site, Washington state", *Applied and Environmental Microbiology*, 70 (7),4230–41, 2004.

[102] R. Ahmad, and M. Sardar, "TiO₂ Nanoparticles as an Antibacterial Agents against E. coli", *International Journal of Innovative Research in Science, Engineering and Technology*, Vol. 2, No. 8, (2013).

[103] S. Rezaei-Zarchi, A. Javed, M. J. Ghani, S. Soufian, F. B. Firouzabadi1, A. B. Moghaddam, and S. H. Mirjalili, "Comparative Study of Antimicrobial Activities of TiO₂ and CdO Nanoparticles against the Pathogenic Strain of Escherichia coli, " *Iranian Journal of Pathology*, Vol. 5, No. 2, pp. 83-89, (2010).

References

- [65] M. T. Cabeen and C. Jacobs-Wagner, “Bacterial Cell Shape”, *Nature Reviews Microbiology*, Vol. 3, pp. 601-610, (2005).
- [104] S. M. Dizaj, A. Mennati, S. Jafari, K. Khezri, and K. Adibkia, “Antimicrobial Activity of Carbon-Based Nanoparticles”, *Advanced Pharmaceutical Bulletin*, Vol.5, No.1, pp.19-23, (2015).
- [105] M. T. Cabeen and C. Jacobs-Wagner, “Bacterial Cell Shape”, *Nature Reviews Microbiology*, Vol. 3, pp. 601-610, (2005).
- [106] P. Judith, and P. Espitia, “Zinc Oxide Nanoparticles: Synthesis, Antimicrobial Activity and Food Packaging Applications”, *Food Bioprocess Technol*, Vol. 5, pp. 1447–1464, (2012).
- [107] T. M. Al-Nori, “Antibacterial Activity of Silver and Gold Nanoparticles against Streptococcus, Staphylococcus aureus and E.coli”, *Al-Mustansiriyah Journal of Science*, Vol. 23, No. 3, pp. 45-54, (2012).
- [108] M. J. Hajipour, K. M. Fromm, A. A. Ashkarran, D. J. de Aberasturi, I. R. de Larramendi, T. Rojo, V. Serpooshan, W. J. Parak and M. Mahmoudi, 114 References “Antibacterial Properties of Nanoparticles”, *Trends in Biotechnology*, Vol. 30, No. 10, pp. 499-511, (2010).
- [109] Hancock, R.E., 1998. Resistance mechanisms in *Pseudomonas aeruginosa* and other nonfermentative gram-negative bacteria. *Clinical Infectious Diseases*, 27(Supplement_1), pp.S93-S99.
- [110] Arancibia, F., Bauer, T.T., Ewig, S., Mensa, J., Gonzalez, J., Niederman, M.S. and Torres, A., 2002. Community-acquired pneumonia due to gram-negative bacteria and *Pseudomonas aeruginosa*: incidence, risk, and prognosis. *Archives of internal medicine*, 162(16), pp.1849-1858.

References

- [111] Miljaković, D., Marinković, J. and Balešević-Tubić, S., 2020. The significance of *Bacillus* spp. in disease suppression and growth promotion of field and vegetable crops. *Microorganisms*, 8(7), p.1037.
- [112] Quiñones-Muñoz, T.A., Villares-Bueno, A.M., Hernández-Ramírez, G., Hernández-Martínez, R., Lizardi-Jiménez, M.A. and Bocanegra-García, V., 2020. *Bacillus* spp. characterization and his intervention as a possible non-traditional etiology of chronic renal insufficiency in Tierra Blanca, Veracruz, Mexico. *Scientific Reports*, 10(1), pp.1-8.
- [113] R. H. Mahdi, “Synthesis and Characterization of CNT-Iron Oxide Nanocomposite by Laser Ablation for Antimicrobial Applications”, PhD thesis, pp. 1-152, (2016).
- [114] P. P. Fu, Q. Xia, H. Hwang, P. C. Ray, and H. Yu, “Mechanisms of Nanotoxicity: Generation of Reactive Oxygen Species”, *Journal of Food and Drug Analysis*, Vol. 22, pp. 64 -75, (2014).
- [115] A. S. Haja Hameed, C. Karthikeyan, V. S. kumar, S. Kumaresan, and G. Ravi, “Impact of Alkaline Metal Ions Mg^{2+} , Ca^{2+} , Sr^{2+} and Ba^{2+} on the Structural, Optical , Thermal and Antibacterial Properties of ZnO Nanoparticles Prepared by Co-precipitation Method”, *Journal of Materials Chemistry B*, Vol. 43, (2013).
- [116] Meyyappan, M., 2004. *Carbon nanotubes: science and applications*. CRC press.
- [117] Kang, S., Pinault, M., Pfefferle, L.D. and Elimelech, M., 2007. Single-walled carbon nanotubes exhibit strong antimicrobial activity. *Langmuir*, 23(17), pp.8670-8673.

References

- [118] Kang, S., Herzberg, M., Rodrigues, D.F. and Elimelech, M., 2008. Antibacterial effects of carbon nanotubes: size does matter. *Langmuir*, 24(13), pp.6409-6413.
- [119] Arias, L.R. and Yang, L., 2009. Inactivation of bacterial pathogens by carbon nanotubes in suspensions. *Langmuir*, 25(5), pp.3003-3012.
- [120] Yang, C., Mamouni, J., Tang, Y. and Yang, L., 2010. Antimicrobial activity of single-walled carbon nanotubes: length effect. *Langmuir*, 26(20), pp.16013-16019.
- [121] Dong, L., Henderson, A. and Field, C., 2012. Antimicrobial activity of single-walled carbon nanotubes suspended in different surfactants. *Journal of Nanotechnology*, 2012.
- [122] Dizaj, S.M., Mennati, A., Jafari, S., Khezri, K. and Adibkia, K., 2015. Antimicrobial activity of carbon-based nanoparticles. *Advanced pharmaceutical bulletin*, 5(1), p.19.
- [123] S. K. Kulkarni, "Nanotechnology: principles and practices", Capital Publishing Company, book. 3rd Edition, ch4,6,11, (2015).
- [124] Bohunicky, B. and Mousa, S.A., 2011. Biosensors: the new wave in cancer diagnosis. *Nanotechnology, science and applications*, 4, p.1.
- [125] Hanahan, D. and Weinberg, R.A., 2011. Hallmarks of cancer: the next generation. *cell*, 144(5), pp.646-674.
- [126] Rasooly, A. and Jacobson, J., 2006. Development of biosensors for cancer clinical testing. *Biosensors and Bioelectronics*, 21(10), pp.1851-1858.
- [127] Selgrad, M., Malfertheiner, P., Fini, L., Goel, A., Boland, C.R. and Ricciardiello, L., 2008. The role of viral and bacterial pathogens in gastrointestinal cancer. *Journal of cellular physiology*, 216(2), pp.378-388.

References

- [128] Zhang, W., Zhang, Z. and Zhang, Y., 2011. The application of carbon nanotubes in target drug delivery systems for cancer therapies. *Nanoscale research letters*, 6(1), pp.1-22.
- [129] Ahmad, S.S., Reinius, M.A., Hatcher, H.M. and Ajithkumar, T.V., 2016. Anticancer chemotherapy in teenagers and young adults: managing long term side effects. *Bmj*, 354.
- [130] Gillet, J.P. and Gottesman, M.M., 2010. Mechanisms of Multidrug Resistance in Cancer BT-Multi-Drug Resistance in Cancer; Zhou, J., Ed.
- [131] Alfarouk, K.O., Stock, C.M., Taylor, S., Walsh, M., Muddathir, A.K., Verduzco, D., Bashir, A.H., Mohammed, O.Y., Elhassan, G.O., Harguindey, S. and Reshkin, S.J., 2015. Resistance to cancer chemotherapy: failure in drug response from ADME to P-gp. *Cancer cell international*, 15(1), pp.1-13.
- [132] Nooter, K. and Stoter, G., 1996. Molecular mechanisms of multidrug resistance in cancer chemotherapy. *Pathology-Research and Practice*, 192(7), pp.768-780.
- [133] Gupta, P.K., 1990. Drug targeting in cancer chemotherapy: a clinical perspective. *Journal of pharmaceutical sciences*, 79(11), pp.949-962.
- [134] Kreuter, J., 2007. Nanoparticles—a historical perspective. *International journal of pharmaceutics*, 331(1), pp.1-10.
- [135] Khanna, S.C., Jecklin, T. and Speiser, P., 1970. Bead polymerization technique for sustained-release dosage form. *Journal of pharmaceutical sciences*, 59(5), pp.614-618.
- [136] Matsumura, Y. and Maeda, H., 1986. A new concept for macromolecular therapeutics in cancer chemotherapy: mechanism of

References

tumorotropic accumulation of proteins and the antitumor agent smancs. *Cancer research*, 46(12 Part 1), pp.6387-6392.

[137] Bae, Y.H. and Park, K., 2011. Targeted drug delivery to tumors: myths, reality and possibility. *Journal of controlled release*, 153(3), p.198.

[138] Ding, C., Tong, L., Feng, J. and Fu, J., 2016. Recent advances in stimuli-responsive release function drug delivery systems for tumor treatment. *Molecules*, 21(12), p.1715.

[139] Li, L., Liu, C., Cao, X., Tan, L. and Lu, W., 2017. Multiplexing determination of cancer-associated biomarkers by surface-enhanced Raman scattering using ordered gold nanohoneycomb arrays. *Bioanalysis*, 9(20), pp.1561-1572.

[140] Chikkaveeraiah, B.V., Bhirde, A.A., Morgan, N.Y., Eden, H.S. and Chen, X., 2012. Electrochemical immunosensors for detection of cancer protein biomarkers. *ACS nano*, 6(8), pp.6546-6561.

[141] Wu, M.S., Shi, H.W., He, L.J., Xu, J.J. and Chen, H.Y., 2012. Microchip device with 64-site electrode array for multiplexed immunoassay of cell surface antigens based on electrochemiluminescence resonance energy transfer. *Analytical chemistry*, 84(9), pp.4207-4213.

[142] Wang, X., Zhou, M., Zhu, Y., Miao, J., Mao, C. and Shen, J., 2013. Preparation of a novel immunosensor for tumor biomarker detection based on ATRP technique. *Journal of Materials Chemistry B*, 1(16), pp.2132-2138.

[143] Song, S.P., Li, B., Hu, J. and Li, M.Q., 2004. Simultaneous multianalysis for tumor markers by antibody fragments microarray system. *Analytica chimica acta*, 510(2), pp.147-152.

References

- [144] Wang, Z., Liu, N. and Ma, Z., 2014. Platinum porous nanoparticles hybrid with metal ions as probes for simultaneous detection of multiplex cancer biomarkers. *Biosensors and Bioelectronics*, 53, pp.324-329.
- [145] Seigneuric, R., Markey, L., SA Nuyten, D., Dubernet, C., TA Evelo, C., Finot, E. and Garrido, C., 2010. From nanotechnology to nanomedicine: applications to cancer research. *Current Molecular Medicine*, 10(7), pp.640-652.
- [146] Wu, X., Patterson, S. and Hawk, E., 2011. Chemoprevention—history and general principles. *Best practice & research Clinical gastroenterology*, 25(4-5), pp.445-459.
- [147] Kukowska-Latallo, J.F., Candido, K.A., Cao, Z., Nigavekar, S.S., Majoros, I.J., Thomas, T.P., Balogh, L.P., Khan, M.K. and Baker, J.R., 2005. Nanoparticle targeting of anticancer drug improves therapeutic response in animal model of human epithelial cancer. *Cancer research*, 65(12), pp.5317-5324.
- [148] Sutradhar, K.B. and Amin, M., 2014. Nanotechnology in cancer drug delivery and selective targeting. *International Scholarly Research Notices*, 2014.
- [149] Pan, Q., Li, Q., Liu, S., Ning, N., Zhang, X., Xu, Y., Chang, A.E. and Wicha, M.S., 2015. Concise review: targeting cancer stem cells using immunologic approaches. *Stem cells*, 33(7), pp.2085-2092.
- [150] Jiang, X., Foldbjerg, R., Miclaus, T., Wang, L., Singh, R., Hayashi, Y., Sutherland, D., Chen, C., Autrup, H. and Beer, C., 2013. Multi-platform genotoxicity analysis of silver nanoparticles in the model cell line CHO-K1. *Toxicology letters*, 222(1), pp.55-63.

References

- [151] Fang, J., Nakamura, H. and Maeda, H., 2011. The EPR effect: unique features of tumor blood vessels for drug delivery, factors involved, and limitations and augmentation of the effect. *Advanced drug delivery reviews*, 63(3), pp.136-151.
- [152] Zhuang, Y., Deng, H., Su, Y., He, L., Wang, R., Tong, G., He, D. and Zhu, X., 2016. Aptamer-functionalized and backbone redox-responsive hyperbranched polymer for targeted drug delivery in cancer therapy. *Biomacromolecules*, 17(6), pp.2050-2062.
- [153] Cherbas, L. and Gong, L., 2014. Cell lines. *Methods*, 68(1), pp.74-81.
- [154] Freshney, R.I., 2006. *Basic principles of cell culture* (pp. 3-22). Hoboken, NJ: John Wiley & Sons, Inc.
- [155] Aschner, M., Suñol, C. and Bal-Price, A. eds., 2011. *Cell Culture Techniques*. Neuromethods: Humana Press.
- [156] Wang, L., Jiang, T. and Gusfield, D., 2000. A more efficient approximation scheme for tree alignment. *SIAM Journal on Computing*, 30(1), pp.283-299.
- [157] Scientific, T., 2016. *Gibco. Cell Culture Basics Handbook*, pp.1-62.
- [158] Riaz, M., van Jaarsveld, M., Hollestelle, A., Prager-van der Smissen, W.J., Heine, A.A., Boersma, A.W., Liu, J., Helmijr, J., Ozturk, B., Smid, M. and Wiemer, E.A., 2013. miRNA expression profiling of 51 human breast cancer cell lines reveals subtype and driver mutation-specific miRNAs. *Breast cancer research*, 15(2), pp.1-17.
- [159] Lacroix, M., Haibe-Kains, B., Henny, B., Laes, J.F., Lallemand, F., Gonze, I., Cardoso, F., Piccart, M., Leclercq, G. and Sotiriou, C., 2004. Gene regulation by phorbol 12-myristate 13-acetate in MCF-7 and MDA-

References

MB-231, two breast cancer cell lines exhibiting highly different phenotypes. *Oncology reports*, 12(4), pp.701-707.

[160] Al-Shammari, A.M., Allak, W.J.K., Umran, M., Yaseen, N.Y. and Hussien, A., 2015. Angiogenesis factors associated with new breast cancer cell line AMJ13 cultured in vitro. *Advances in Breast Cancer Research*, 4(04), p.100.

[161] Qiu, G.H., Xie, X., Xu, F., Shi, X., Wang, Y. and Deng, L., 2015. Distinctive pharmacological differences between liver cancer cell lines HepG2 and Hep3B. *Cytotechnology*, 67(1), pp.1-12.

[162] Hinson, A.R., Jones, R., Crose, L.E., Belyea, B.C., Barr, F.G. and Linardic, C.M., 2013. Human rhabdomyosarcoma cell lines for rhabdomyosarcoma research: utility and pitfalls. *Frontiers in oncology*, 3, p.183.

[163] Burgess, R., 2012. *Understanding nanomedicine: an introductory textbook*. CRC Press.

[164] Bianco, A., Kostarelos, K. and Prato, M., 2005. Applications of carbon nanotubes in drug delivery. *Current opinion in chemical biology*, 9(6), pp.674-679.

[165] Hampel, S., Kunze, D., Haase, D., Krämer, K., Rauschenbach, M., Ritschel, M., Leonhardt, A., Thomas, J., Oswald, S., Hoffmann, V. and Büchner, B., 2008. Carbon nanotubes filled with a chemotherapeutic agent: a nanocarrier mediates inhibition of tumor cell growth.

[166] Beg, S., Rizwan, M., Sheikh, A.M., Hasnain, M.S., Anwer, K. and Kohli, K., 2011. Advancement in carbon nanotubes: basics, biomedical applications and toxicity. *Journal of pharmacy and pharmacology*, 63(2), pp.141-163.

References

- [167] Jin, H., Heller, D.A. and Strano, M.S., 2008. Single-particle tracking of endocytosis and exocytosis of single-walled carbon nanotubes in NIH-3T3 cells. *Nano letters*, 8(6), pp.1577-1585.
- [168] Liu, Z., Chen, K., Davis, C., Sherlock, S., Cao, Q., Chen, X. and Dai, H., 2008. Drug delivery with carbon nanotubes for in vivo cancer treatment. *Cancer research*, 68(16), pp.6652-6660.
- [169] Wu, W., Li, R., Bian, X., Zhu, Z., Ding, D., Li, X., Jia, Z., Jiang, X. and Hu, Y., 2009. Covalently combining carbon nanotubes with anticancer agent: preparation and antitumor activity. *ACS nano*, 3(9), pp.2740-2750.
- [170] Li, Y., Cousins, B.G., Ulijn, R.V. and Kinloch, I.A., 2009. A Study of the Dynamic Interaction of Surfactants with Graphite and Carbon Nanotubes using Fmoc– Amino Acids as a Model System. *Langmuir*, 25(19), pp.11760-11767.
- [171] Liu, Z., Tabakman, S.M., Chen, Z. and Dai, H., 2009. Preparation of carbon nanotube bioconjugates for biomedical applications. *Nature protocols*, 4(9), pp.1372-1381.
- [172] Rosca, I.D., Watari, F., Uo, M. and Akasaka, T., 2005. Oxidation of multiwalled carbon nanotubes by nitric acid. *Carbon*, 43(15), pp.3124-3131.
- [173] Prato, M., Kostarelos, K. and Bianco, A., 2008. Functionalized carbon nanotubes in drug design and discovery. *Accounts of chemical research*, 41(1), pp.60-68.
- [174] Liu, Z., Sun, X., Nakayama-Ratchford, N. and Dai, H., 2007. Supramolecular chemistry on water-soluble carbon nanotubes for drug loading and delivery. *ACS nano*, 1(1), pp.50-56.

References

- [175] Klumpp, C., Kostarelos, K., Prato, M. and Bianco, A., 2006. Functionalized carbon nanotubes as emerging nanovectors for the delivery of therapeutics. *Biochimica et Biophysica Acta (BBA)-Biomembranes*, 1758(3), pp.404-412.
- [176] Bekyarova, E., Ni, Y., Malarkey, E.B., Montana, V., McWilliams, J.L., Haddon, R.C. and Parpura, V., 2005. Applications of carbon nanotubes in biotechnology and biomedicine. *Journal of biomedical nanotechnology*, 1(1), pp.3-17.
- [177] Salam, M.A., Obaid, A.Y., El-Shishtawy, R.M. and Mohamed, S.A., 2017. Synthesis of nanocomposites of polypyrrole/carbon nanotubes/silver nano particles and their application in water disinfection. *RSC advances*, 7(27), pp.16878-16884.
- [178] Bai, Y., Wang, C., Gao, J., Su, J. and Ma, W., 2015. A study on dispersion and antibacterial activity of functionalizing multi-walled carbon nanotubes with mixed surfactant. *Journal of Surfactants and Detergents*, 18(6), pp.957-964.
- [179] Engel, M., Hadar, Y., Belkin, S., Lu, X., Elimelech, M. and Chefetz, B., 2018. Bacterial inactivation by a carbon nanotube–iron oxide nanocomposite: a mechanistic study using *E. coli* mutants. *Environmental science: nano*, 5(2), pp.372-380.
- [180] Wang, S., Haldane, D., Liang, R., Smithyman, J., Zhang, C. and Wang, B., 2012. Nanoscale infiltration behaviour and through-thickness permeability of carbon nanotube buckypapers. *Nanotechnology*, 24(1), p.015704.
- [181] Karam, L., Jama, C., Nuns, N., Mamede, A.S., Dhulster, P. and Chihib, N.E., 2013. Nisin adsorption on hydrophilic and hydrophobic surfaces: evidence of its interactions and antibacterial activity. *Journal of Peptide Science*, 19(6), pp.377-385.

References

- [182] Vardharajula, S., Ali, S.Z., Tiwari, P.M., Eroğlu, E., Vig, K., Dennis, V.A. and Singh, S.R., 2012. Functionalized carbon nanotubes: biomedical applications. *International journal of nanomedicine*, 7, p.5361.
- [183] Ibrahim, K.S., 2013. Carbon nanotubes-properties and applications: a review. *Carbon letters*, 14(3), pp.131-144.
- [184] Iijima, S., 1991. Helical microtubules of graphitic carbon. *nature*, 354(6348), pp.56-58.
- [185] Veetil, J.V. and Ye, K., 2009. Tailored carbon nanotubes for tissue engineering applications. *Biotechnology progress*, 25(3), pp.709-721.
- [186] Yang, W., Thordarson, P., Gooding, J.J., Ringer, S.P. and Braet, F., 2007. Carbon nanotubes for biological and biomedical applications. *Nanotechnology*, 18(41), p.412001.
- [187] Thostenson, E.T., Ren, Z. and Chou, T.W., 2001. Advances in the science and technology of carbon nanotubes and their composites: a review. *Composites science and technology*, 61(13), pp.1899-1912.
- [188] Smith, S.C. and Rodrigues, D.F., 2015. Carbon-based nanomaterials for removal of chemical and biological contaminants from water: a review of mechanisms and applications. *Carbon*, 91, pp.122-143.
- [189] Ali, N.H. and Mohammed, A.M., 2021. Biosynthesis and characterization of platinum nanoparticles using Iraqi Zahidi dates and evaluation of their biological applications. *Biotechnology Reports*, 30, p.e00635.
- [190] Khashan, K.S., Abdulameer, F.A., Jabir, M.S., Hadi, A.A. and Sulaiman, G.M., 2020. Anticancer activity and toxicity of carbon nanoparticles produced by pulsed laser ablation of graphite in water. *Advances in Natural Sciences: Nanoscience and Nanotechnology*, 11(3), p.035010

References

- [191] Kushwaha, S.K.S., Ghoshal, S., Rai, A.K. and Singh, S., 2013. Carbon nanotubes as a novel drug delivery system for anticancer therapy: a review. *Brazilian Journal of Pharmaceutical Sciences*, 49(4), pp.629-643.
- [192] Bianco, A., Kostarelos, K. and Prato, M., 2005. Applications of carbon nanotubes in drug delivery. *Current opinion in chemical biology*, 9(6), pp.674-679.
- [193] Shen, M., Wang, S.H., Shi, X., Chen, X., Huang, Q., Petersen, E.J., Pinto, R.A., Baker Jr, J.R. and Weber Jr, W.J., 2009. Polyethyleneimine-mediated functionalization of multiwalled carbon nanotubes: synthesis, characterization, and in vitro toxicity assay. *The Journal of Physical Chemistry C*, 113(8), pp.3150-3156.
- [194] Buchman, Y.K., Lellouche, E., Zigdon, S., Bechor, M., Michaeli, S. and Lellouche, J.P., 2013. Silica nanoparticles and polyethyleneimine (PEI)-mediated functionalization: a new method of PEI covalent attachment for siRNA delivery applications. *Bioconjugate chemistry*, 24(12), pp.2076-2087.
- [195] Arola, O.J., 2000. Saraste A, Pulkki K, Kallajoki M, Parvinen M, and Voipio-Pulkki LM. Acute doxorubicin cardiotoxicity involves cardiomyocyte apoptosis. *Cancer Res*, 60, pp.1789-1792.
- [196] Yang, C.C., Cohen, S., Shaw, T., Wang, P.C., Nogami, T. and Edelstein, D., 2010. Characterization of "Ultrathin-Cu"/Ru (Ta)/TaN liner stack for copper interconnects. *IEEE Electron Device Letters*, 31(7), pp.722-724.
- [197] Elhissi, A., Ahmed, W., Hassan, I.U., Dhanak, V. and D'Emanuele, A., 2012. Carbon nanotubes in cancer therapy and drug delivery. *Journal of drug delivery*, 2012.
- [198] Sobhani, Z., Dinarvand, R., Atyabi, F., Ghahremani, M. and Adeli, M., 2011. Increased paclitaxel cytotoxicity against cancer cell lines using

References

a novel functionalized carbon nanotube. *International journal of nanomedicine*, 6, p.705.

[199] Landeros, J.M., Belmont-Bernal, F., Pérez-González, A.T., Pérez- Padrón, M.I., Guevara-Salazar, P., González-Herrera, I.G. and Guadarrama, P., 2017. A two-step synthetic strategy to obtain a water-soluble derivative of curcumin with improved antioxidant capacity and in vitro cytotoxicity in C6 glioma cells. *Materials Science and Engineering: C*, 71, pp.351-362.

[200] Jogi, H., Maheshwari, R., Raval, N., Kuche, K., Tambe, V., Mak, K.K., Pichika, M.R. and Tekade, R.K., 2018. Carbon nanotubes in the delivery of anticancer herbal drugs. *Nanomedicine*, 13(10), pp.1187-1220.

[201] Mehdipoor, E., Adeli, M., Bavadi, M., Sasanpour, P. and Rashidian, B., 2011. A possible anticancer drug delivery system based on carbon nanotube–dendrimer hybrid nanomaterials. *Journal of Materials Chemistry*, 21(39), pp.15456-15463.

[202] Adeli, M., Soleyman, R., Beiranvand, Z. and Madani, F., 2013. Carbon nanotubes in cancer therapy: a more precise look at the role of carbon nanotube–polymer interactions. *Chemical Society Reviews*, 42(12), pp.5231-5256.

[203] Uzair, M., Arshad, M., Abbasi, S.S., Arshad, A., Khattak, J.Z., Tabassum, S. and Zakaria, U.B., 2021. Review: Biomedical Applications of Carbon Nanotubes. *Nano Biomed. Eng*, 13(1), pp.82-93.

[204] Saliev, T., 2019. The advances in biomedical applications of carbon nanotubes. *C*, 5(2), p.29.

[205] Hamzat, W.A., Abdulkareem, A.S., Bankole, M.T., Tijani, J.O., Kovo, A.S. and Abubakre, O.K., 2019. Adsorption studies on the treatment of battery wastewater by purified carbon nanotubes (P-CNTs) and polyethylene glycol carbon nanotubes (PEG-CNTs). *Journal of Environmental Science and Health, Part A*, 54(9), pp.827-839.

الخلاصة

تضمنت هذه الدراسة ثلاثة أجزاء، تضمن الجزء الأول تفعيل (SWCNTs) باستخدام (HCl) ومزيج من حامضي (HNO_3 H_2SO_4) لتحويلها الى (SWCNTs-COOH)، لوحقت بعدها عملية استرهل (SWCNTs-COOH) ب (PEG, PEG-PEI)، تم إجراء تفاعل الأستر بين مجموعة الأحماض الكربوكسيلية لأنابيب الكربون أحادية الجدران (SWCNTs) ومجموعة هيدروكسيل البولي إيثيلين جلايكول (PEG) والبولي اتلين امينين (PEI) باستخدام مواد كيميائية. بعد ذلك تم دراسة الخصائص الفيزيائية باستخدام التقنيات XRD، FTIR، UV-Vis، TEM، AFM و RS لتوصيف المركب (PEG-SWCNTs, PEG-PEI-SWCNTs). كان لـ SWCNTs قمة حادة عند (291 نانومتر) في مطياف الأشعة المرئية- فوق البنفسجية، في حين أن (PEG -SWCNTs) كان لها قمة عند (289 نانومتر)، بينما تظهر قمة (PEG-PEI-) (SWCNTs) عند (300.98 نانومتر). في تحويلات فورير لمطياف الأشعة تحت الحمراء (FTIR)، يمكن رؤية رابطة (OH) قوية لكلا المادتين، وكذلك رابطة (C-H) لـ (PEG-SWCNTs)، كما أظهرت رابطة (C-H)، NH، C-N لـ (PEG-PEI-SWCNTs). تمتلك أنابيب الكربون أحادية الجدران قمة حادة عند ($2\theta = 25.6299^\circ$)، والتي ترتبط بالمستوي (002) مع تباعد ($d = 3.4729 \text{ \AA}$) بينما يتوافق تفعيل (PEG - SWCNTs) مع قمة واسعة عند 2θ ($= 23.4473^\circ$) مع تباعد ($d = 3.8447 \text{ \AA}$)، بينما يتوافق تفعيل (PEG-PEI-SWCNTs) مع قمة واسعة عند ($2\theta = 23.51^\circ$) مع تباعد ($d = 7816 \text{ \AA}$). قيم الحجم البلوري لـ (SWCNTs)، (PEG-SWCNTs, PEG-PEI-SWCNTs) تساوي (3 نانومتر)، (7.7 نانومتر). (8.48 نانومتر)، على التوالي. تُظهر صور مجهر القوة الذرية (AFM) صور أنابيب الكربون النانوية أنبوباً نانويًا واحدًا من الكربون بحجم حبيبات (60 نانومتر). في (PEG-SWCNTs) و (PEG-PEI-SWCNTs) يزداد حجم الحبوب الرئيسي مع التفعيل إلى (83.60 نانومتر). (80.68 نانومتر). في التحليل الطيفي لرامان، نلاحظ حصول إزاحة في نطاق (D,G) لكلا المادتين. في TEM، تكون SWCNTs الخام عبارة عن مجاميع منحنية طويلة، والتي يبدو أنها حزمة من التجمعات غير المتجانسة تتكون من العديد من الأنابيب، والبنية الأنبوبية لـ (PEG-SWCNTs) PEI خشنة، وتكون بعض الجسيمات متصلة وموزعة على طول جدران أنابيب الكربون النانوية، ربما يشير إلى أن مجموعات PEG و PEI مرتبطة بأنابيب الكربون النانوية.

يتضمن الجزء الثاني تحميل النانو كركمين (N. Cur) على SWCNTs التي تحتوي على البولي إيثيلين جلايكول (PEG) والبولي إيثيلين أمين (PEI)، والتي تحتوي على مجموعات

أمينية، تم تصنيعها (PEG-PEI-SWCNTs). تم تحليل الخصائص الطيفية والهيكلية لـ (PEG-PEI-SWCNTs-N. Cur) بشكل شامل بواسطة TEM ,RS ,UV-Vis ,FTIR,XRD وAFM. كشفت أنماط XRD أن PEG-PEI-SWCNTs لها هياكل وعيوب بلورية مختلفة، بالإضافة إلى تباعد أعلى بين الطبقات. أظهرت نتائج AFM أن (SWCNTs) بحجم حبة رئيسي (60 نانومتر)، بينما كشفت (PEG-PEI-SWCNTs) عن تجمع (SWCNTs) بحجم الحبوب الرئيسي (79.6 نانومتر) بعد تحميل مستخلص الكركمين N. Cur، والذي تم التحقق منه بفحص TEM. ظهرت رابطة OH قوية في أطياف FTIR. علاوة على ذلك، يبدو أن قمم امتصاص الأشعة فوق البنفسجية المرئية عند (289، 300.98، (425،282) و (431،273)) نانومتر مرتبطة بـ SWCNTs، PEG-PEI-SWCNTs، مستخلص الكركمين N.Cur، و PEG-PEI-SWCNTs-N. Cur أطياف رامان لـ (PEI-SWCNTs- N. Cur) ، ونطاق (D) ، (النطاق G) ، و (النطاق ثنائي الأبعاد 2D) التي تتحول إلى (RBM) ، ونطاق (D) ، (النطاق G) ، و (النطاق ثنائي الأبعاد 2D) التي تتحول إلى (171,264), 1283, 1593,2131 ((1428 و 939) cm^{-1}) في العينة المحملة بالدواء بسبب تغليف النانو ويشير إلى تحميل دواء ناجح. الخطوط عند (716 و 853) cm^{-1}) يمكن ان تشير إلى اهتزازات التمدد C-N.

تضمن الجزء الثالث استخدام جميع العينات في الأجزاء الثلاثة في الدراسة في ثلاثة أنواع من التطبيقات الحيوية، النوع الأول من التطبيقات الحيوية يشمل تأثير PEG-PEI-SWCNTs و SWCNTs على نوعين من السلالة البكتيرية المضادة للبكتيريا سالبة الجرام *Pseudomonas aeruginosa* وموجبة الجرام *Bacillus spp.* تم تعريض السلالة البكتيرية لسلسلة من التراكيز من (PEG-SWCNTs و SWCNTs) المحضرة ((25-100) $\mu g/ml$). أظهرت النتائج نشاطاً مثبتاً معنوياً وأن معدل تثبيط نمو البكتيريا يزداد مع زيادة التركيز. النوع الثاني من التطبيقات الحيوية يشمل تأثير (PEG-SWCNTs و PEG-PEI-SWCNTs و PEG-SWCNTs) على نوعين من الخلايا السرطانية خط خلايا سرطان الثدي (AMJ13) وخط خلايا سرطان الكبد (HepG2) بتراكيز ((6.25-100) $\mu g/ml$) ، وتم قياس معدل تثبيط النمو في الخلايا لمدة (72hr). أظهر فحص السمية الخلوية أن هناك تأثيراً شديداً للسمية على الخلايا السرطانية. النوع الثالث من التطبيقات الحيوية يشمل التأثير (SWCNTs و PEG-SWCNTs و PEG-PEI-SWCNTs و PEG-PEI-SWCNTs-NCur) على خط الخلايا الطبيعي (RD). معدلات التثبيط في خط الخلية الطبيعي RD بتأثير تركيزات مختلفة

PEG-PEI- و PEG-PEI-SWCNTs و SWCNTs) من ((6.25-100) $\mu\text{g/ml}$)
(SWCNTs-N.Cur) لفترة تعرض (٧٢ ساعة) ودرجة حرارة (٣٧ درجة مئوية).



جمهورية العراق
وزارة التعليم العالي والبحث العلمي
جامعة ديالى - كلية العلوم - قسم الفيزياء



تأثير مترابكات SWCNTs – Polymers النانوية على تطبيقات الخطوط

الخلوية السرطانية

اطروحة مقدمة إلى

مجلس كلية العلوم - جامعة ديالى

وهي جزء من متطلبات نيل درجة الدكتوراه فلسفة

في الفيزياء

من قبل

مروه رشيد جوامير

بكالوريوس علوم فيزياء ٢٠١٠

ماجستير علوم فيزياء ٢٠١٦

أشراف

أ.د. فرح طارق محمد نوري

أ.د. صباح أنور سلمان

٢٠٢٢ م

١٤٤٤ هـ